LAPPEENRANTA UNIVERSITY OF TECHNOLOGY
LUT School of Energy Systems
LUT Mechanical Engineering

Joel Salo

FATIGUE STRENGTH OF WELDED JOINTS IN SUPER-DUPLEX STAINLESS STEEL

Examiners: Prof. Timo Björk
D. Sc. (Tech.) Mari Lindgren

ABSTRACT

Lappeenranta University of Technology
LUT School of Energy Systems
LUT Mechanical Engineering

Joel Salo

Fatigue strength of welded joints in super-duplex stainless steel

Master's thesis

2016

93 pages, 72 figures, 20 tables and 7 appendices

Examiners: Prof. Timo Björk
D.Sc. (Tech.) Mari Lindgren

Keywords: super-duplex, 2507, EN 1.4410, fatigue, welded joints, HiFIT post-weld treatment, static test

In this thesis, there is studied the fatigue and static strength of welded joints in super-duplex 2507 stainless steel and the effect of post-weld treatment HiFIT in the fatigue strength.
In the work a literature research on relevant subjects is performed and experimental tests on static performance and fatigue strength. Also, measurements on residual stresses and hardness are made to the specimens. FE-analysis are performed by ENS-method to all joints with FEMAP/NxNastran-program. The joint that are studied in this thesis are limited to tensile loading cases and they are: butt welded joint, non-load carrying joint, load carrying joint and the effect of different cutting methods is studied. Butt welded and non-load carrying joints are tested in as-welded and HiFIT treated conditions.

In static tests the ultimate tensile strength was 870–900 MPa. All the specimens broke from the base material. In fatigue testing, the as-welded condition had better characteristic fatigue values than the IIW recommendations are. With HiFIT treatment the fatigue strength didn't improve compared to the as-welded condition and partly they were worse.

Based on the results HiFIT treatment is not suggested on this material. With the same manufacturing methods and quality as in the as-welded condition there is suggested new characteristic fatigue values that are: for cut edges 200 MPa, butt welds 112 MPa, non-load carrying joints 90 MPa and load carrying joints 71 MPa.

TIIVISTELMÄ

Lappeenrannan teknillinen yliopisto
LUT School of Energy Systems
LUT Kone

Joel Salo

Hitsattujen liitosten väsymiskestävyys super-duplex ruostumattomassa teräksessä

Diplomityö

2016

93 sivua, 72 kuvaa, 10 taulukkoa ja 7 liitettä

Tarkastajat: Professori Timo Björk
TkT Mari Lindgren

Hakusanat: super-duplex, 2507, EN 1.4410, väsyminen, hitsatut liitokset, HiFIT jälkikäsittely, staattinen koe

Tässä diplomityössä tutkitaan super-duplex 2507 ruostumattoman teräksen hitsattujen liitosten staattisia ja väsymiskestävyys ominaisuuksia sekä hitsauksen jälkikäsittely menetelmän HiFIT vaikutusta väsymiskestävyyteen.

Työssä tehdään kirjallisuustutkimuksen lisäksi staattisia- sekä väsytyskokeita. Lisäksi tutkitaan jäännösjännityksiä, kovuuskoe tuloksia sekä tehdään liitoksista FE-analyysit ENS-menetelmällä käyttäen FEMAP/NxNastran-ohjelmaa. Tutkittavat liitokset tässä työssä rajoitetaan vetokuormitus tapauksiin ja ne ovat: päittäisliitos, kuormaa kantamaton liitos, kuormaa kantava liitos ja lisäksi tutkitaan eri menetelmillä leikatun perusmateriaalin reunan vaikutusta. Päittäisliitokset ja kuormaa kantamattomat liitokset ovat testattu myös jälkikäsiteltynä.

Staattisissa kokeissa saatiin murtolujuudeksi 870–900 MPa. Kaikki kappaleet hajosivat perusmateriaalista. Väsytyskokeissa, ilman jälkikäsittelyä, saavutettiin huomattavasti parempia karakteristisia väsymisluokkia kuin IIW:n suositukset ovat. Jälkikäsitellyillä koekappaleilla ei saavutettu pitempiä elinikiä verrattuna hitsattuun kuntoon ja osittain tulokset olivat huonompia. HiFIT jälkikäsittelyä ei tulosten perusteella suositella tehtäväksi tälle materiaalille. Väsytyskokeiden perusteella, koekappaleiden valmistuksessa käytetyillä valmistusmenetelmillä ja laadulla suositellaan uusiksi karakteristisiksi FAT-luokiksi leikatuille reunoille 200 MPa, päittäisliitoksille 112 MPa, kuormaa kantamattomille liitoksille 90 MPa ja kuormaa kantaville liitoksille 71 MPa.

FOREWORDS

I would like to thank Professor Timo Björk and D. Sc. (Tech.) Mari Lindgren for guidance and feedback along this work. The experimental part of this work could not happen without the employees of LUT laboratory of steel structures especially Matti Koskimäki, Olli-Pekka Pynnönen and Jari Koskinen were a great help. Also, the help of Ville Strömmer from Outotec and other students in LUT is held in great value. I would like to thank FIMECC's BSA program for funding this thesis. Additionally, I would like to thank my family for their support throughout my studies and this thesis.

Joel Salo

Lappeenranta 01.11.2016

TABLE OF CONTENTS

APPENDIXES:

LIST OF SYMBOLS AND ABBREVIATIONS

A	Cross-sectional area [mm]
a	Weld throat thickness [mm]
A_5	Elongation [%]
b_0	Plate width [mm]
E	Modulus of elasticity [MPa]
e	Axial misalignment [mm]
F	Force [N]
F_{max}	Maximum force [N]
F_{min}	Minimum force [N]
FAT_{char}	Characteristic fatigue resistance value [MPa]
FAT_{mean}	Mean fatigue resistance value [MPa]
I	Second moment of area [mm^4]
K	Stress intensity factor
K_m	The stress concentration factor for misalignment
$K_{m,calculated}$	Stress magnification factor that is obtained by equations
$K_{m,already\ covered}$	Stress magnification factor covered in FAT classes
$K_{m,angular}$	The magnification factor for angular misalignment
$K_{m,axial}$	The magnification factor for axial misalignment
$k_{m,tot}$	Total stress magnification factor including axial and angular misalignments
K_s	The stress concentration factor for structural detail
l_0	Length of plate [mm]
l_1	Length of plate [mm]
M	Moment [Nm]
m	Slope of the S-N curve
N	Number of cycles
R	Stress ratio
r	Fillet rounding radius [mm]
Ra	Surface roughness arithmetic average [µm]
R_m	Tensile strength [MPa]

$R_{p0.2}$	Yield strength based on 0.2 % permanent elongation [MPa]
Rz	Surface roughness between highest peak and lowest valley [µm]
t	Thickness [mm]
ν	Poisson's ratio
y	The distance from the natural axis [mm]
y_1	Intermediate factor for angular misalignment
α	Angular misalignment
β	Intermediate factor for angular misalignment
ΔF	Force fluctuation [N]
$\Delta\sigma$	Stress fluctuation [MPa]
$\Delta\sigma_{nom}$	Nominal stress range [MPa]
$\Delta\sigma_{n,w}$	Nominal stress in weld [MPa]
$\Delta\sigma, structural$	Structural stress range [MPa]
ε_x	Strain in x-direction
ε_y	Strain in y-direction
λ	Misalignment factor dependent on restrains
σ	Stress [MPa]
σ_{hs}	Hot spot stress [MPa]
σ_m	Nominal mean stress [MPa]
σ_{max}	Maximum stress [MPa]
σ_{min}	Minimum stress [MPa]
$\sigma_{0.4t}$	Stress located 0.4 times plate thickness from the weld root [MPa]
$\sigma_{1.0t}$	Stress from one plate thickness away from the weld root [MPa]

BM	Base material
BSA	Breakthrough steels and applications
BW	Butt weld
ENS	Effective notch stress
FAT	Fatigue resistance value [MPa]
FCW	Flux-cored arc welding
FEM	Finite element method
FIMECC	Finnish Metals and Engineering Competence Cluster
GMAW	Gas metal arc welding

GTAW	Gas tungsten arc welding
HAZ	Heat affected zone
HFMI	High frequency mechanical impact
HiFIT	High frequency impact treatment
IIW	International Institute of Welding
L1	Load carrying joint 1
L2	Load carrying joint 2
NDT	Nondestructive testing
NL	Non-load carrying
PAW	Plasma arc welding
PC	Plasma cut
PREN	Pitting resistance equivalent number
SAW	Submerged arc welding
SCC	Stress corrosion cracking
SD	Super-duplex
SMAW	Shielded metal arc welding
TIG	Tungsten inert gas welding
UIT	Ultrasonic impact treatment
WC	Water cut edge specimen
WPS	Welding procedure specification
XRD	X-ray diffraction

1 INTRODUCTION

In this work the fatigue and static strength of welded joints in super-duplex stainless steel is investigated. The aggressive environment in many industries such as pulp and paper, oil, chemistry etc. creates a need for materials that can last in the corrosive environments. Modern structures need to be efficient which has led to using of higher strength materials. The commonly used 300-series austenitic stainless steels have a good corrosion resistance but a low strength and commonly used carbon steels, such as high strength structural steels, have good strength but low corrosion resistance. Super-duplex stainless steels have a good combination of both corrosion resistance and high strength. Welded structures have to perform in a reliable manner for safety reasons and disturb-free operation is essential from the economical point of view. Because super-duplex stainless steels are much more expensive than 300-series stainless steels the optimum usage of the material is important. For these reasons the assessments of fatigue strength of welded joints in super-duplex stainless steels is needed. This thesis is founded by FIMECC's (Finnish Metals and Engineering Competence Cluster) BSA (Breakthrough steels and applications) program.

This thesis is carried out by using two methods, a literature survey which is used to obtain background data for the experimental and the actual experimental investigation which is carried out in the LUT (Lappeenranta University of Technology) laboratory. The experimental results will be used to evaluate the current workshop quality of the specimen manufacturer. The material in this research is 2507 grade (EN 1.4410) super-duplex stainless steel. It will be referred shortly by 2507 in this paper. For this material, fatigue and static testing for butt welded, non-load carrying and load carrying joints are performed. The effect of post weld treatment technique HiFIT (high frequency impact treatment) is also investigated. To evaluate the results hardness measurements, scanning electron microscopy examination, residual stress measurements and FEM (finite element method) are utilized.

This thesis is limited to joints subjected only to tensile loading. The real-world applications can vary a lot, so in this thesis, the welding joints are simplified to three different types of joints: butt weld, non-load carrying and load carrying joints. Fatigue testing is performed in

the high-cycle fatigue regime, cycles before fracture are kept under the knee point of N = 10^7. It is expected that 2507 has a good static strength and fatigue performance.

2 MATERIAL AND FATIGUE THEORY

The literature review for the material information and theory was performed mostly by NELLI (National Electronic Library Interface), SCOPUS bibliographic database and Google's Scholar search engine but other sources were also utilized such as Science Direct. In this chapter, duplex and super-duplex stainless steels are first introduced. Then a look is taken at the theory of fatigue and at the experimental methods used in this study.

2.1 Duplex stainless steels

Duplex stainless steels have a microstructure of about 50 % of austenite and 50 % of ferrite. This kind of steels has been produced from the 1930's. In the 1930's in Sweden a duplex stainless steel was created for the sulfite paper industry. Those grades were made by alloying steels with chromium, nickel and molybdenum. They were created to reduce corrosion problems. The general performance of these first duplex stainless steels was good but there were problems with the HAZ (heat-affected zone) in the welding of the materials. The welding HAZ had too much ferrite which leads to low toughness and lower corrosion resistance than the base material which had an equal amount of austenite and ferritic in the microstructure. In the 1970's the steel production techniques improved, nitrogen was added and carbon content lowered in the duplex stainless steels. This helped to stabilize the austenite content in the HAZ and also improved the corrosion resistance in the as-welded condition. (Alvarez-Armas 2008, p. 51.)

The second generation of duplex steels came in the late 1970's. Offshore gas and oil fields and applications where an excellent chloride corrosion resistance was needed, started to use the 2205 duplex stainless steel widely. 2205 had a high strength which enabled to reduce weight and which made the 2205 the most used duplex stainless steel with nearly 60 % of the total duplex usage. Modern duplex stainless steels can be divided into five different groups, according to their corrosion resistance. The corrosion resistance is approximated by PREN (Pitting Resistance Equivalent Number). PREN can be calculated based on the alloy content of chromium Cr, molybdenum Mo and nitrogen N, by their weight percent. The five different groups of duplex stainless steels are according to International Molybdenum Association (IMOA) (2014, p. 5–6.):

1. “Lean duplex without deliberate Mo addition, such as 2304;
2. Molybdenum-containing lean duplex, such as S32003;
3. Standard duplex with around 22% Cr and 3% Mo, such as 2205, the workhorse grade accounting for nearly 60 % of duplex use;
4. Super duplex with approximately 25% Cr and 3% Mo, with PREN of 40 to 45, such as 2507;
5. Hyper duplex with higher Cr and Mo contents than super duplex grades and PREN above 45, such as S32707.”

Typical PREN values for different grades of the lean duplex is around 21–27, lean duplex with the additional molybdenum 27–34, standard duplex 33–38, super-duplex 40–45 and hyper duplex 49–53 (International Molybdenum Association (IMOA) 2014, 5–6). The PREN value does not describe the absolute corrosion resistance of the material in every corrosion environment but it gives an approximation of the expected resistance to pitting corrosion in an aqueous chloride solution (Alvarez-Armas 2008, p. 53).

Stainless steel production is increasing on average by 6 % by year. However, stainless steel production is still less than 1 % of carbon steel production. Most of the duplex stainless steel products are made from hot rolled 2205. Duplex grades production in 2007 had increased by almost 100 % in a decade but it is still less than 1 % of total stainless steel production. Super-duplex grades, mostly 2507, represent about 10 % of the duplex production. (Charles 2007, pp. 2–5.)

Duplex grading commonly goes by the numbers that reflect their typical content of chromium and nickel by weight percent. For example, the 2507 grade has about 25 % Cr and 7 % Ni and 2205 grade has 22 % Cr and 5 % Ni. (Alvarez-Armas 2008, p. 52.)

2.2 2507 grade super-duplex stainless steels

2507 grade super-duplex stainless steels are also known in North American designation system UNS S32750, EN number 1.4410 and EN name X 2 CrNiMoN 25-7-4. The 2507 grade is typically characterized by (Sandvik 2015, p. 1):

– “Excellent resistance to stress corrosion cracking (SCC) in chloride-bearing environments

- Excellent resistance to pitting and crevice corrosion
- High resistance to general corrosion
- Very high mechanical strength
- Physical properties that offer design advantages
- High resistance to erosion corrosion and corrosion fatigue
- Good weldability".

It is available for example as seamless and welded pipes and tubes, flanges, sheets, bars and forged and cast products. Its applications are typically chloride-containing environments like seawater cooling and handling, oil and gas exploration and production, pulp and paper production, chemical processing and other mechanical components that require high strength in for example seawater. (Sandvik 2015, p. 1, 18.) The typical values of the chemical composition of 2507 are showed in table 1**.** The mechanical properties of 2507 are presented in table 2.

Table 1. The typical values of 2507 chemical composition by its weight percent (Outokumpu 2013, p. 1).

Element	Carbon (C)	Nitrogen (N)	Chromium (Cr)	Nickel (Ni)	Molybdenum (Mo)
Content %	0.02	0.27	25.0	7.0	4.0

Table 2. The mechanical properties of cold rolled 2507 according to Outokumpu (2013, p. 3).

Yield strength	Tensile strength	Elongation A_5	Impact toughness	Modulus of elasticity
$R_{p0.2}$ [MPa]	R_m [MPa]	%	EN 10028 [J]	20°C [GPa]
550	750	20	60	200

The yield strength of 2507 is 550 MPa which is over two and a half times of 316L stainless steel. The tensile strength is reported by Outokumpu to be 750 MPa but for smaller sizes, it is reported to be more. For 1mm thick cold rolled sheet it is informed to be 940 MPa. Also, other manufacturers like Sandvik informs the tensile strength to be 800–1000 MPa (Sandvik 2015, p. 2). Elongation is slightly lower for the 2507 than the less alloyed stainless steels but

the ductility is good compared to carbon steels. The yield strength at elevated temperatures and a comparison to other stainless steels is showed in figure 1. (International Molybdenum Association (IMOA) 2014, pp. 26–28.)

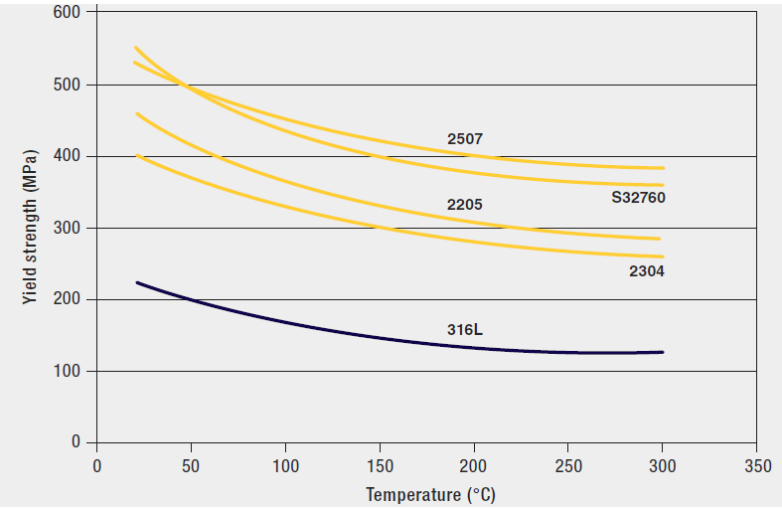

Figure 1. The yield strength of 2507 in elevated temperatures and comparison to other stainless steels (International Molybdenum Association (IMOA) 2014, p. 26).

2507 microstructure has almost equal amounts of ferrite and austenite like other duplex stainless steels. In figure 2, the microstructure of the austenite and ferrite in the rolling-transverse direction is shown. 2507 super-duplex has increased chromium, molybdenum and nitrogen contents compared to conventional duplex stainless steels. These alloying elements add corrosion resistance and especially the nitrogen increases the strength of the material. (International Molybdenum Association (IMOA) 2014, pp. 8–10.)

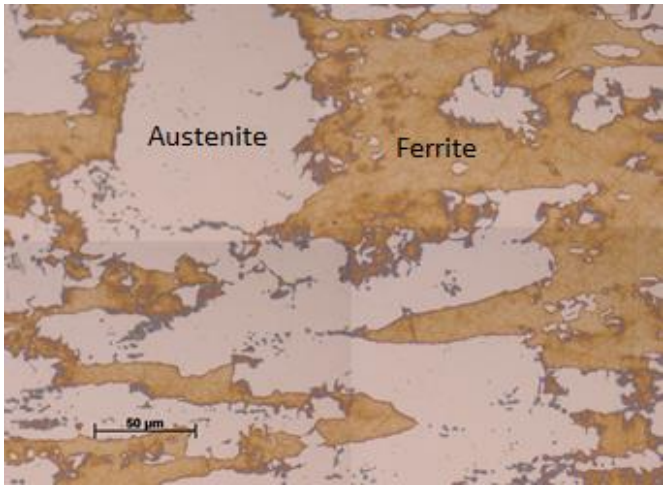

Figure 2. The microstructure of 2507, showing austenite and ferrite.

2507 is prone to the formation of a sigma phase at temperatures between 800–1000°C. The sigma phase can reduce the toughness, ductility and corrosion resistance significantly. The sigma phase can precipitate from the ferrite in high temperatures if the cooling rate is too slow. The increased alloying contents of molybdenum and chromium allows the precipitates to form more quickly. The corrosion resistance is reduced because of sigma phase depletes chromium and molybdenum from the surrounding areas which decreases the pitting resistance of the material, as these alloying elements are responsible for the formation of the protective passive layer. For this reason, the time in high temperatures must be minimized when for instance welding. (International Molybdenum Association (IMOA) 2014, pp. 10–12.)

Weldability of 2507 is good. Most of the methods that can be used in other stainless steels can also be applied to 2507. These methods are for example SMAW (shielded metal arc welding), GTAW (Gas tungsten arc welding), GMAW (gas metal arc welding), FCW (flux-cored arc welding), PAW (plasma arc welding), and SAW (submerged arc welding). 2507 does not need preheating or post-weld annealing. Cooling down is important when welding with multiple passes and the temperature should be under 150°C before next pass. When welding 2507 with GTAW or PAW methods nitrogen should be added to the welding gas so that the pitting resistance does not decrease. The used arc energy should follow the recommendations when welding because otherwise, the balance between austenite and ferrite could change. (Outokumpu 2013, p. 9.) Sandvik suggests that the heat input range should be between 0.2–1.5 kJ/mm (Sandvik 2015, p. 17).

In cutting most of the same processes can be used as with austenitic stainless steels. Plasma and laser cutting are suitable for 2507. However, the mechanical cutting is more difficult because of the material’s high strength. With powerful machinery sawing and shearing is not a problem, some adjustments in the parameters may be needed to get optimal results. (International Molybdenum Association (IMOA) 2014, p. 31.) Machining is harder for 2507 than 300-series austenitic stainless steels. The yield strength is over twice as high as for the austenitic steels and the initial work hardening rate is at least at the same level. The chips from duplex stainless steels are strong and abrasive for the tools. There are high cutting forces so the machinery needs to be powerful and the mountings need to be rigid.

(International Molybdenum Association (IMOA) 2014, p. 36.) The relative machinability of different duplex stainless steels and 316 austenitic stainless steel is presented in figure 3.

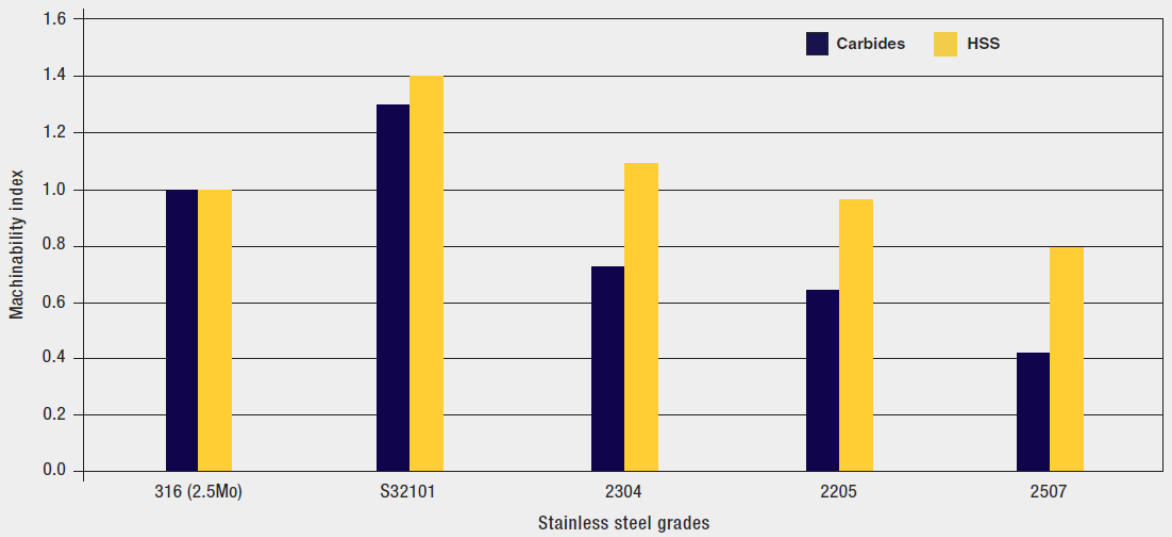

Figure 3. The relative machinability of 2507 is more challenching than other duplex stainless steels and 316 austenitic stainless steel with cemented carbide tooling and high-speed steel tooling (International Molybdenum Association (IMOA) 2014, p. 36).

2.3 Fatigue with welded structures

In welded structures fatigue is the most common cause of failure because weld toe or root side has commonly some small crack-like defects and they are often under the influence of high secondary stresses. Fatigue failure in the welded structures is caused by for instance structural irregularities, local notch effect or by crack-like flaws. Usually, they can be found at the same place which causes a cumulative effect. It is noted that the fatigue performance does not depend on the strength of the material in welded condition. The crack growth rate is about the same in steels with different yield strength steels. High strength is only beneficial in crack initiation phase. (Niemi 2003, p. 16, 95.)

2.3.1 Fatigue phases

Fatigue process can be divided into three different stages: crack initiation, crack propagation and fracture. If peak stress in the bottom of the notch is over twice the yield strength, there is presented back on forth plastic deformation of the material. This is presented in figure 4 on the left side and on the right side there is a simplified version of crack initiation. When the load grows happens sliding that exposes new material. When the load decreases, the

situation does not recover fully. This repeats until a crack-like flaw is generated. It is generally considered that the as-welded condition does not have initiation stage as cracks start to propagate immediately from the small welding imperfections in the weld toe. (Niemi & Kemppi 1993, p. 236.)

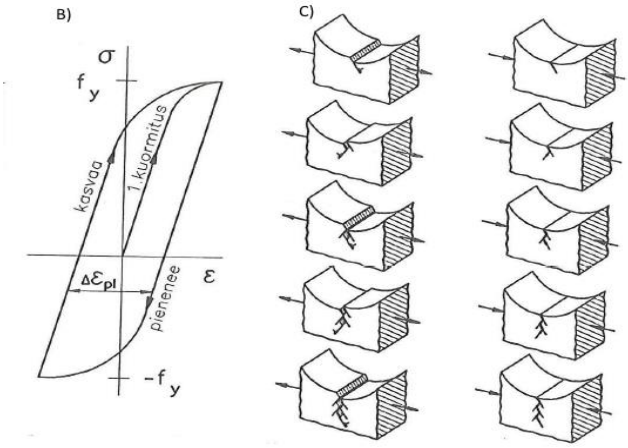

Figure 4. The crack initiation stage (kasvaa = growing, 1. kuormitus = 1. load, pienenee = decreases) (Niemi & Kemppi 1993, p. 237).

Crack propagation stage works similarly as the initiation stage in the tip of the crack but now the plastically deformed area is small compared to the depth of the crack. In the propagation stage, the stress field and plastically deforming zone are described by the stress intensity factor *K*. When the crack has proceeded to be so long that the remainder section cannot take the maximum load anymore, a fracture happens. The more ductile the material is, the longer crack length is needed for the fracture. (Niemi & Kemppi 1993, p. 238.)

2.3.2 Fatigue loading

Fatigue loading is cyclic with a constant or a variable amplitude. The most important feature in fatigue loading is the stress range which means the difference between the maximum and minimum stress. In the as-welded condition, there is assumed to be yield strength high welding stress in the location of the initial crack. Nominal mean stress influence is low in the as-welded joints because the welding stresses keep the real stress level high. (Niemi 2003, p. 92.) Stress ratio *R* can be calculated as (Niemi & Kemppi 1993, p. 240):

$$R = \frac{\sigma_{min}}{\sigma_{max}} \tag{1}$$

In equation 1, σ_{min} is the minimum stress and σ_{max} is the maximum stress.

The constant and variable amplitude loading and the stress factors maximum stress σ_{max}, minimum stress σ_{min}, nominal mean stress σ_m and stress fluctuation $\Delta\sigma$ are shown in figure 5.

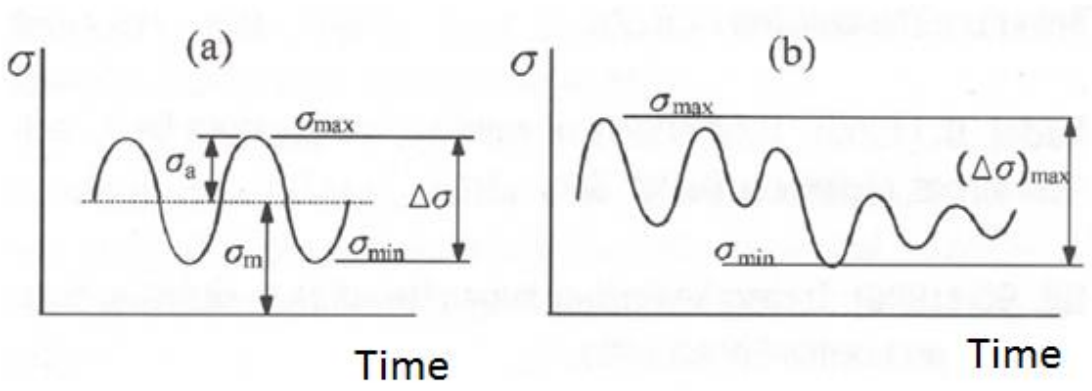

Figure 5. The variable and constant amplitude loading and stress factors (modified from Niemi 2003, p. 92).

In figure 6 there is shown different stress ratios *R*. The last one on the right describes the influence of the welding stresses.

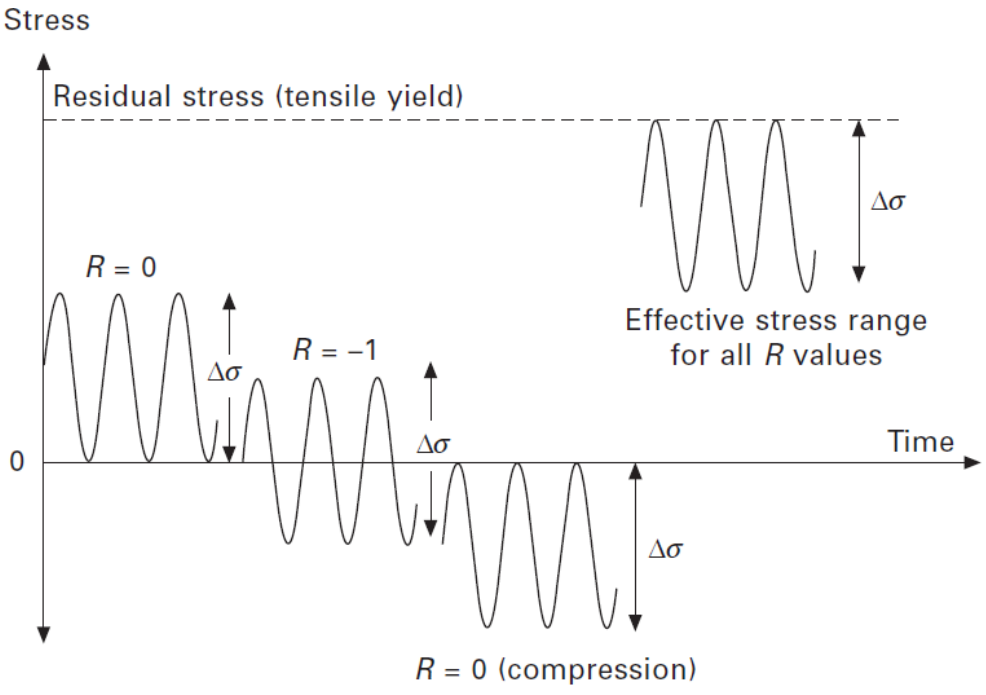

Figure 6. Different stress ratios R (Maddox 2011, p. 174).

In research, usually specimens nominal stress ratios without taking account of the welding stresses are used (Niemi & Kemppi 1993, p. 241).

2.3.3 Fatigue life evaluating and stresses

Fatigue life of welded joints can be evaluated by multiple different methods. Three common types of methods can be separated by what kind of irregularities and notches are considered when calculating the stresses (Niemi & Kemppi 1993, p. 231):

- Nominal stress
- Structural hot spot stress
- Effective notch stress.

In these three methods, the fatigue life is expressed in a Wöhler curve which is also known as an S-N curve. S stands for the stress range and N means the number of stress cycles needed for the fracture. (Niemi 2003, p. 95.) The S-N curves are based on the results from constant amplitude tests. The fatigue resistance in the S-N curves represents a survival probability of at least 95 % in the IIW (International Institute of Welding) recommendations. An example of S-N curves is shown in figure 7, in which there are also shown the recommendations of FAT (fatigue resistance value) classes for the nominal stress method. (Hobbacher 2014, p. 17, 40.)

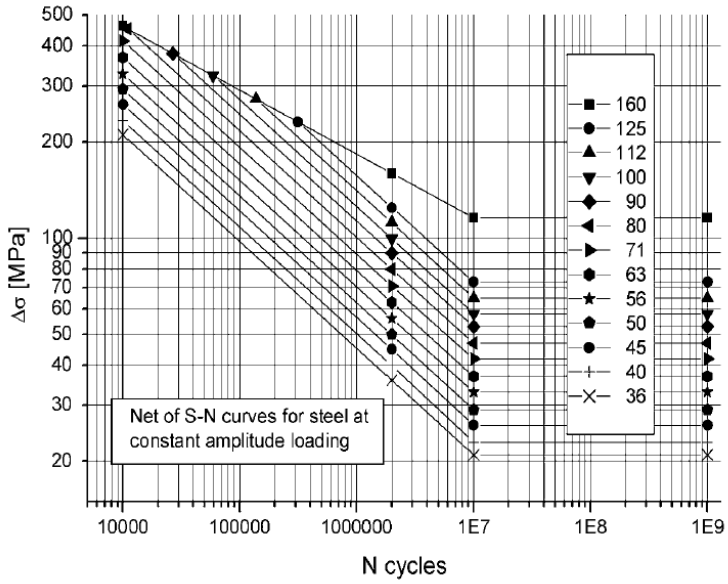

Figure 7. The S-N curve that shows different FAT classes for the nominal stress ranges (Hobbacher 2014, p. 42).

2.3.4 Nominal stress method

Nominal axial tension can be calculated from the beam theory. It is the stress in the cross-sectional area of the structure with macro-geometrical effects but without the consideration of the local stress effects of the welding joints. Large manufacturing imperfections are also considered for instance if there is an axial or angular misalignment. Figure 8 shows a beam-like structure nominal stresses. (Hobbacher 2014, pp. 15–17.)

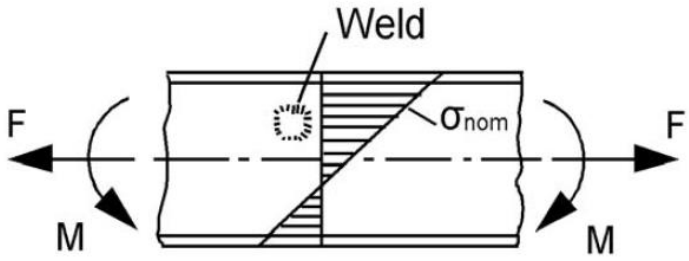

Figure 8. The nominal stress of a beam-like structure (Hobbacher 2014, p. 15).

For the beam in figure 8 the nominal stress can be calculated as (Niemi & Kemppi 1993, p. 232):

$$\sigma = \frac{F}{A} + \frac{M}{I} y \tag{2}$$

, where F is the force, A is the cross-sectional area, M is moment, I second moment of area and y is the distance from the natural axis.

From the nominal stress assessments of classified structural details and welded joints are made. These are estimated by the maximum principal stress range in those sections that will most likely have fatigue cracking. Fatigue curves are made from experimental research using repetitive testing of different types of joints. The fatigue strength of the joint type is described by FAT which means the fatigue strength at 2 million cycles in MPa. FAT class can get values from 36 to 160 MPa. The maximum value of 160 MPa is for the steel material without welded joints and the details should not normally exceed this value. However, the base material can exceed this if it can be verified by tests. (Hobbacher 2014, pp. 41–44.) The S-N curves are presented in the log-log scale and the curves in realistic applications have 1:3 slope (m = 3). Some specimens might have a milder slope but these are forced to 1:3 ratio to

describe the real-life joints more accurately. (Niemi 2003, p. 95.) Since the fatigue curves are based on experimental results they include according to Hobbacher (2014, p. 41) the effects of:

- "structural hot spot stress concentrations due to the detail shown
- local stress concentrations due to the weld geometry
- weld imperfections consistent with normal fabrication standards
- direction of loading
- high residual stresses
- metallurgical conditions
- welding process (fusion welding, unless otherwise stated)
- inspection procedure (NDT), if specified
- post weld treatment, if specified".

Macro-structural hot spot concentrations for instance holes or large manufacturing imperfections has not been taken account in the joint geometry. They need to be taken account in the stress range by different stress concentration factors or by FEM. This is called modified nominal stress. Fatigue curves are not affected by the tensile strength of the material. With constant amplitude loading fatigue curves have a point when the fatigue lifetime can be expected to last forever. This knee point is assumed commonly to match to $N = 10^7$ cycles. (Hobbacher 2014, pp. 41–43.) In fatigue testing the nominal stress range $\Delta\sigma_{nom}$ can be calculated as follows (Niemi et al. 2004, p. 30):

$$\Delta\sigma_{nom} = \frac{F_{max} - F_{min}}{A} = \frac{\Delta F}{A} \tag{3}$$

, where F_{max} is maximum force, F_{min} is minimum force and ΔF is force fluctuation.

2.3.5 Structural hot spot stress

Structural stress in the weld toe position where a crack often develops is called a hot spot stress. In the welded structures, there are many irregularities that cause stress concentrations. These differ from macro-geometrical irregularities because they are included in the fatigue tests. In figure 9 some examples of structural stress concentrations are presented. (Niemi et al. 2004, p. 7)

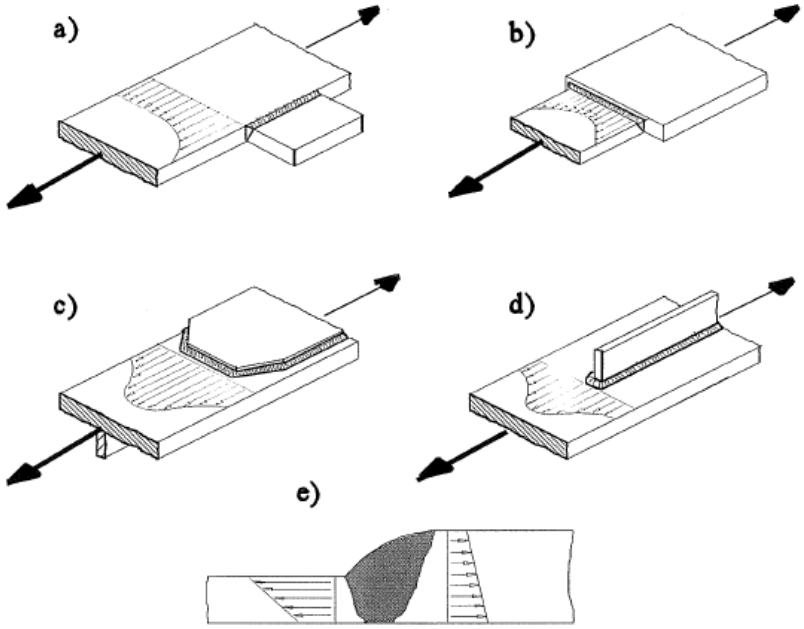

Figure 9. Examples of structural stress with a) side attachment or junction of a beam, b) load carrying attachment, c) end of covering plate, d) end of a long attachment, e) misalignment due change in plate thickness (Niemi et al. 2004, p. 7).

Hot spot stress does not consider the non-linear peak stress which is caused by a local notch in the weld toe for this, there is ENS (effective notch stress method). Hot spot stress is used if the nominal stress is hard to calculate because of geometrical effects or the structure is not equal to the classified structural details. (Hobbacher 2014, p.19.) Hot spot method does not work if the crack grows from the weld root or inside the weld (Niemi et al. 2004, p. 14). Hot spot stress can be defined by three different methods: 1: measuring stresses from a specimen by two or more strain gauges, 2: calculating by using FEM using fine meshing or 3: multiplying the nominal stress by the intensity factor K_S. When using strain gauges or FEM the notch effect must be avoided. That is why the measurements are done by reference points first from $0.4t$, where t is the plate thickness, and the second point is at $1.0t$. (Niemi et al. 2004, pp.6–8.) Then the stress or strain is linearly extrapolated to the welding toe as follows (Hobbacher 2014, p. 24):

$$\sigma_{hs} = 1.67\sigma_{0.4t} - 0.67\sigma_{1.0t} \quad (4)$$

, where σ_{hs} is hot spot stress, $\sigma_{0.4t}$ is stress located 0.4 times plate thickness from the weld root and $\sigma_{1.0t}$ stress from one plate thickness away from the weld root. Three points can also be used with different locations and multipliers. If the stress is not dependent on plate thickness then there is measured the stresses at the distance of 4 mm, 8 mm and 12 mm from the weld toe. (Hobbacher 2014, pp. 24–28.) This is shown in figure 10 along with the extrapolation with two points.

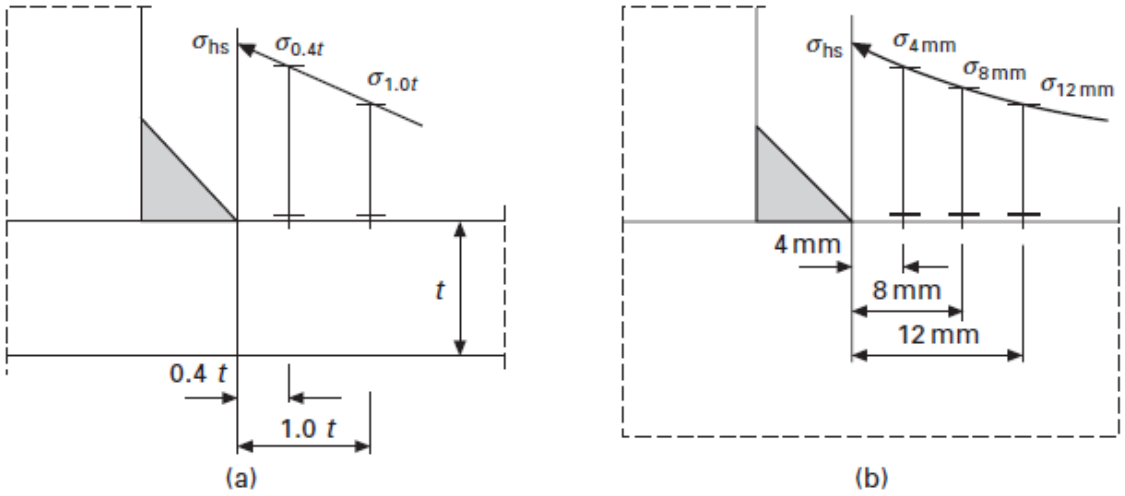

Figure 10. The extrapolation of structural hot spot stress using a) two points on plate surface and b) three points when the plate thickness is not determining (Fricke 2011, p. 120).

The fatigue strength can be estimated after the hot spot stress is determined using a correct FAT class as (Hobbacher 2014, p. 36):

$$FAT = \Delta\sigma_{hs} * \sqrt[m]{\frac{N}{2 * 10^6}} \quad (5)$$

, where *FAT* is the hot spot FAT class, m = 3 the slope of S-N curve and N is the expected number of cycles. The hot spot stress can also be calculated by the stress concentration factors. For structural stress concentration, there is the factor K_s and for the stress concentration caused by axial or angular misalignment, there is the factor K_m. These factors can be calculated from equations presented in later in this work. The hot spot stress can be then calculated. (Niemi et al. 2004, p. 43.)

$$\Delta\sigma_{hs} = K * \Delta\sigma_{nom} \quad (6)$$

Where the K is the relevant stress concentration factor and $\Delta\sigma_{nom}$ is nominal stress. When measuring the stress level from structures using a strain gauge the stress can be calculated as (Niemi et al. 2004, p. 29):

$$\sigma_{hs} = E * \varepsilon_x * \frac{1 + v\frac{\varepsilon_y}{\varepsilon_x}}{1 - v^2} \quad (7)$$

, where E is the modulus of elasticity, ε_x is strain in the x-direction, ε_y is strain in the y-direction and v is the poison's ratio. When strain is occurring only in one direction the equation can be reduced as (Niemi et al. 2004, p. 29):

$$\sigma_{hs} = 1.1 * E * \varepsilon_x \quad (8)$$

2.3.6 Effective notch stress

ENS predicts the crack initiation stage. Welding face and weld toe geometry generates a peak stress near the weld toe. It does not change the average stress in the cross-section but makes it non-linear to the thickness direction of the plate, so that the peak is near the surface. This is presented in figure 11. (Niemi et al. 2004, pp. 8–9.)

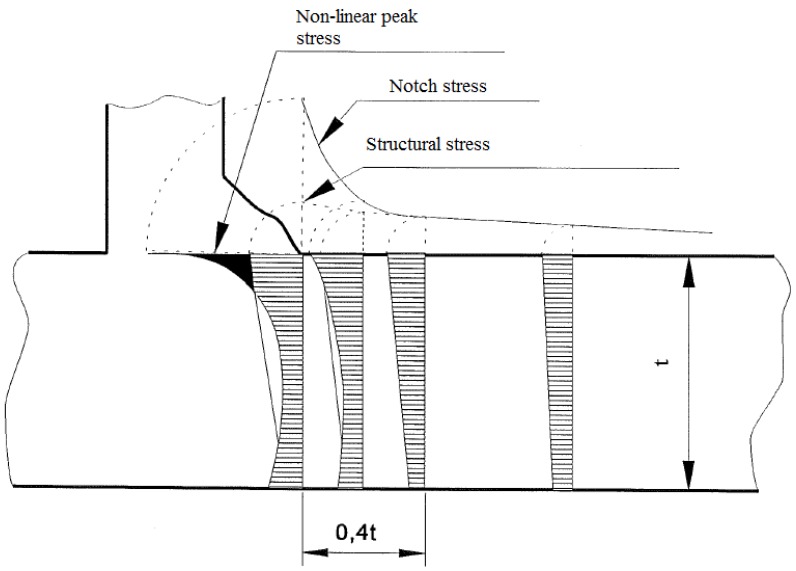

Figure 11. The notch stress in the fillet weld (modified from Niemi et al. 2004, p. 8).

In practice the welding notch stress cannot be measured from the weld toe or root. The measurement device would need to be very small and be placed at the weld toe. (Niemi & Kemppi 1993, p. 232.) The notch stress can be obtained by FEM, by rounding the notch root for example to 1 mm and then the notch stress can be calculated. After assessments of the notch stress, together with FAT classes for the notch stress, the fatigue life can be calculated. This method is limited to the plate thickness of 5 mm and over. Also, the element size needs special attention around the radius, element sizes should be 1/6 or smaller than the radius for linear elements and for higher order elements is should be 1/4 or smaller. For 1 mm radius this means using 0.25 mm or smaller size elements with mid-side nodes and for linear elements 0.15 mm or smaller. The locations where to apply the notch stress radius is presented in figure 12. For the maximum principle stress criteria, a FAT class of 225 is used for steel. (Hobbacher 2014, pp. 29–31, 79.)

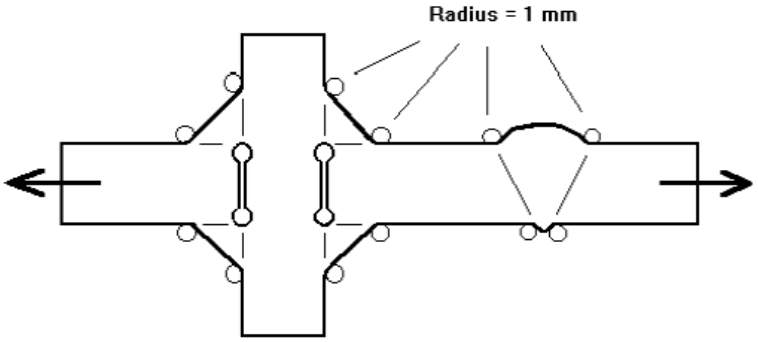

Figure 12. The locations of notch stress rounding's (Hobbacher 2014, p. 30).

2.3.7 Welding imperfections

Welding of materials causes always some kind of imperfections. If they are within the guidelines of the relevant standards they are called imperfections. Otherwise, if they are out of the relevant standard limits they are called defects. Welding defects needs correcting procedures. Welding imperfections has a negative impact on fatigue strength of structures. (Fricke 2011, p. 127.) These imperfections are for example imperfect shape; axial misalignment, angular misalignment, flank angle, added material from the weld, undercut, volumetric discontinuities; pores, slag and planar discontinuities; all crack-like flaws. Misalignment introduces secondary shell bending stresses that increase the stress in the welded joints, which leads to lower fatigue life. These additional stresses can be considered as structural stresses. (Hobbacher 2014, p. 98, 100.)

IIW document: recommendations for fatigue design of welded joints and components, allow axial misalignment of 5–10 % of plate thickness for butt welds depending on FAT class. For cruciform joints, it is 15 % of the primary plate thickness. (Hobbacher 2014, pp. 47–48, 59–60.) In figure 13 the axial misalignment for two plate's butt weld is presented.

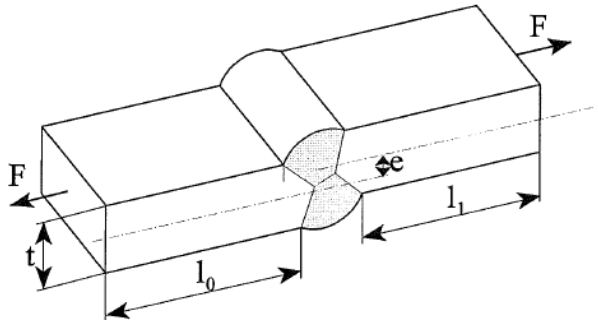

Figure 13. The axial misalignment of the butt welded plates (Niemi et al. 2004, p. 63).

The stress magnification factor K_m can be calculated for the axial misalignment as (Niemi et al. 2004, p. 63):

$$K_{m,axial} = 1 + 6\frac{e\, l_0}{t(l_0 + l_1)} \tag{9}$$

, where $K_{m,axial}$ is the magnification factor for axially misalignment, e is axial misalignment, l_0 and l_1 are the length of the plates. The plate lengths can be set as even if the load is far away from the joint. Angular misalignment is shown in figure 14.

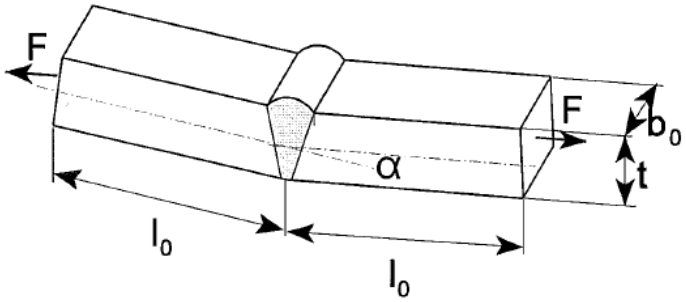

Figure 14. The angular misalignment for butt welded plates (Niemi et al. 2004, p. 66).

The angular misalignment magnification factor $K_{m,angular}$ for plates that are rigidly supported can be calculated as (Niemi et al. 2004, p. 66):

$$K_{m,angular} = 1 + \frac{3\,y_1}{t}\frac{\tanh\left(\beta/2\right)}{\beta/2} \tag{10}$$

, where $K_{m,angular}$ is magnification factor for angular misalignment and intermediate factors β & y_1 can be calculated as follows (Niemi et al. 2004, p. 67):

$$\beta = \frac{2 * l_0}{t}\sqrt{\frac{3\sigma_{nom}}{E}} \tag{11}$$

σ_{nom} can be calculated as:

$$\sigma_{nom} = \frac{F}{t\,b_0} \tag{12}$$

, where b_0 is plate width shown before in figure 14.

$$y_1 = l_0 \sin\left(\alpha/2\right) \tag{13}$$

, where α is the angular misalignment. For cruciform joints, axial misalignment is shown in figure 15. The magnification factor can be calculated as (Niemi et al. 2004, p. 69):

$$K_{m,axial} = 1 + \lambda\frac{e\,l_0}{t(l_0 + l_1)} \tag{14}$$

, where $l_0 = l_1$ if the load is far away from joint and then factor λ, which is dependent on restrains is 6.

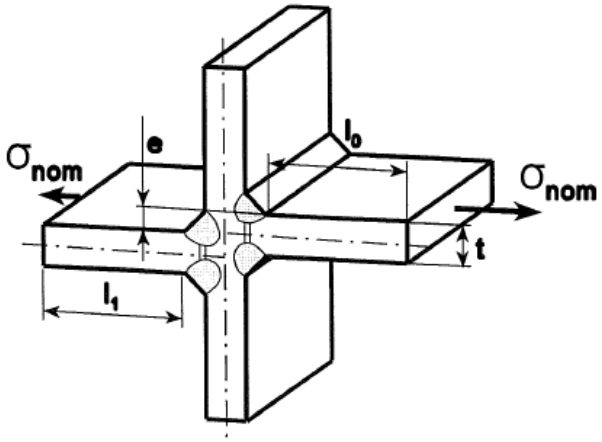

Figure 15. The axial misalignment for cruciform joints.

Angular misalignment for cruciform joints is shown in figure 16. The magnification factor can be calculated as (Niemi et al. 2004, p.69):

$$K_{m,angular} = 1 + \alpha \frac{l_0\, l_1}{t(l_0 + l_1)} \tag{15}$$

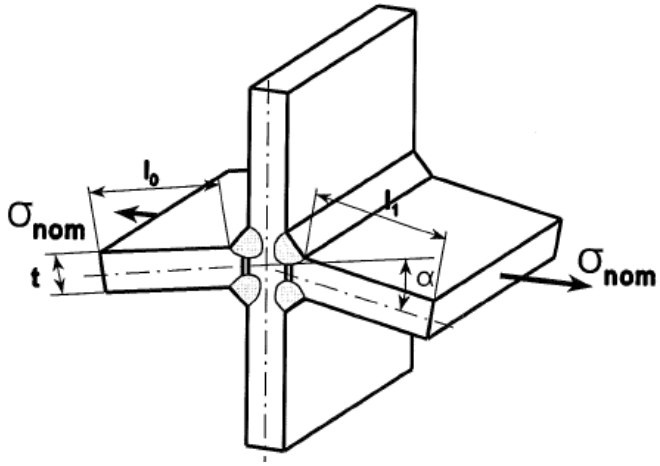

Figure 16. The angular misalignment of cruciform joints (Niemi et al. 2004, p.70).

If a joint contains both axial and angular misalignment then the combined stress magnification can be calculated as (Niemi et al. 2004, p. 44):

$$K_m = 1 + \left(K_{m,axial} - 1\right) + \left(K_{m,angular} - 1\right) \tag{16}$$

Then the stress can be calculated using the equation 6 presented earlier. In classified structural details by IIW: Recommendations for fatigue design of welded joints and components, there are allowed some misalignment. For nominal stress method, there is covered K_m of 1.15 for butt joint made in a workshop in a flat position, 1.30 for other butt joints and 1.45 for cruciform joints in the FAT classes. If the stress magnification K_m is calculated from equations an effective stress magnification factor can be used, which can be calculated as (Hobbacher 2014, p. 101):

$$K_{m,eff} = \frac{K_{m,calculated}}{K_{m,already\ covered}} \tag{17}$$

, where $K_{m,calculated}$ is stress magnification factor that is obtained by equations and $K_{m,already\ covered}$ is stress magnification factor covered in FAT classes. (Hobbacher 2014, pp. 100–101.)

2.4 Post-weld treatment methods

Post-weld treatment methods are made to improve the fatigue performance compared to the as-welded condition. Post-weld treatment methods can be divided into two different types: methods that reduce the geometrical stress concentrations and methods that increase the materials resistance to crack formation by introducing residual compressive stress and hardening of the surface layer. Post-weld treatment methods and their operation ideas are presented in figure 17. (Ummenhofer et al. 2010, p. 18.)

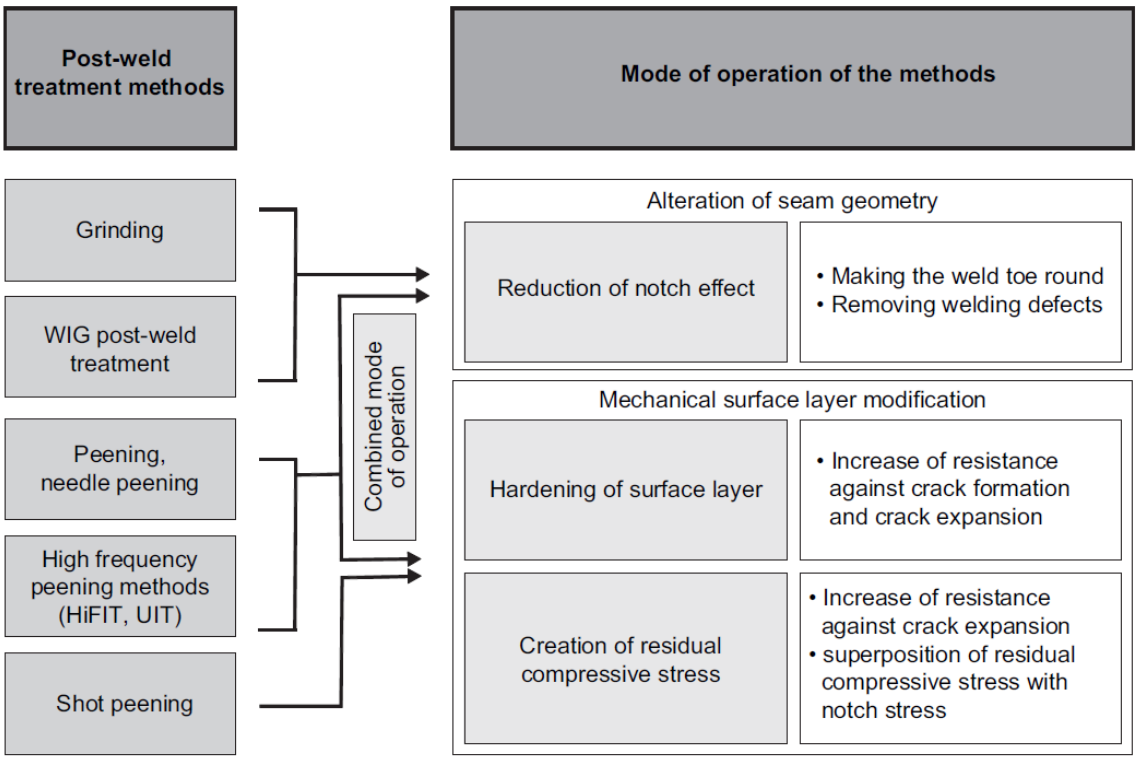

Figure 17. Post-weld treatment methods operation principle (Ummenhofer et al. 2010, p. 18).

Reduction of the stress concentration is often made by grinding or using TIG (tungsten inert gas welding) or plasma welding to re-melt the weld toe. With these methods, the transition between weld and base material is made smoother which reduces the local stress concentration. Grinding can reduce or remove altogether imperfections like undercut, cold laps and crack-like flaws. Usually, 0.5 to 1 mm of material needs to be removed to get rid of the imperfections. If the crack-like flaws are removed then a longer crack initiation period, compared to the as-welded condition, is introduced. TIG or plasma dressing are used to achieve the same results but instead of removing material these methods are used to re-melt the weld toe. The TIG and plasma dressing are made without any use of filler material (Maddox, Doré & Smith 2010, p. 8, 11.)

Generating compressive residual stresses to the weld toe by peening methods, does not necessarily remove the weld imperfections but as it causes compression by plastic deformation. The fatigue loading is then still locally in compression which is better for the fatigue life. Also, there are geometrical advantages as the notch effect is lowered when the weld toe fillet radius is increased. (Maddox, Doré & Smith 2010, p. 8.)

Conventional peening methods are for example hammer and needle peening. In the hammer peening, there is pneumatically operated hammer with rounded tip tool that has 3–7 mm radius. Optimal results are obtained with multiple passes with a pit depth of 0.2–0.5 mm. With hammer peening, residual stress to about max 2 mm below the worked surface is introduced. A similarly shaped groove as in grinding is obtained. Needle peening is like hammer peening but multiple round tip tools are used simultaneously. This method is used when there is a need to work on large areas. (Haagensen 2011, pp. 316–317.) These methods work in the frequency range of 20–100 Hz. There are now newer methods called high frequency peening methods that have frequencies over 180 Hz. Common examples of this method are UIT (ultrasonic impact treatment) and HiFIT. (Ummenhofer et al. 2010, p. 20.)

2.4.1 Post-weld treatment method HiFIT

HiFIT is a peening method where a single pin with a diameter of 2–4 mm is actuated to high frequencies by compressed air. The peening frequency in HiFIT is about 180 Hz to 250 Hz and it is affected by the motion speed, the geometry of the pin and the treated material. It operates in a similar way as hammer peening by introducing compressive residual stresses and reducing the notch effect, but in higher frequency. The surface layer under treatment is plastically deformed but the deeper layers behave elastically. After the treatment, the elastic layers rebounds but the plastically deformed surface layer prevents this from happening which causes residual stress formation with compressive stresses in the surface layer. Plastic deformation in surface layers may be also followed by strain hardening for about 0.2–0.3 mm from the surface. An example of the surface hardness comparison between the as-welded condition and after the HiFIT treatment is shown in figure 18. A noticeable increase in the hardness of the surface layer can be observed. In figure 19 there is showed what the HiFIT treatment looks like in fillet welds. (Ummenhofer et al. 2010, pp. 20–23.)

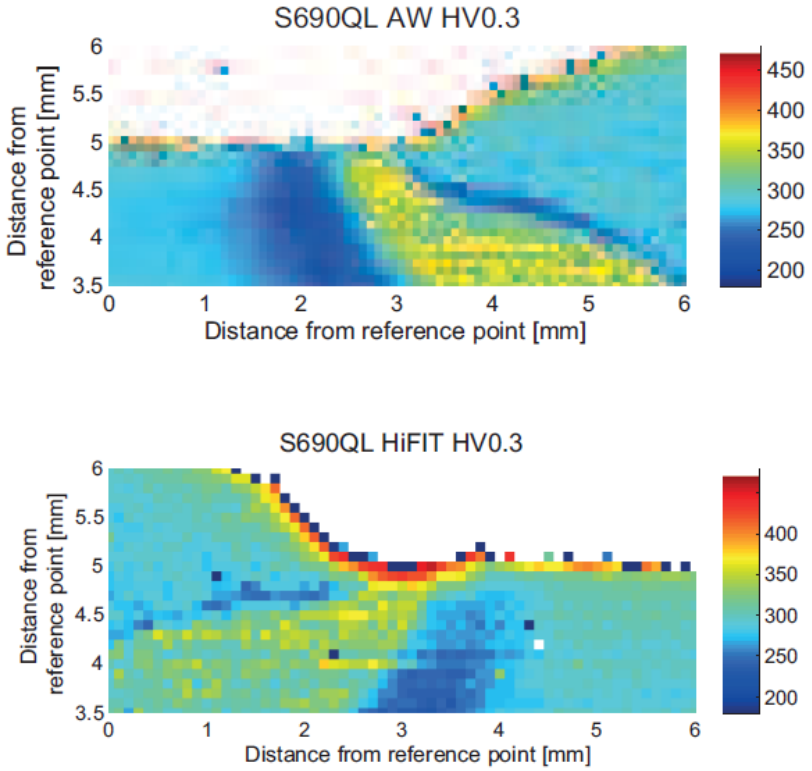

Figure 18. The surface hardness in S690 QL in the as-welded and HiFIT treated condition (Ummenhofer et al. 2010, p. 23).

Figure 19. The weld toe before and after HiFIT treatment (Pfeifer 2009, p. 9).

The motion speed of HiFIT treatment is about 5 mm/s and the required air pressure is 6–8 bar with about 400 l/min of air flow rate. The structure of HiFIT device is shown in figure 20.

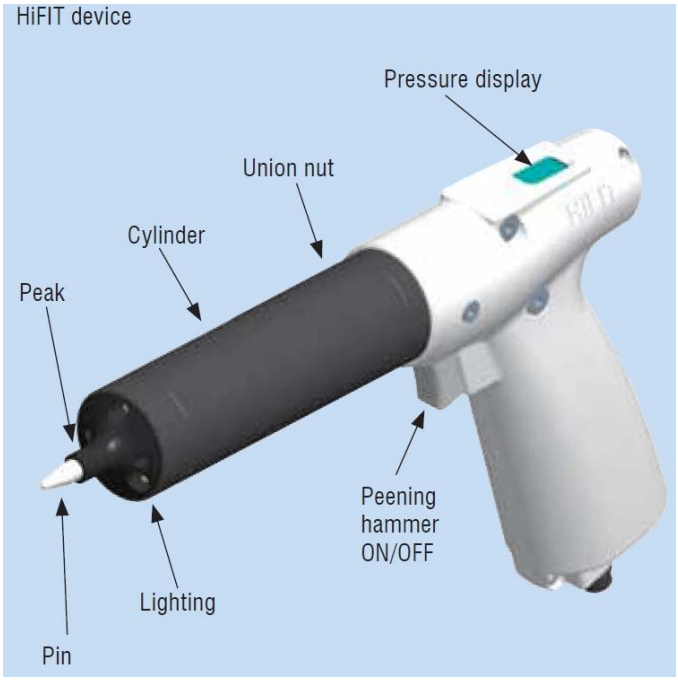

Figure 20. The design of HiFIT device (Pfeifer 2009, p. 8).

HiFIT treatment like other peening treatments works only for the weld toes. HiFIT cannot improve the fatigue life if the crack is initiated from the welding root. Some suitable and unsuitable applications for the HiFIT treatment are summarized in figure 21. (Pfeifer 2009, p. 8).

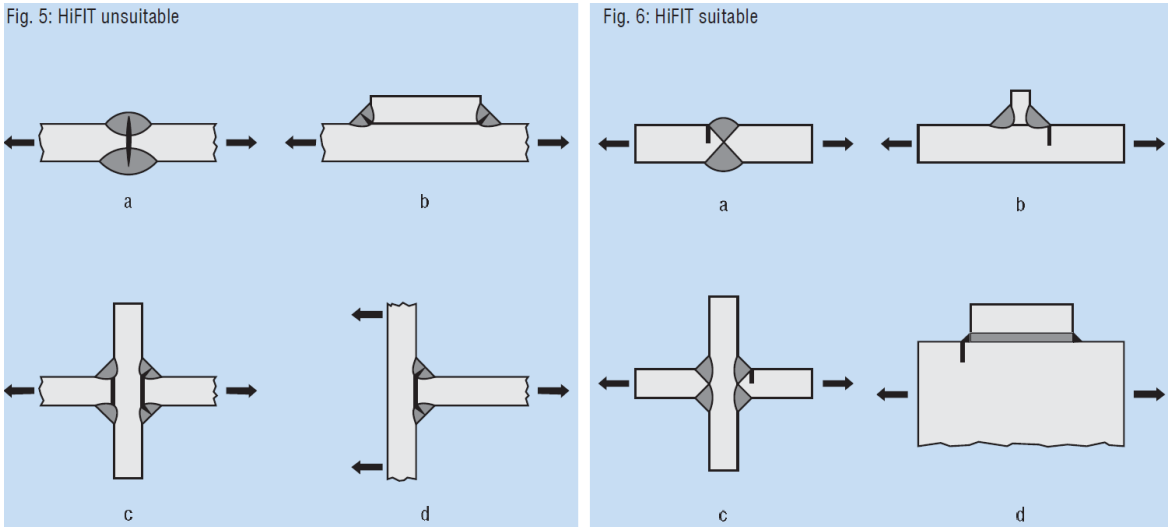

Figure 21. Weld defects that can and cannot be treated by HiFIT (Pfeifer 2009, p. 7).

For high strength steels with over 355 MPa yield strength hammer peening improves the fatigue strength by a factor of 1.5, when the FAT class is 90 or under (Hobbacher 2014, p.

88). This would lead to three fatigue class increases. FAT class limit of 90 is because of higher FAT classes include non-welded details which may lead to failure because of other details than weld toe. Test data suggests that the S-N slope of $m = 5$ could be used for HFMI (high frequency mechanical impact) methods including HiFIT. For steels with a yield strength of under 355 MPa the suggested increase in FAT classes are 4. But for higher strength steels the multiplier would increase by one for every 200 MPa increase in the yield strength. For transverse non-load carrying joint with FAT class of 80 in the as-welded condition an example is showed in figure 22, where the S-N slope of $m = 5$ is used and the new FAT class according to yield strength of the material. (Marquis & Barsoum 2013, pp. 99–100.)

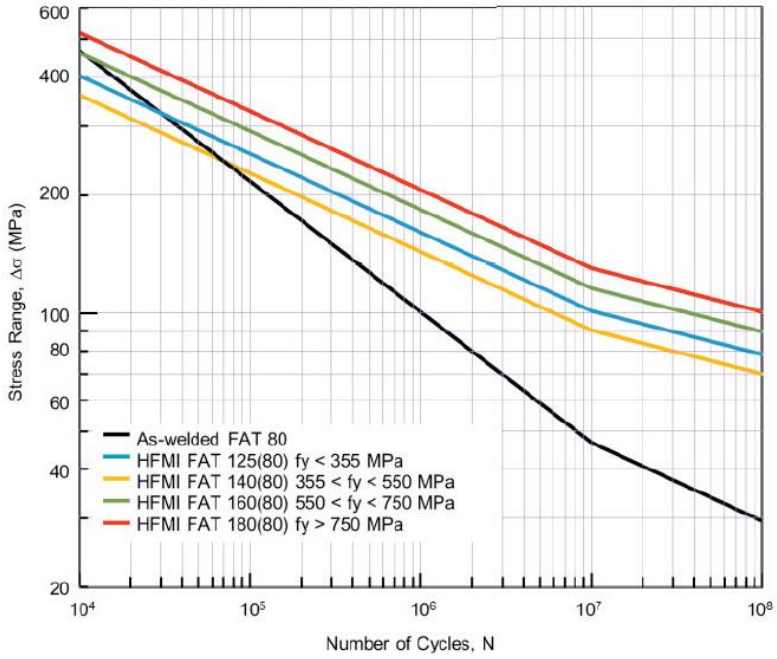

Figure 22. Fatigue life improvement to as-welded FAT 80 class by HFMI for different yield strength steels (Marquis & Barsoum 2013, p. 100).

However, some researches say that the fatigue strength improvement depends on the R-ratio of the loading. It is suggested that with the peening methods the real benefit in fatigue life is fully utilized when $R \leq 0.15$, for $0.15 < R \leq 0.28$ the improvement is one FAT class less, $0.28 < R \leq 0.4$ two FAT classes less and $R > 0.4$ improvement can be claimed only if shown by fatigue tests. (Yildirm & Marquis 2012, p. 175.)

3 EXPERIMENTAL RESEARCH

In this work fatigue and static testing of welded joints made of 2507 grade super-duplex stainless steel are carried out. The specimens are manufactured from cold rolled plate with the thickness of 5 mm. Specimen were cut in the rolling direction. The total number of tests are 43 of which five are static tests and the other are fatigue tests. Testing is performed at an ambient temperature of about 20 ºC.

3.1 Specimen design

The test matrix for the experimental tests is shown in table 3. There is specified the different joint types with three different loading cases.

Table 3. The test matrix for this research.

Preparing of joints		**Number of tests**					
Specimen or joint type	Post-treatment	Loading					Total number
		Static	Fatigue				
			stress range levels	R-value		number of fatigue tests	
				0.1	0.5		
Water cut edges	no	1	2	1	1	4	**5**
Plasma cut edges	no	0	2	1	1	4	**4**
Butt weld	no	1	3	1	1	6	**7**
	HiFIT	0	3	1	1	6	**6**
Non-load carrying joint	no	1	3	1	1	6	**7**
	HiFIT	0	3	1	1	6	**6**
Load-carrying joint, $a = 4$	no	1	3	1	1	6	**7**
Load-carrying joint, $a = 3$	no	1	0	0	0	0	**1**
∑		5				38	**43**

Cut edges specimens are cut straight to their dimensions by water and plasma cutting. Plasma cutting was performed in water. In the water cutting, additional abrasive sand was used. Dimensions of cut edges and the other specimens without the welding joint are shown in figure 23.

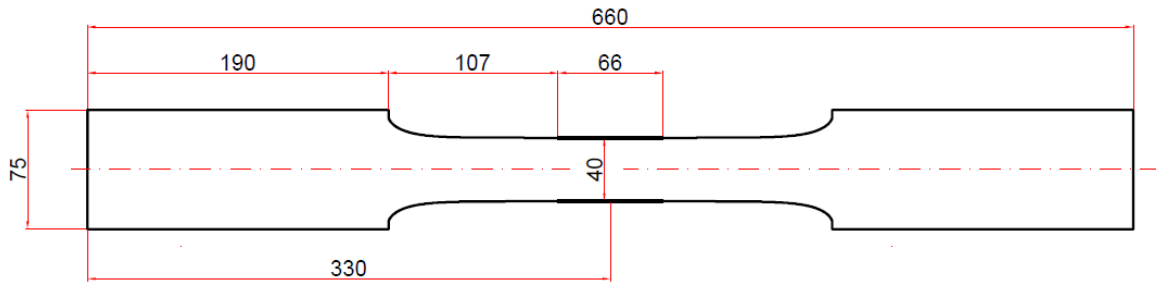

Figure 23. The specimen design for the cut edges and the dimensions of the other specimens without welding joint.

The welding joints are placed in the middle of the specimen. Butt weld specimen was manufactured from two halves that are welded together by a butt weld. Non-load carrying joint has two attachments on opposite sides of the main plate which are welded by fillet welds with the throat thickness of a = 3 mm. Load carrying joints are cruciform joints with two different sizes of throat thickness. For the welded joints the base plate was manufactured by laser cutting and the edges was grinded, so that the fatigue damage is not expected to happen in the cut edges of the specimen. In figure 24 the surface qualities after different cutting methods and grinding are presented.

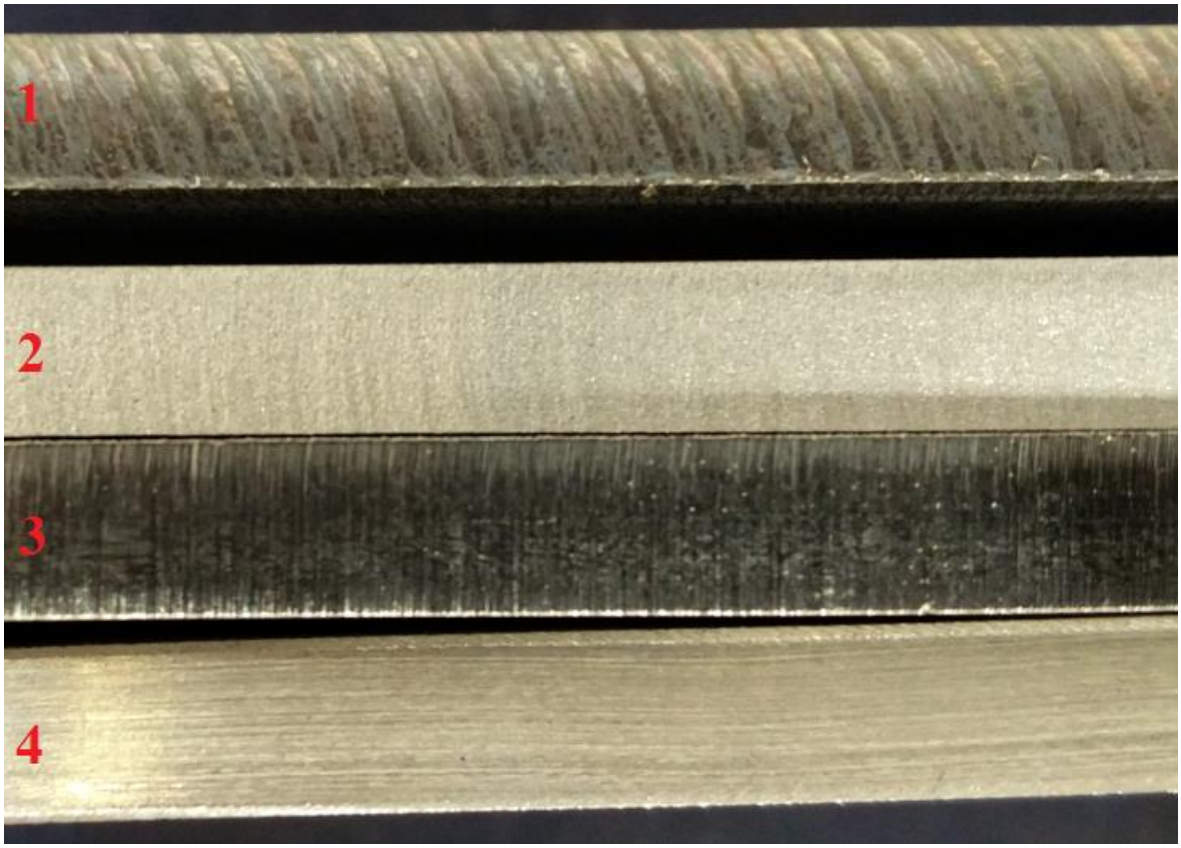

Figure 24. Different cut edges: 1. underwater plasma cutting, 2. water cutting, 3. laser cutting and 4. grinded edge of butt welded specimen after fatigue testing.

Dimensions of the load carrying and non-load carrying joints are shown in figure 25**.** Load carrying specimens are 5 mm longer than others because it was manufactured from same halves as the butt weld specimen, but a middle plate was added between the halves. IIW fatigue recommendation for the fat class of base material is 160 MPa with m = 5, for butt welds FAT = 90 m = 3, for non-load carrying joints FAT = 80 m = 3 and for load carrying fillet welded joints FAT = 63 m = 3 (Hobbacher 2014, pp. 45–63). These fatigue classifications are shown in appendix II.

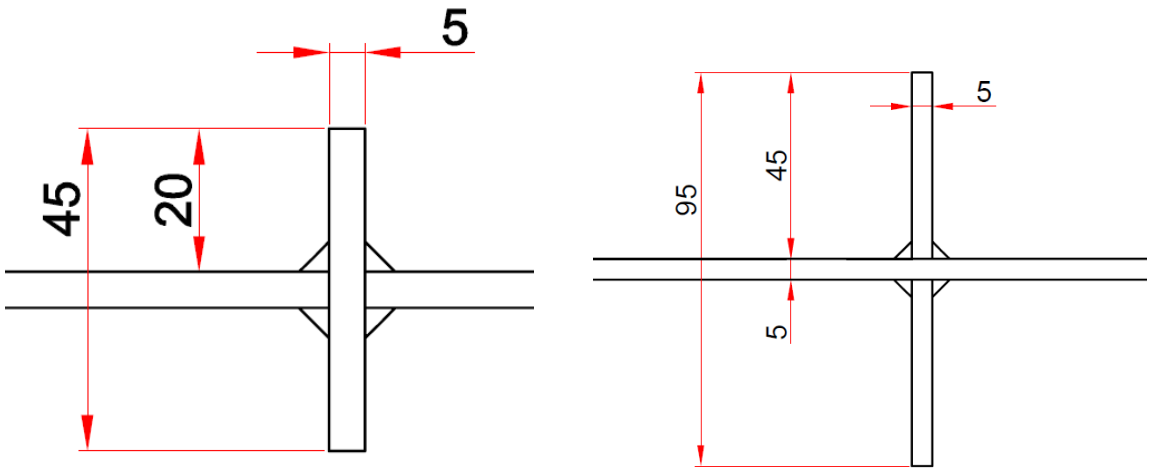

Figure 25. Load-carrying joint design on the left and non-load carrying design on the right.

The specimens were manufactured with an extra ledge in the welding location because then the starting and ending point of welding could be machined off. This is made to remove all possible welding imperfections and defects caused by starting and ending point of the welds. Welding and post-weld treatment were carried out by Outotec Turula Oy according to their own WPS (welding procedure specification). Welding was performed by three to four different welders with no special arrangements, consequently the quality represents the typical workshop quality in Turula. Welding was made by manual MAG welding, process number 136, using Ar+18% CO_2 shielding gas, Tetra S D57L filler metal with a diameter of 1.2 mm. The welding filler material has higher mechanical properties than the base material, R_m is 950 MPa, $R_{p0,2}$ is 830 MPa and elongation A_5 is 22 % (Welding Alloys 2016). Welding was performed without any pre- or post-heating treatments with the max interpass temperature of 100 °C and heat input between 0.8–1.5 kJ/mm. Butt welded specimens were welded from both sides. The machining off of the extra ledge was performed by LUT for the butt welded specimen and for the cruciform joint types by Outotec. A specimen before the extra ledges were machined off, from the dashed red line, is presented in figure 26. The butt welded specimens were brushed near the joint location after welding, which caused problems in residual stress measurements. This is shown in figure 27. Brushing were made to clean the specimen after welding and before HiFIT treatment, but it was not made to cruciform joints. Brushing as a cleaning method was in the WPS.

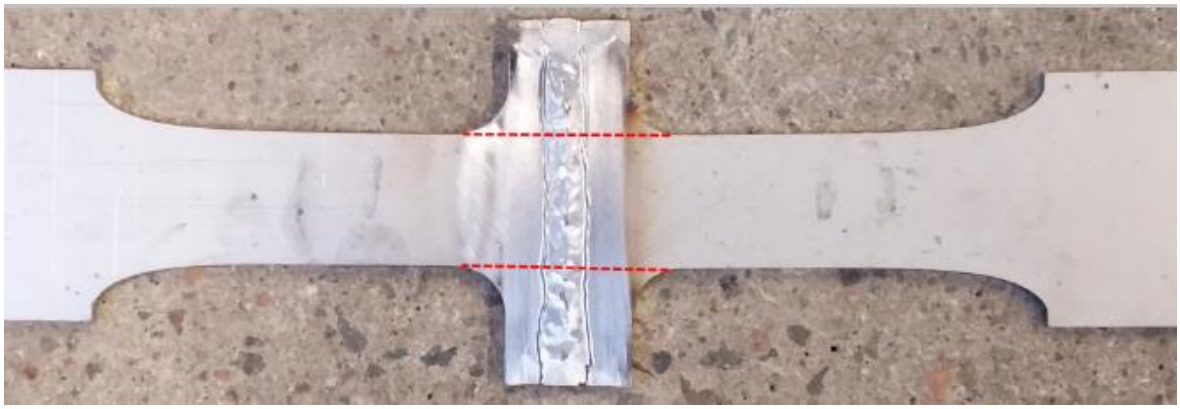

Figure 26. Butt welded HiFIT treated specimen before machining the extra ledge out.

Figure 27. The polished area near in the joint of fatigue tested SDBW.4H specimen.

The specimens are referred by a 5 to 7 character long name which consists of SD (Super-Duplex), joint type (WC = water cut, PC = plasma cut, BW = butt weld, NL = non-load carrying, L1 = load carrying joint with bigger weld throat thickness of 4 mm and L2 = load carrying with smaller weld throat thickness of 3 mm), S denotes to a static test and other are fatigue tests. If there is an H in the end of the name, the specimen is HiFIT post-weld treated and J means a specimen is continued with higher loads after run out. For different specimens in the same series, continuous numbering was used. Specimen sides are named by letters A, B, C and D. This is shown in figure 28. These letters are used to determine for instance the locations of fracture or a strain gauge. In figure 29 there is shown a strain gauge near the weld toe in D side of a butt welded specimen.

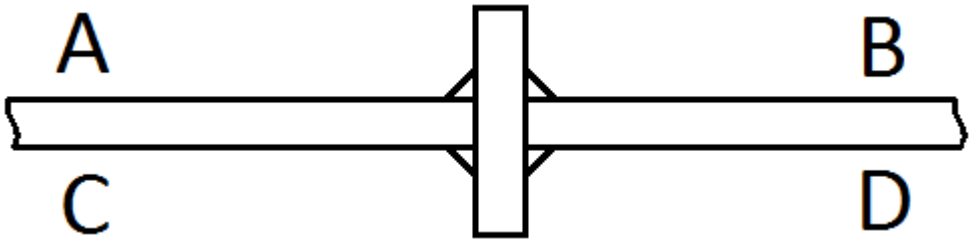

Figure 28. The side marking in the specimens.

Figure 29. The location of a strain gauge in a butt welded specimen.

3.1.1 Material information

The material for the specimen was delivered by Outokumpu Stainless AB, Sweden.
The plate is cold rolled and the chemical composition and mechanical properties per material certificate EN 10204-3.1 are presented in tables 4 and 5. There are two sets of material. The only specimens that were made from the second set, was the plasma cut edges specimens.

Table 4. The Chemical composition weight % for the two different sets of 5 mm 2507 super-duplex stainless steel per the material certificates.

Element:	C	Si	Mn	P	S	Cr	Ni	Mo	Cu	N
Series 1:	0.015	0.39	0.83	0.024	0.001	25.02	6.94	3.80	0.34	0.277
Series 2:	0.016	0.40	0.85	0.030	0.001	25.26	6.83	3.79	0.37	0.281

Table 5. Mechanical properties for 5 mm plate of 2507 super-duplex stainless steel per the material certificates at +20 °C.

		Yield strength		Tensile strength	Elongation	Hardness
		$R_{p.0.2}$ [MPa]	$R_{p.1.0}$ [MPa]	R_m [MPa]	*A5* [%]	*HB*
Set 1	Front	712	801	917	29	285
	Back	715	801	917	29	278
Set 2	Front	716	800	919	33	278
	Back	719	800	922	31	282

The chemical composition is close to its nominal values presented earlier in table 1. The biggest difference is in molybdenum content where the specimen material had 0.2 % less than nominal value. The nominal values are presented in table 2. Yield strength $R_{p0.2}$ and tensile strength R_m are both over 160 MPa better than the nominal values. Elongation is also at least 9 % higher. Differences between two different sets of materials are small.

3.1.2 Weld throat thickness assessment for load carrying joints

For the load carrying joints two different fillet weld sizes are used. The bigger one is calculated so that the weld toe and root have the same fatigue strength in terms of numbers of cycles. The calculations are based on IIW fatigue recommendations structural details 413 and 414. Cruciform joint with fillet welds have the FAT class of 63 for weld toe and 36 MPa for root, respectively (Hobbacher 2014, p. 59). The calculation is based on equation 5. The nominal stress in weld root can be calculated from the equation 18 (Fricke 2011, p. 119):

$$\sigma_{n,w} = \frac{\Delta\sigma_{nom} * t}{2a} \tag{18}$$

, where $\Delta\sigma_{n,w}$ is nominal stress in weld and a is the weld throat thickness. The calculation is presented in appendix 1.

3.2 FE-analysis

FE-analysis was performed by Femap version 11.2.1 with NX Nastran static analysis. Effective notch stress method was used to determine the fatigue strength of joints and comparing with experimental results. The material had a modulus of elasticity of 200 GPa and Poisson's ratio of 0.3. In modeling 20-node solid elements with mid-side nodes were used but also 8 node quadrilateral elements were applied. For the as-welded toe and root a fillet rounding of r = 1mm was used according to IIW recommendations. HiFIT treatment models were rounded according to measurement data in the real test specimens. Welded joints were modeled to have the same height, width and throat thickness as in the test specimens. Fillet weld profile was simplified to be straight and the same side of the specimen which broke in fatigue testing was modeled. Element size was kept smaller than it is required in the literature. The models for butt welded specimen had about 31 000 to 33 000 elements. FAT class of 225 was used to calculate the ENS fatigue strength. FAT class 225 has survival probability of 97.7 % (Fricke 2010, p. 17). Because of the ENS FAT class and nominal stress method FAT classes have survival probability of 95 % or 97.7 % there is a safety factor of 1.37 (Sonsino et al. 2012, p. 7). The conversions from characteristic FAT classes to mean FAT classes for both nominal stress method and ENS method are presented in table 6.

Table 6. The transformation between characteristic FAT classes and mean FAT classes by a safety margin of 1.37.

Method	Nominal stress				ENS
FAT_{char} [MPa]	63	80	90	160	225
FAT_{mean} [MPa]	86	110	123	219	308

Only half of the structure was modeled because the structure is symmetrical and constraints were applied in the symmetry lines. Constraints for the half model was set so that in the thickness direction, z-axis, in symmetry line only translation in the thickness direction is allowed and in the height direction, y-axis, only the translation in the height direction is allowed. Also for the symmetry surface, in the middle of the joint, translation in the loading direction, x-axis, was prevented.

There are two ways of including misalignments in FEM, including axial and angular misalignments in the model or by using stress magnification factor $k_{m,tot}$ (Fricke 2010, p. 15). In this work, axial and angular misalignments were considered by using stress magnification factors. Loading is set to coincide the nominal stress range in the fatigue testing. Loading was set as elemental pressure of 1 MPa normal to elements in the negative x-axis direction. Then the stress concentration factor was multiplied by the fatigue test nominal stress to get ENS stress. In figures 30–33 there is presented an example of a model and elements mesh in the different joint types.

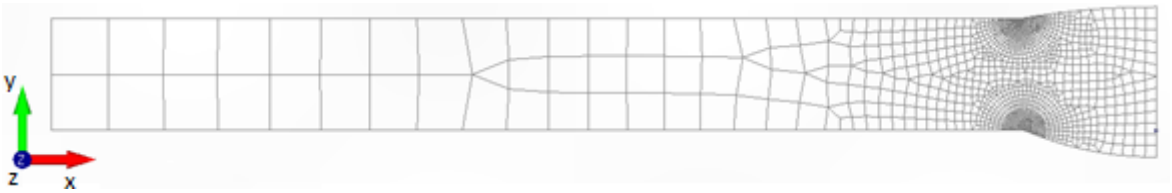

Figure 30. FEM-model side view of butt welded specimens.

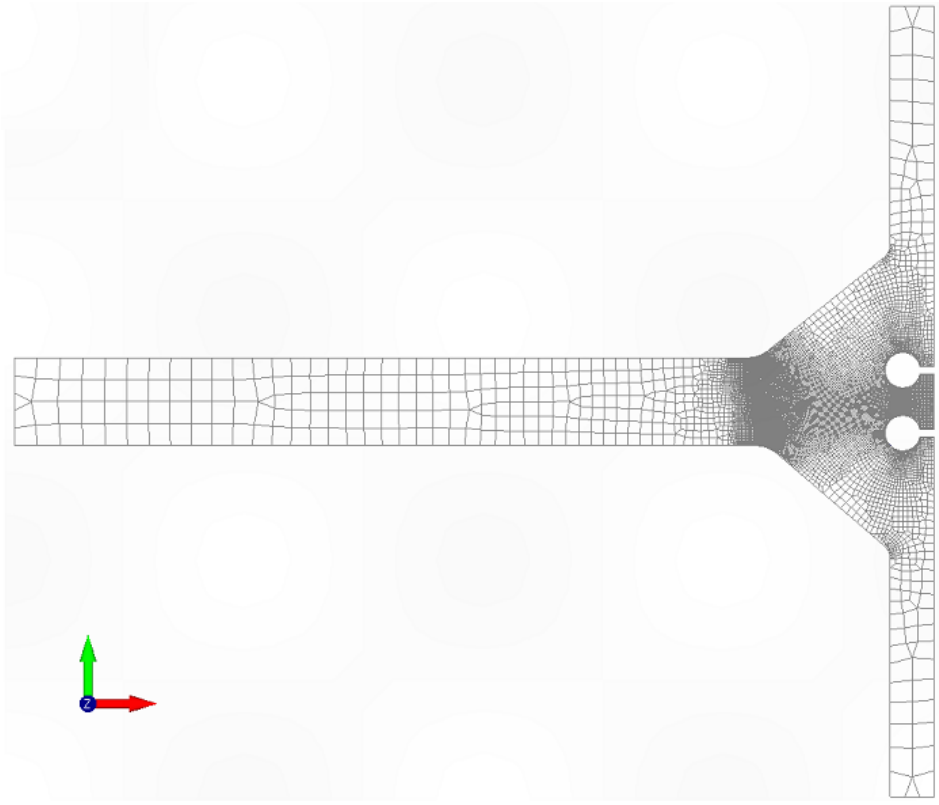

Figure 31. FEM-model side view of non-load carrying specimens.

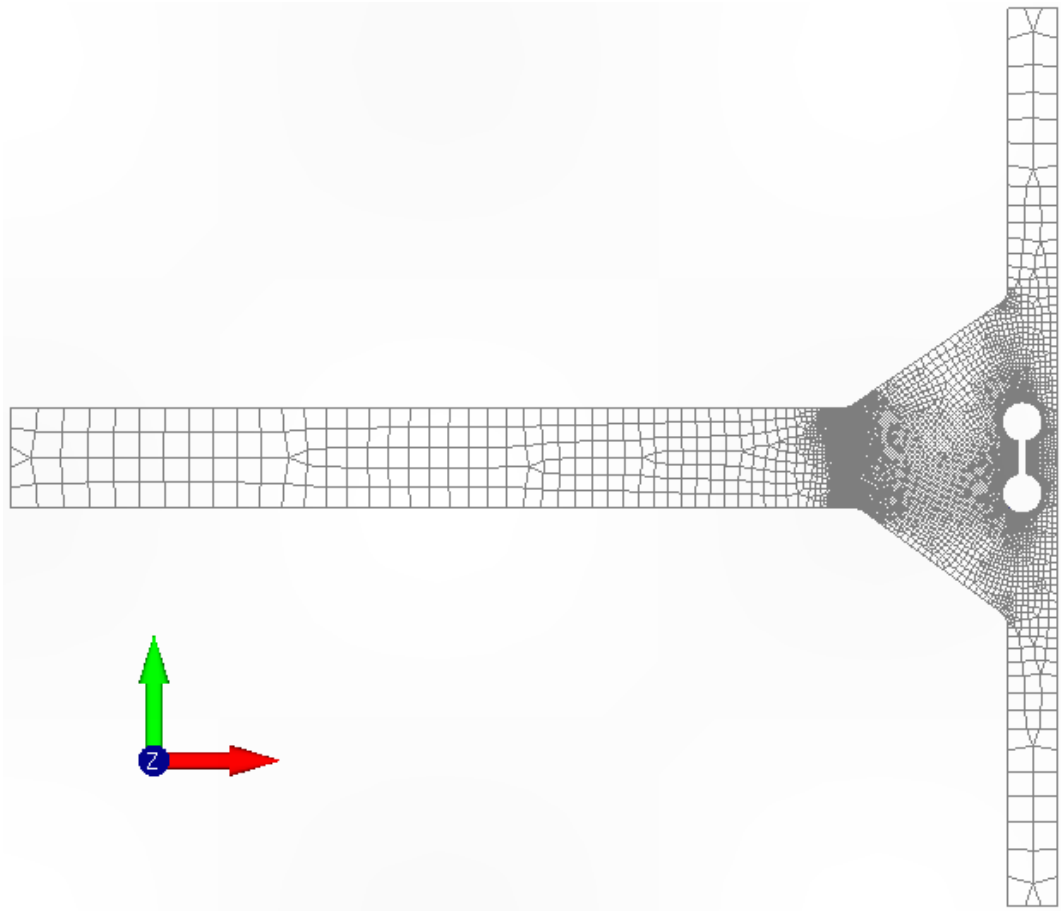

Figure 32. FEM-model side view of the load carrying specimens.

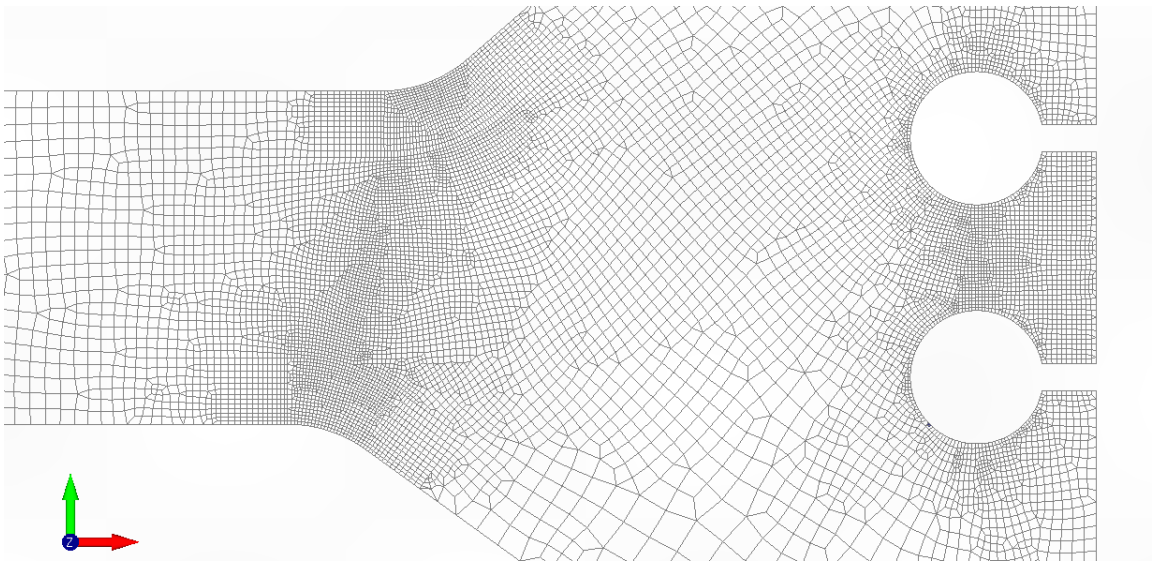

Figure 33. A close-up of smaller elements near the notch radius in the weld toe and weld root.

3.3 Static tests

Static tests were carried out for each joint type but not for HiFIT post-weld treated specimen because the post-weld treatments affect only the fatigue strength. Static tests were performed by LUT steel structures 400 kN test machine. Strain gauges was used for water cut specimen and digital image correlation method, in this study ARAMIS equipment, is utilized during every static test. ARAMIS equipment is based on optical 3D deformation analysis. ARAMIS can be used as a non-contact measuring device to follow 3D coordinates, 3D displacements and velocities, surface strain values and strain rates. ARAMIS follows the small movements of painted points in the specimen by two cameras and generates real-time data. (GOM 2016.) The ARAMIS equipment and 400kN test machine used in a static test for water cut specimen is presented in figure 34. Static testing was carried out by manually controlling the strain in the specimen.

Figure 34. The ARAMIS and 400kN test equipment in static testing.

3.4 Fatigue tests

Fatigue tests were carried out by laboratory of steel structures at LUT, with two different fatigue testing machines 150 kN and 400 kN. During the testing, it was preferred to use R-value of 0.5 rather than 0.1 which means higher mean stresses. However, some R-value 0.1 test was also done as reference points. For the cut edge specimens two different stress levels were used but for welded joint specimen four different stress levels were tested. For the fatigue test results, FAT curves with Matlab were calculated so that they could be compared with the literature results. The characteristic curves were calculated by suggestions in IIW Fatigue Recommendations 2014. The frequency of the fatigue testing was between 4 and 8 Hz.

Fatigue tests were performed for four test specimens in cut edges series and for welded specimen there were six of each type of joint and post-weld treatment. Post-weld treatment HiFIT was applied only for butt welded and non-load carrying specimen. Strain gauges were used in all test specimens. For all specimen, first multiple static tensile loadings from zero strain to the maximum strain were made. They were done until specimen stabilized.

The fatigue test run out limit was set in this work at 5 million cycles if there was not any evidence of specimen breaking in the near future. With these run out specimen, fatigue testing continued with higher loads.

3.5 Shape measurements

All the tested specimens are measured for axial and angular misalignment. From the data, the misalignment of the plate is calculated in degrees and the axial misalignment in millimeters was estimated. The measurements were carried out by LUT steel structures laboratory with laser shape measurement device showed in figure 35. The measurements were made from the middle of the specimen. For the cut edges specimens, the measurement was made from one side for the whole length of the specimen and for the welded specimen for both sides but only for about 50 mm on both sides of the welding joint. Also, the thickness and width of the specimens are measured and marked in the test report.

Figure 35. The laser shape measurement device.

3.6 Residual stress measurements

Duplex steels have a two-phase microstructure of austenitic and ferritic phases. These phases have different thermal expansion rates and mechanical properties. When heat is applied in welding to the material residual stresses, called homogeneous micro stresses, appear between the phases because of temperature changes. Residual stresses can affect the mechanical properties of the material, especially the fatigue properties. There are two common ways of measuring residual stresses: a destructive method such as hole-drilling and nondestructive method such as XRD (x-ray diffraction). XRD is based on measurements of the XRD device on changes of the interplanar lattice spacing because of stress and strain. In this work, there was used Stresstech Xstress G3 device for measuring residual stresses using XRD. The equipment is shown in figure 36. (Lindgren & Lepistö 2002, pp. 279–280.)

Figure 36. The XRD device used to measure residual stresses.

Residual stresses were measured for each cruciform joint type. Measurements were done in the middle of the specimen on 4 points located in weld toe or HiFIT treatment, 2 mm, 4 mm and 6 mm from weld toe. 2 mm is also equal to 0.4*t* which is the location of the strain gauge. Also, the measurements were performed on all four sides A, B, C and D of the specimen. Measurements for non-load carrying, non-load carrying HiFIT treated and load carrying joints were made with 65 seconds shutter time, the maximum angle of tilt to the left 40° and to the right 15° and tilted three on both directions.

4 RESULTS

In this chapter, there are presented the results obtained in the experimental part of this study. The analysis and discussion of the results are presented in the next chapter.

4.1 Shape measurements results

After the shape measurement data were collected, for angular and axial displacement, the total structural stress magnification K_m factor was calculated according to equation 16. $\Delta\sigma_{nom}$ was obtained from the fatigue tests using nominal stress, $\Delta\sigma_{hs}$ *meas* is measured from the specimen using a strain gauge by keeping track of max and min strain in strain gauge and then the difference in MPa could be calculated. Info column tells the side of measurements, the location of the strain gauge which is the expected location of fracture based on shape measurements. For welded structures, the measured hotspot stress was calculated from the equation 8. Since the stress magnification factors are calculated differently of butt welds and cruciform joints the results are presented in two different tables, table 7 for butt welds and cut edges and in table 8 for cruciform joints.

Table 7. The shape measurements and calculated stress for cut edges and butt welds.

Specimen	e [mm]	α [deg]	t [mm]	$K_{m,tot}$	$\Delta\sigma_{nom}$ [MPa]	$\Delta\sigma_{hs}$, *Calc* [MPa]	$\Delta\sigma_{hs}$ *meas* [MPa]	info
SDWC.11	0.00	0.13	5.06	1.07	534	572	546	A/B, A
SDWC.12	0.00	0.05	5.04	1,03	296	306	301	A/B, A
SDWC.51	0.00	0.09	5.05	1.05	337	355	348	A/B. A
SDWC.52	0.00	0.16	5.07	1.09	606	657	646	A/B, A
SDPC.1	0.00	0.72	5.03	1.22	487	594	488	A/B. A
SDPC.2	0.00	0.86	5.04	1.25	540	675	564	A/B. A
SDPC.3	0.00	0.21	5.00	1.08	280	302	269	A/B. A
SDPC.3J	0.00	0.21	5.00	1.08	302	326	313	A/B. A
SDPC.4	0.00	0.88	5.05	1.33	297	396	301	A/B, A
SDBW.1	0.06	0.31	5.06	1.13	402	456	486	A/B, A

Table 7 continues. The shape measurements and calculated stress for cut edges and butt welds.

SDBW.2	0.33	0.34	5.00	1.30	468	610	540	A/B, B
SDBW.3	0.25	0.48	5.05	1.35	251	338	326	A/B, A
SDBW.3J	0.25	0.48	5.05	1.33	317	421	398	A/B, A
SDBW.4	0.17	0.90	5.05	1.44	310	446	359	A/B, A
SDBW.5	0.25	0.26	5.06	1.27	158	201	205	C/D, D
SDBW.5J	0.25	0.26	5.06	1.25	253	317	320	C/D, D
SDBW.6	0.005	0.32	5.05	1.12	300	337	349	A/B, D
SDBW.1H	0.17	0.08	5.04	1.13	408	460	453	C/D, D
SDBW.2H	0.12	0.28	5.06	1.15	550	634	544	A/B, A
SDBW.3H	0.28	1.80	5.06	1.87	271	509	351	A/B, B
SDBW.4H	0.44	0.90	5.03	1.59	327	520	358	A/B, D
SDBW.5H	0.03	0.48	5.02	1.20	297	356	349	A/B, B
SDBW.6H	0.61	0.30	5.05	1.49	229	341	326	A/B, A

For cut edges and butt welded specimens the obtained misalignment total structural stress magnification factor was mostly between 1.03–1.35. Four specimens had higher factors: SDBW.4 with 1.45, SDBW.3H with 1.91, SDBW.4H with 1.60 and SDBW.6H.

Table 8. The shape measurement data and calculated stress for the cruciform joints.

Specimen	e [mm]	α [deg]	t [mm]	$K_{m,\,tot}$	$\Delta\sigma_{nom}$ [Mpa]	$\Delta\sigma_{hs}$, *Calc* [MPa]	$\Delta\sigma_{hs}$ *meas* [MPa]	info
SDNL.1	0.07	0.27	5.04	1.11	399	444	396	C/D, A
SDNL.2	0.05	0.07	5.06	1.05	456	478	493	A/B, A
SDNL.3	0.13	0.09	5.06	1.10	300	331	339	A/B, A
SDNL.4	0.05	0.38	5.06	1.13	268	302	320	A/B, D
SDNL.5	0.06	1.79	5.06	1.50	225	336	299	A/B, B
SDNL.6	0.16	1.55	5.06	1.50	188	281	272	A/B, B
SDNL.1H	0.17	0.44	5.04	1.22	290	543	407	A/B, A
SDNL.2H	0.11	0.80	5.07	1.27	383	488	502	C/D, D

Table 8 continues. The shape measurement data and calculated stress for the cruciform joints.

SDNL.3H	0.01	1.82	5.07	1.47	252	372	327	A/B, A
SDNL.4H	0.02	2.55	5.07	1.67	249	415	330	A/B, B
SDNL.5H	0.03	0.54	5.04	1.16	295	342	295	C/D, A
SDNL.6H	0.01	2.08	5.01	1.55	220	342	282	A/B, A
SDL1.1	0.08	0.69	5.00	1.23	276	338	344	A/B, B
SDL1.2	0.17	0.16	5.05	1.15	474	542	452	A/B, B
SDL1.3	0.17	0.44	5.04	1.22	290	353	346	A/B, A
SDL1.4	0.03	0.26	5.06	1.08	303	328	324	C/D, C
SDL1.5	0.41	2.16	5.05	1.80	188	340	304	A/B, A
SDL1.6	0.01	3.26	5.02	1.86	153	283	272	A/B, A

Non-load carrying joints in the as-welded and HiFIT treated conditions had a total structural stress magnification factors of 1.05–1.67. Load carrying joints had the total structural stress magnification factor between 1.08 and 1.86 with four specimens under 1.25 and two over 1.80.

For the different cutting methods, the surface roughness arithmetic average *Ra* and maximum difference between highest peak and lowest valley *Rz* was measured. These results are presented in table 9.

Table 9. The surface roughness measurement results.

Cutting method:	*Ra* [µm]	*Rz* [µm]
Water cutting	4.07	24.9
Plasma cutting	2.23	8.26
Laser cutting	5.96	15.38

4.2 Static test results

Static test results are presented in figure 37 and table 10. Ultimate strength was calculated with maximum force and measured area of the specimen before testing.

Table 10. Results from static tests.

Specimen	Ultimate strength [MPa]	Max Force [kN]	Maximum elongation [mm]	Info
SDWCS1	871	175.29	59.1	Broke from base material
SDBWS1	878	176.76	54.8	Broke from base material
SDNLS1	877	176.27	54.2	Broke from base material
SDL1S1	903	182.13	52.7	Broke from base material
SDL2S1	867	174.32	53.4	Broke from base material

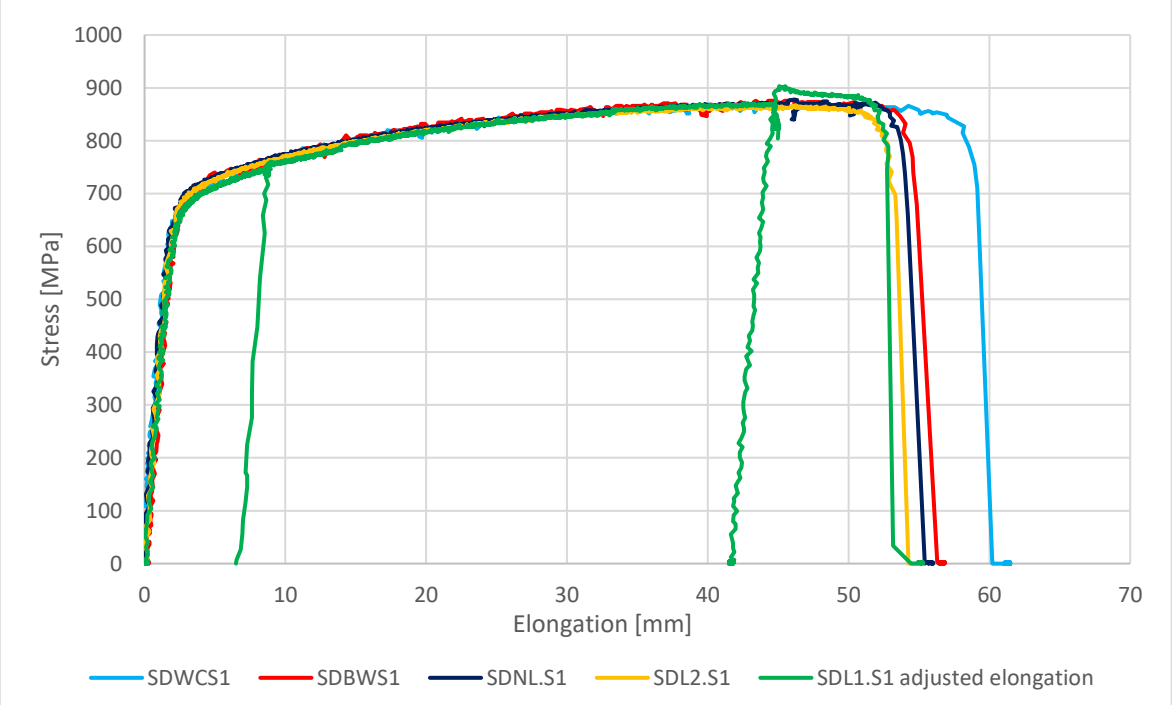

Figure 37. The stress strain curves from static tests.

Static tests showed very similar results on all tested specimens. All specimens had ultimate tensile strength of 870–900 MPa. The lowest result was with the load carrying joint with the smallest throat thickness of nominal 3 mm and the highest ultimate strength was with load carrying joint with bigger weld throat thickness. The load carrying test specimen SDL1.S1 static testing was restarted twice because the deformation limit was set too low in the test equipment. Therefore, the result is a combination of three different tests on one specimen.

Testing speed was about 3 mm/min. The calculated modulus of elasticity from the water cut specimen is 204 GPa. This was calculated by the means of measured force and strain gauge data. All the specimens broke at the base material about 60 mm from the weld. In figure 38 there is shown the breaking point in a non-load carrying joint.

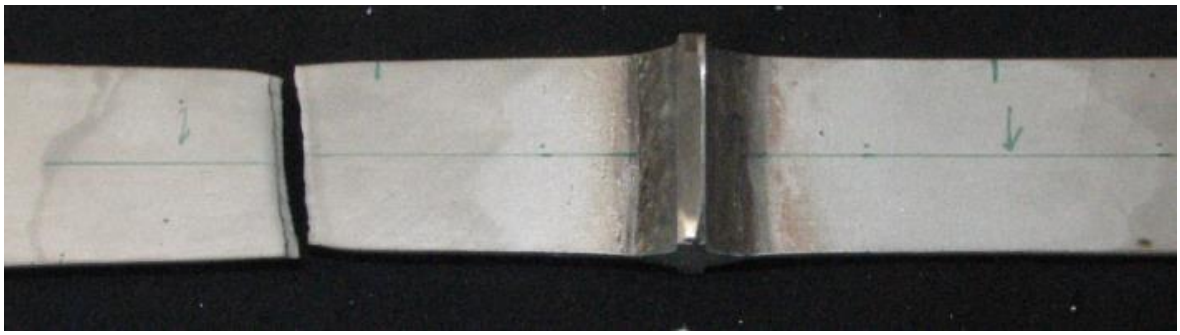

Figure 38. The breaking point of non-load carrying specimen SDNL.S1.

4.3 Fatigue test results

Fatigue test results are shown in the S-N curve, where are FAT curves from IIW recommendations for each joint detail and for the fatigue testing results there are calculated FAT_{mean} and FAT_{char} curves. FAT_{mean} and FAT_{char} characteristic curves mean survival probability of 50 % and 95 % respectively. Fatigue results are calculated using stress values obtained from the measured maximum and minimum force by using equation 3. In figures 39 and 40, there are presented all the fatigue data points. In table 11 there are explanations for the names of figures 39–50. In tables 12–14 there are numerical values from the fatigue tests and in tables 15–18 there are summarized the FAT values in nominal stress if not otherwise notified. $\Delta\sigma, structural$ includes the structural misalignments and angular effects. This is to represent the actual stress range which is located at the weld toe where the crack initiated.

Table 11. The explanations of the specimen names.

Specimen name part:	Explanation:
R 0.1	*R*-value 0.1
R 0.5	*R*-value 0.5
HiFIT	HiFIT treated specimen
SDWC	Water cut edges
SDPC	Underwater plasma cut edges
SDBW	Butt welded specimen
SDNL	Non-load carrying specimen
SDL1	Load carrying specimen with bigger weld throat thickness

Figure 40. The combined S-N curve for all fatigue test results with nominal stress.

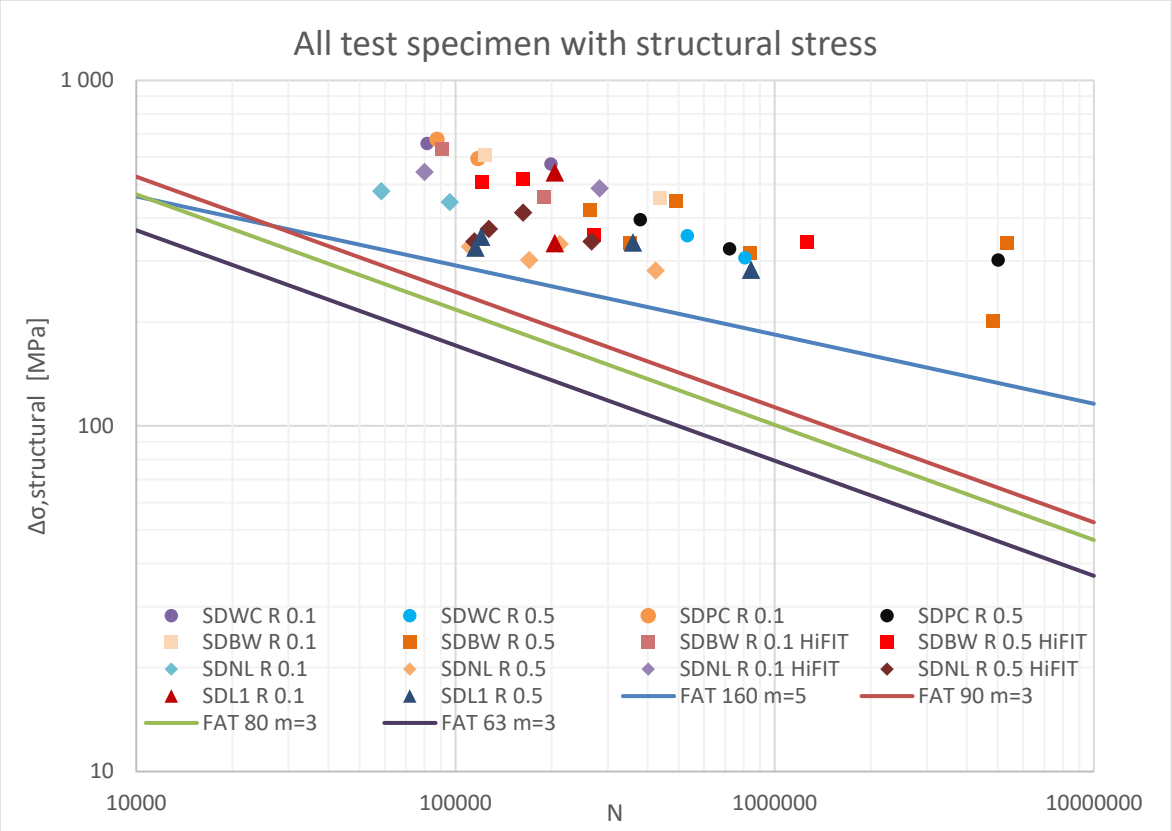

Figure 39. The fatigue results with axial and angular misalignment taken into account.

Table 12. The numerical results of the cut specimen from fatigue testing.

Specimen	R-value	σ_{max} [MPa]	σ_{min} [MPa]	$\Delta\sigma_{nom}$ [MPa]	N	$FAT_{50\%}$ m=3	$FAT_{50\%}$ m = 5	Comments
SDWC.11	0.08	592	49	543	199004	252	342	-
SDWC.12	0.49	583	285	296	806455	219	247	Broke from lower clamp
SDWC.51	0.47	642	302	337	532346	217	259	-
SDWC.52	0.04	644	27	646	81511	222	340	-
SDPC.1	0.10	541	53	487	117468	189	276	-
SDPC.2	0.11	604	63	540	87470	190	289	-
SDPC.3	0.49	553	273	280	5008821	380	336	Runout
SDPC.3J	0.54	652	302	302	722264	215	246	Broke from grinded area
SDPC.4	0.55	655	358	297	378 955	171	213	-

Table 13. The numerical results of butt welded specimen from fatigue testing.

Specimen	R-value	σ_{max} [MPa]	σ_{min} [MPa]	$\Delta\sigma_{nom}$ [MPa]	N	$FAT_{50\%}$ m=3	$FAT_{50\%}$ m = 5	Breaking point
SDBW.1	0.11	449	47	402	438935	242	296	A-side
SDBW.2	0.09	516	48	468	123405	185	268	C-side
SDBW.3	0.49	498	246	251	5 367 862	349	306	Unbroken, runout
SDBW.3J	0.48	608	292	317	263186	161	211	A-side
SDBW.4	0.48	598	288	310	489366	194	234	C-side
SDBW.5	0.49	311	154	158	4833103	212	188	Unbroken, runout
SDBW.5J	0.50	503	250	253	836130	189	212	Crack initiated from B side
SDBW.6	0.50	600	299	301	352648	169	212	Crack initiated from C side
SDBW.1H	0.09	460	42	418	189377	190	261	D-side HiFIT
SDBW.2H	0.08	601	51	550	90954	196	296	B-side, HiFIT
SDBW.3H	0.46	505	233	271	120951	107	155	Crack initiated from B-side HiFIT
SDBW.4H	0.44	588	261	327	162664	142	198	A-side, HiFIT
SDBW.5H	0.51	608	310	297	270407	153	199	Crack initiated from B side HiFIT
SDBW.6H	0.49	453	224	229	1 265 620	196	209	D-side, HiFIT

Table 14. The numerical results of cruciform joint type specimens in fatigue testing.

Specimen	R-value	σ_{max} [MPa]	σ_{min} [MPa]	$\Delta\sigma_{nom}$ [MPa]	N	$FAT_{50\%}$ m=3	$FAT_{50\%}$ m=5	Breaking point
SDNL.1	0.12	453	53	399	95 966	145	218	D-side weld toe
SDNL.2	0.10	508	52	456	58 500	141	225	C-side weld toe
SDNL.3	0.52	630	330	300	111033	114	168	D-side weld toe
SDNL.4	0.51	549	281	268	170129	118	164	C-side weld toe
SDNL.5	0.46	418	193	225	211655	106	143	A-side weld toe
SDNL.6	0.46	350	162	188	423383	112	138	B-side weld toe
SDNL.1H	0.13	494	65	429	79 955	147	225	C-side HiFIT
SDNL.2H	0.08	417	34	383	282979	200	259	D-side HiFIT
SDNL.3H	0.50	504	252	252	127284	101	145	A-side HiFIT
SDNL.4H	0.46	463	214	249	162978	108	151	A-side HiFIT
SDNL.5H	0.52	620	325	295	114702	114	166	C-side HiFIT
SDNL.6H	0.46	405	185	220	267126	113	147	A-side HiFIT
SDL1.1	0.09	304	28	276	204886	129	175	A/C root
SDL1.2	0.09	518	45	474	204891	222	300	A/C root
SDL1.3	0.50	581	290	290	120457	114	166	B/D root
SDL1.4	0.50	606	303	303	115329	117	171	A/C root
SDL1.5	0.45	346	157	188	359833	106	134	A-side weld toe
SDL1.6	0.44	274	121	153	843377	114	128	B-side weld toe

The fatigue testing results are also shown in their own S-N curves for each joint type. There are also presented the IIW recommended FAT class for the relevant joint type. These are shown in figures 41–42, 44–45 and 47–50. Different FAT classes calculated from the results are available in appendix III, where is calculated the characteristic curves and the suitable slope of the curve. Run out specimens are marked with a short line.

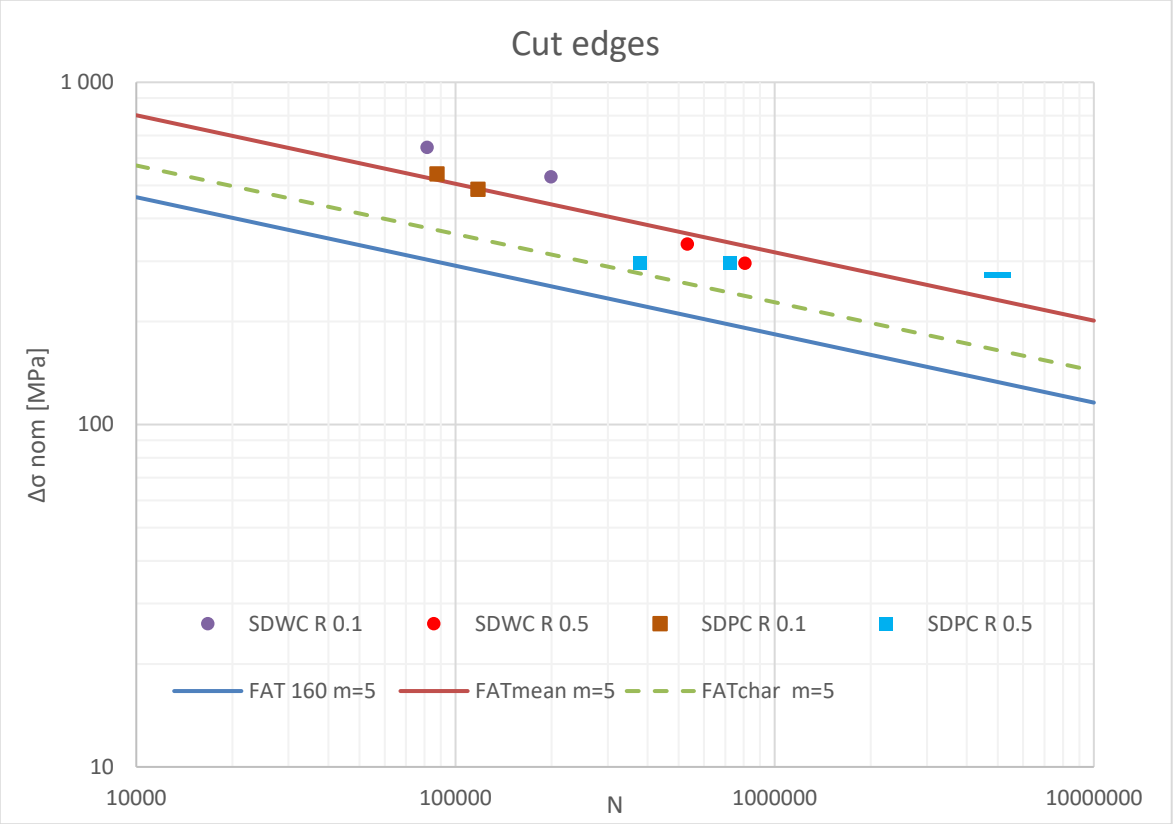

Figure 41. The S-N curve for cut edges with nominal stress

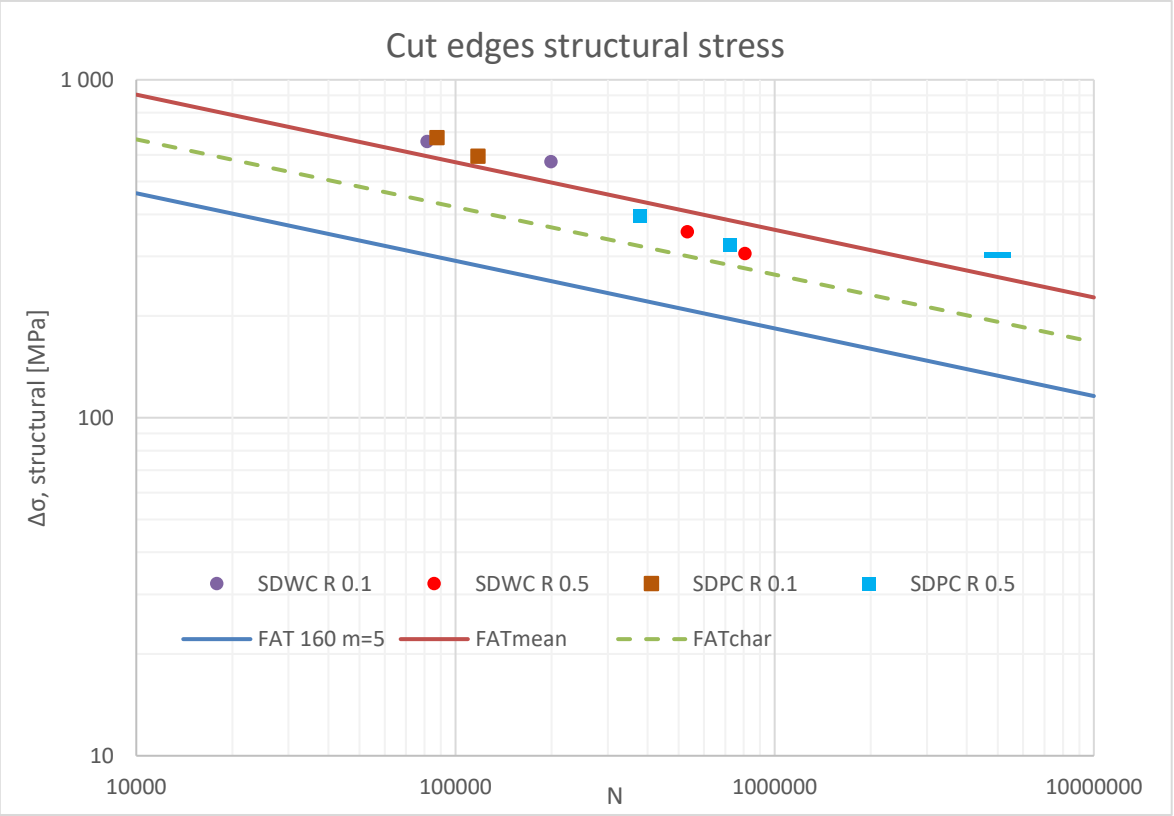

Figure 42. The S-N curve for cut edges with structural stress

Table 15. Summary of the fatigue test results for cut edges specimens.

	Water cut specimens [MPa]	Plasma cut specimens [MPa]	All cut edges specimens [MPa]	All cut edges with structural stress [MPa]
FAT_{mean} m=5	294	267	278	313
FAT_{char} m=5	195	183	198	230
m calculated	2.70	4.40	3.49	3.55
FAT_{mean} with m calculated	212, $m = 2.70$	256, $m = 4.40$	239, $m = 3.49$	282, $m = 3.55$
FAT_{char} with m calculated	181, $m = 2.70$	168, $m = 4.40$	163, $m = 3.49$	198, $m = 3.55$

Plasma cut specimen SDPC.3 fatigue testing was stopped as run out result and continued with higher loads. Specimens SDWC.12 and SDPC.3J broke from the little wider grinded area of the baud curve. This is shown in figure 43. The surface finishes were shown in figure 24. The underwater plasma cut specimens had the roughest edge whereas water cut had a smoother matt finish. Laser cutting had smoother edges than plasma cutting. Laser cut specimen edges were not tested as the edges were polished.

Figure 43. The location of fracture in SDPC.3J was in grinded are of baud curve.

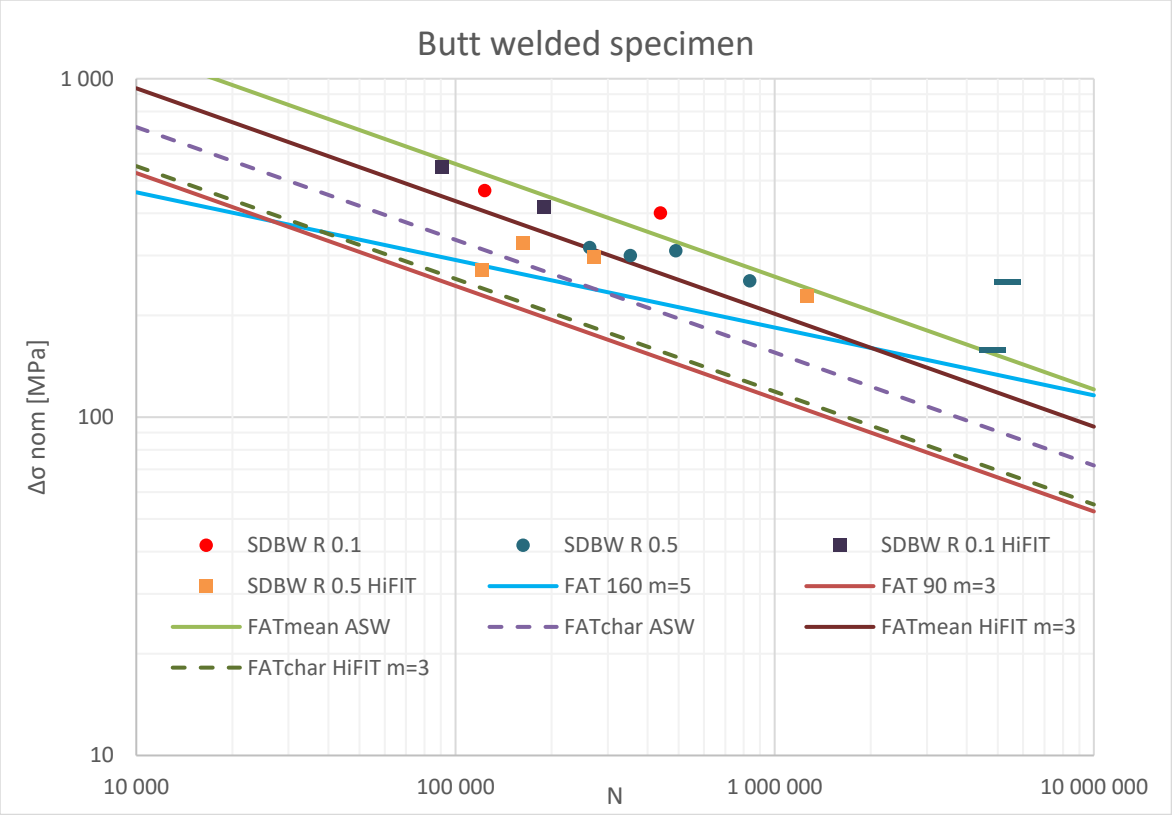

Figure 44. The S-N curve for as-welded and HiFIT treated butt welded specimen.

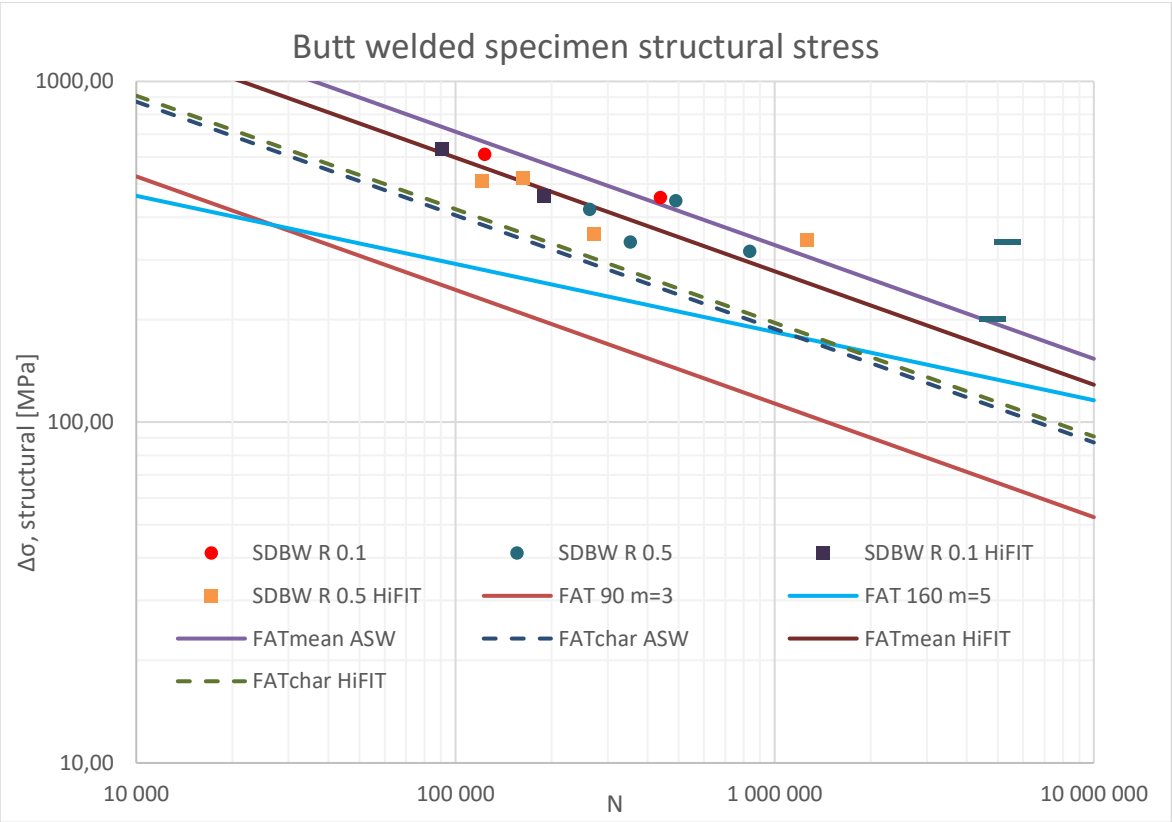

Figure 45. The S-N curve for butt welded specimen with structural stress.

Table 16. Summary of the fatigue test results for butt welded specimens.

	Butt welded [MPa]	Butt welded HiFIT [MPa]	Butt welded structural [MPa]	Butt welded HiFIT structural [MPa]
FAT_{mean} m=3	206	160	262	220
FAT_{char} m=3	123	94	149	155
m calculated	3.44	2.07	3.28	3.38
FAT_{mean} with m calculated	216, m = 3.44	155, m = 2.07	271, m = 3.28	239, m = 3.38
FAT_{char} with m calculated	139, m = 3.44	57, m = 2.07	162, m = 3.28	176, m = 3.38

Tests with specimens SDBW.3 and SDBW.5 were stopped as run-outs results and continued with higher loads. All the specimens broke from the weld toe or HiFIT treated area. In figure 46 is shown the location of fracture which was found in all HiFIT treated specimen. In appendix V there are more figures of HiFIT treatment.

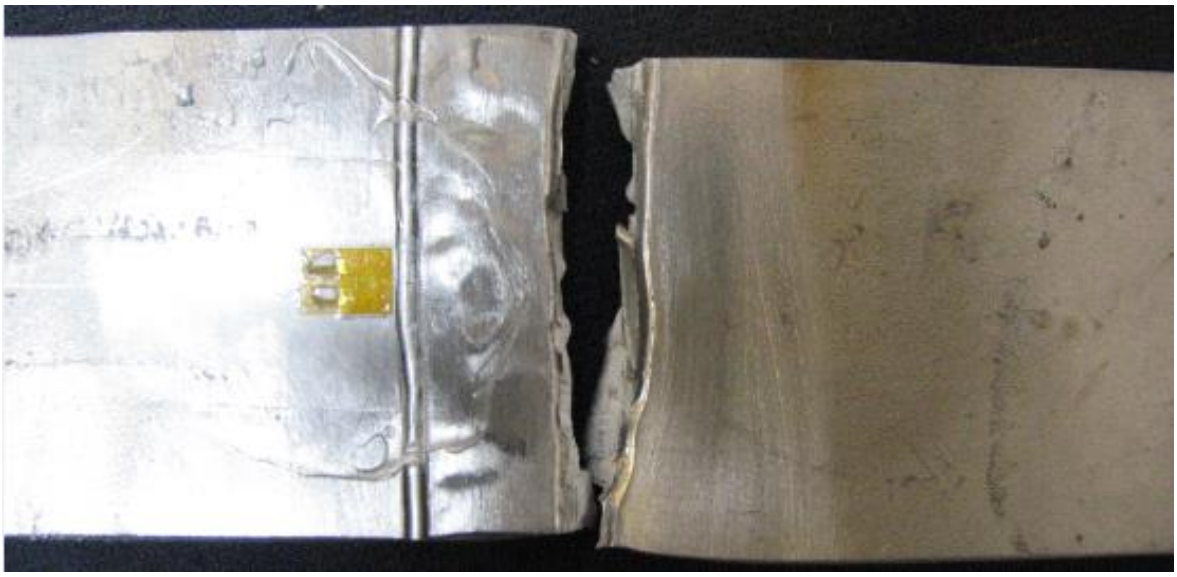

Figure 46. The SDBW.2H and other butt welded HiFIT treated specimens broke from the HiFIT treated area.

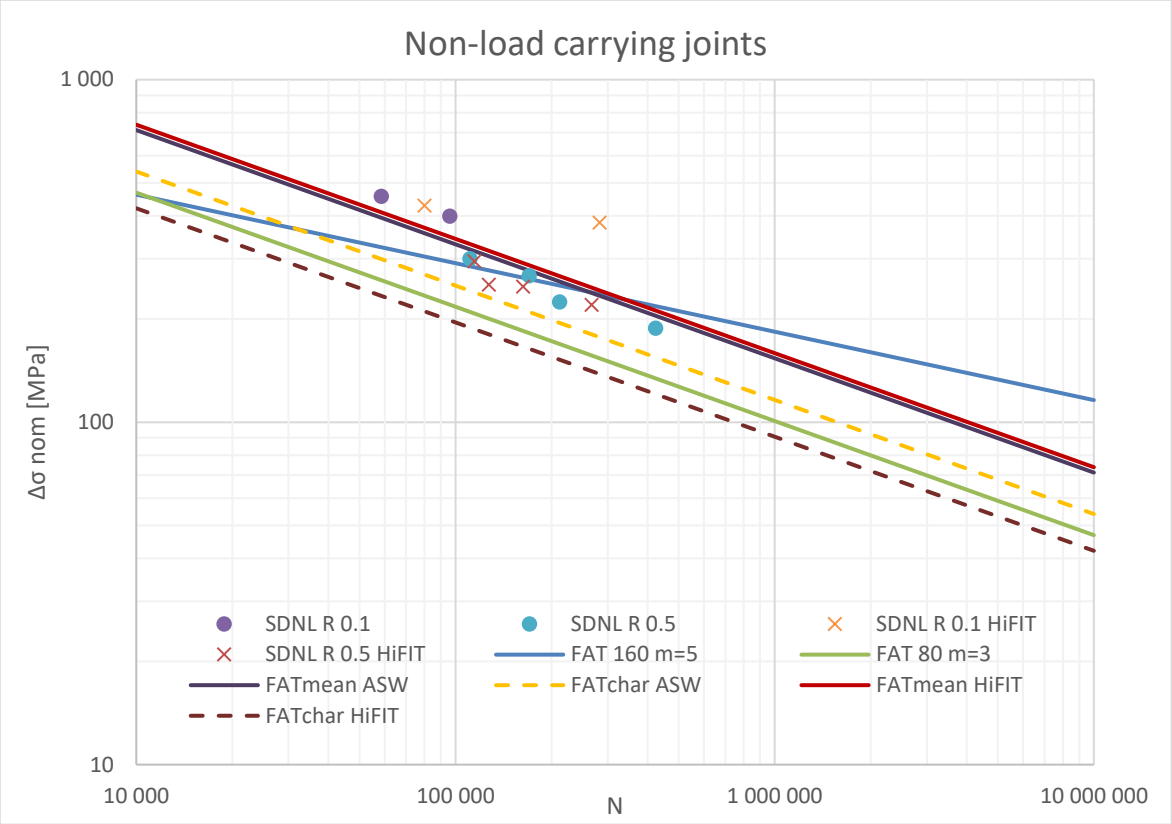

Figure 47. The S-N curve for non-load carrying joints

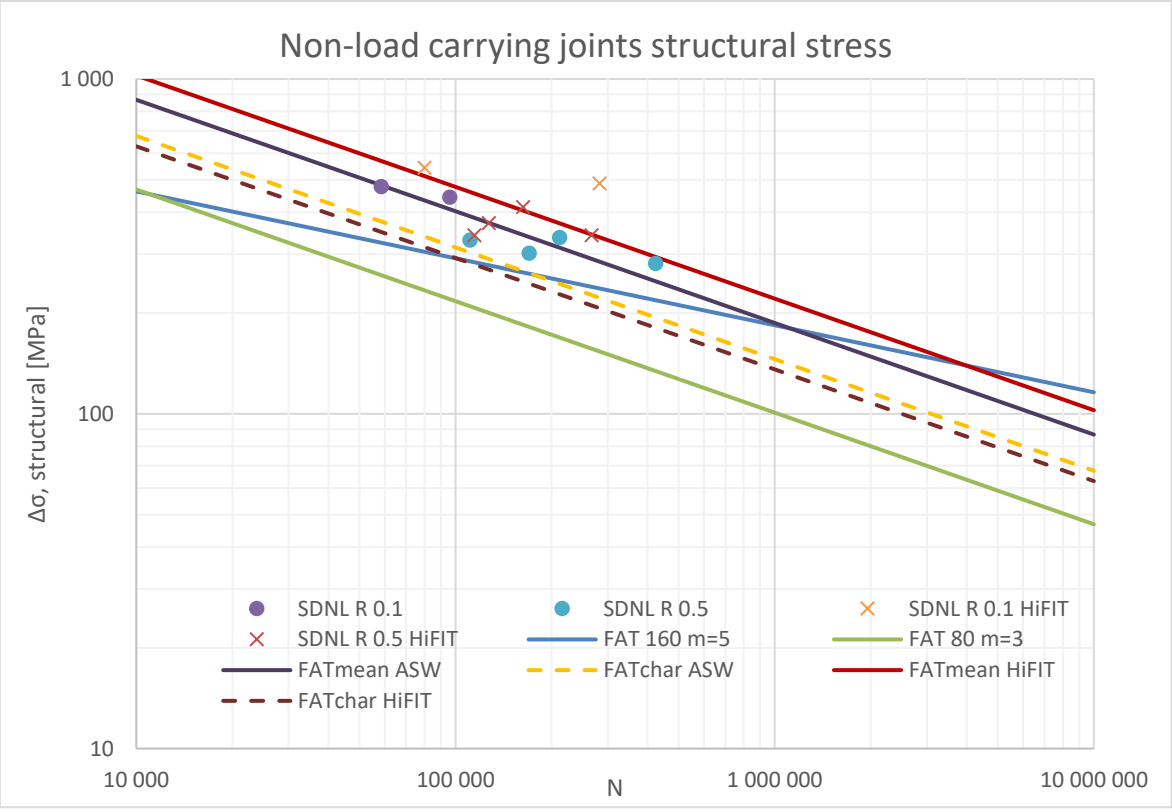

Figure 48. The S-N curve for non-load carrying joints with structural stress

Table 17. Summary of the fatigue test results for non-load carrying specimens.

	Non-load carrying [MPa]	Non-load carrying HiFIT [MPa]	Non-load carrying structural [MPa]	Non-load carrying HiFIT structural [MPa]
FAT_{mean} m=3	122	126	148	175
FAT_{char} m=3	92	72	116	108
m calculated	1.98	0.65	2.85	0.57
FAT_{mean} with m calculated	78, *m = 1.98*	6, *m = 0.65*	140, *m = 2.85*	4.7, *m = 0.57*
FAT_{char} with m calculated	64, *m = 1.98*	1.3, *m = 0.65*	108, *m = 2.85*	0.3, *m = 0.57*

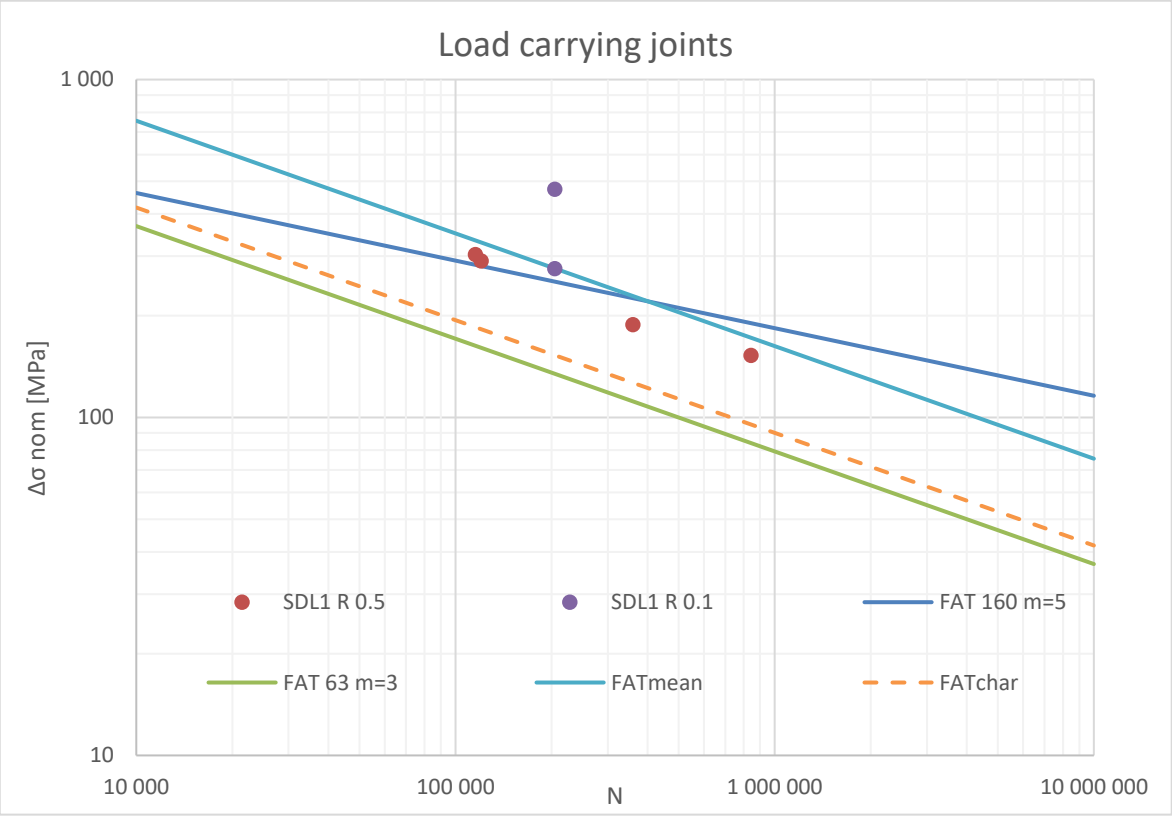

Figure 49. The S-N curve for Load carrying joints.

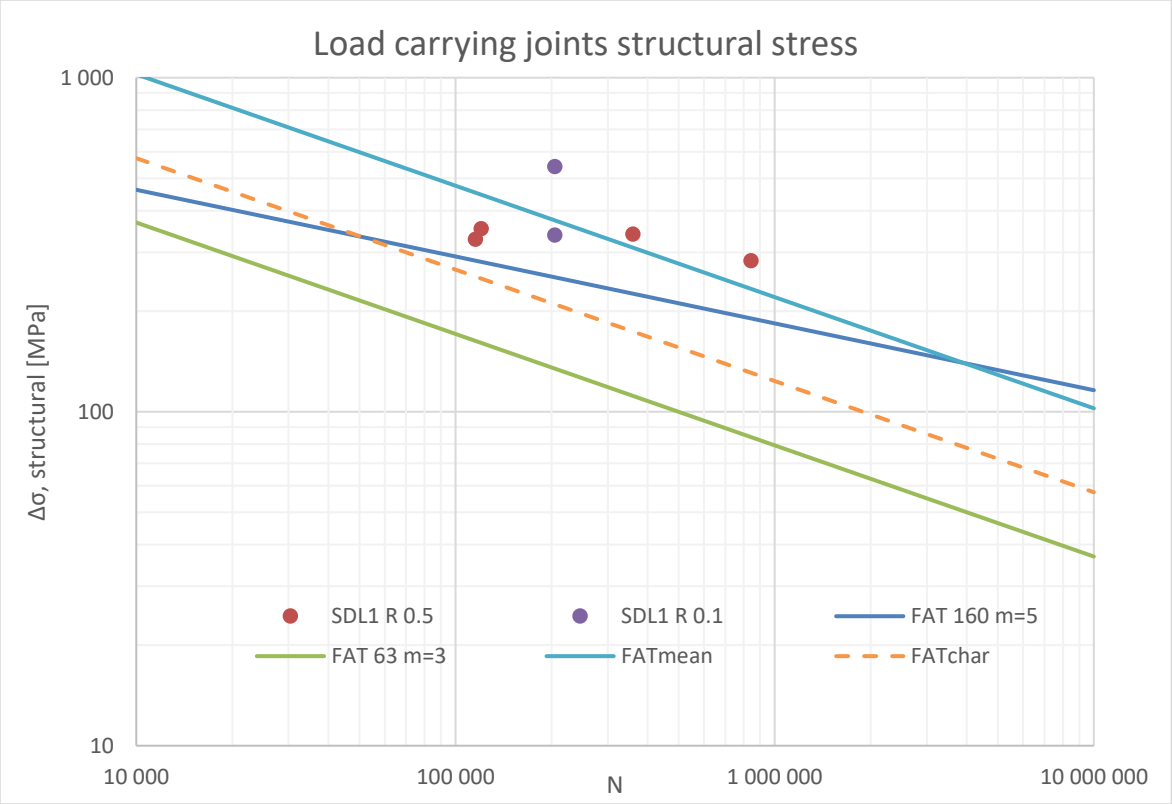

Figure 50. The S-N curve for load carrying joints with structural stress.

Table 18. Summary of the fatigue test results for load carrying specimens.

	Load carrying [MPa]	Load carrying structural [MPa]
FAT_{mean} m=3	129	175
FAT_{char} m=3	71	98
m calculated	1.39	1.24
FAT_{mean} with m calculated	57, m = 1.39	64, m = 1.24
FAT_{char} with m calculated	26, m = 1.39	19, m = 1.24

Four of the six specimens broke from the root of the weld and only SDL1.5 and SDL1.6 broke from the weld toe.

4.4 FE-analysis results

Maximum principle stress and the relevant FAT_{mean} class of 308 MPa was used in FE-analysis. The loading in FE-analysis is the same as nominal stress range in fatigue testing. The used loading, misalignment factor from shape measurements, combined ENS stress, fatigue strength by means of ENS method and fatigue testing and a comparison between tested real fatigue strength and ENS method are presented in table 19.

Table 19. FEM results using FAT class of 308 MPa with 50 % survival probability.

Specimen	$\Delta\sigma_{nom}$ MPa	σ_{ENS} MPa	*Km*	σ_{ENS} *Km MPa	N_{ENS}	*N* fatigue test	$FAT_{50\ \%,\ ENS,\ real}$	$FAT_{ENS,\ real}/FAT_{ENS}$ [%]
SDBW.1	402	694	1.13	787	119 673	438 935	475	154
SDBW.2	468	783	1.30	1 021	54 964	123 105	403	131
SDBW.3	251	416	1.35	560	333 531	5 367 862	778	252
SDBW.3J	317	525	1.33	697	172 380	263 186	355	115
SDBW.4	310	510	1.44	734	147 908	489 366	459	149
SDBW.5	158	281	1.27	358	1 272 086	4 833 103	481	156
SDBW.5J	253	450	1.25	564	325 204	836 130	422	137
SDBW.6	300	498	1.12	559	334 323	352 648	314	102
SDBW.1H	408	695	1.13	784	121 103	189377	357	116
SDBW.2H	550	869	1.15	1 003	57 970	90 954	358	116
SDBW.3H	271	478	1.87	895	81 427	120 951	351	114
SDBW.4H	327	526	1.59	836	99 939	162 664	362	118
SDBW.5H	297	513	1.20	615	251 206	270 407	316	102
SDBW.6H	229	374	1.49	557	337 567	1 265 620	478	155
SDNL.1	399	895	1.11	996	59 163	95 966	362	117
SDNL.2	456	975	1.05	1 020	55 007	58 500	314	102
SDNL.3	300	718	1.10	873	87 942	111033	333	108
SDNL.4	268	571	1.13	644	218 894	170 129	283	92
SDNL.5	225	539	1.50	806	111 771	211 655	381	124

Table 19 continues. FEM results using FAT class of 308 MPa with 50 % survival probability.

SDNL.6	188	399	1.50	597	274 279	423 383	356	116
SDNL.1H	429	773	1.27	980	62 126	79 955	330	109
SDNL.2H	383	645	1.27	821	105 430	282 979	428	139
SDNL.3H	252	437	1.47	644	218 684	127 284	257	83
SDNL.4H	249	466	1.67	777	124 736	162 978	337	109
SDNL.5H	295	492	1.16	572	313 035	114 702	220	72
SDNL.6H	220	360	1.55	560	332 673	267 126	286	93
SDL1.1	276	643	1.23	790	118 629	204 886	370	120
SDL1.2	474	1070	1.15	1 225	31 812	204 891	573	186
SDL1.3	290	688	1.22	836	100 027	120 457	328	106
SDL1.4	303	670	1.08	725	153 094	115 329	280	91
SDL1.5	188	423	1.80	764	131 187	359 833	431	140
SDL1.6	153	345	1.86	640	222 700	843 377	480	156

FEM results suggested lower fatigue strength in all but five cases. With the butt welded specimens the average model had 37 % higher calculated ENS FAT_{mean} class based on fatigue testing strength and the cruciform joints had 15 % higher.

4.5 Hardness measurements and microstructure

Hardness tests results from 2507 welded specimens are summarized in table 20. The BM (base material) test is made by macrohardness with 5 kg (HV5) and detailed tests from HAZ and weld area is made by 100 grams (HV0.1). Also, the hardness was previously measured separately for the austenite and ferrite phases in 2507 stainless steel. Hardness measurements were carried by Outotec. The different areas of measurement points, base material, HAZ, weld and HiFIT, were estimated from the microstructure pictures. Also, there were made additional test to the fusion line of the cruciform joints.

Table 20. The hardness results in a summary from a butt weld on 2507.

Specimen design	Hardness [HV5] BM	Micro-hardness [HV0.1] BM	Micro-hardness [HV0.1] HAZ	Micro-hardness [HV0.1] Weld	Micro-hardness [HV0.1] BM, austenite	Micro-hardness [HV0.1] BM, ferrite	Micro-hardness [HV0.1] Near, HiFIT
Previous tests	290±7	290±12	290±14	280±12	320±10	300±10	-
Butt weld	289±12	330±20	324±8	329±15	-	-	-
Butt weld HiFIT	276±8	363±40	396±30	398±90	-	-	431±20
Non-load carrying	288±13	294±14	298±15	302±20	-	-	-
Non-load carrying HiFIT	276±21	366±40	388±7	378±30	-	-	407±34
Load carrying	279±20	294±23	289±21	302±27	-	-	-

Macrohardness measurements for different as-welded and HiFIT treated specimens are presented in figures 51–55. Also, the profiles of welds are shown in the same figures. In figure 56 there is combined microhardness measurements for butt weld specimen. For the rest of specimens, the microhardness measurement figures are shown in appendix V. In butt welded specimen in as-welded and HiFIT treated condition, there was found some sigma phase about 2 mm from HAZ to the main plate. This is shown in figure 57.

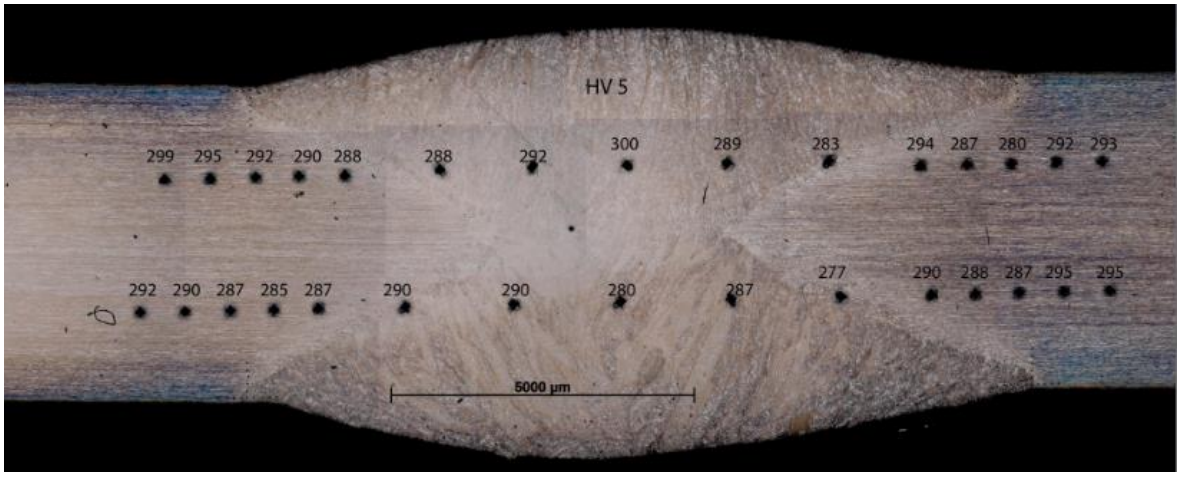

Figure 51. Macrohardness measurements and weld profile for a butt weld.

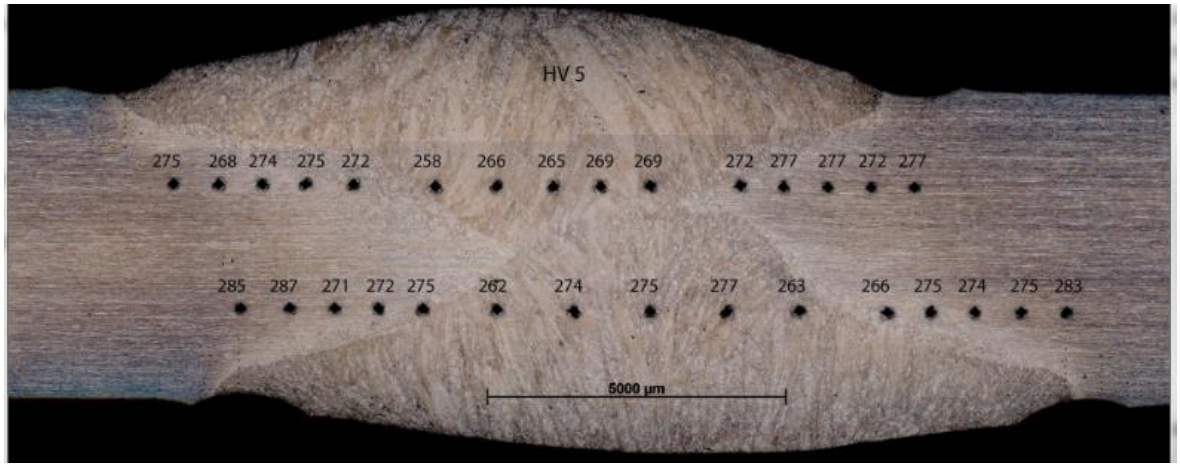

Figure 52. Macrohardness measurements and weld profile for HiFIT treated butt weld.

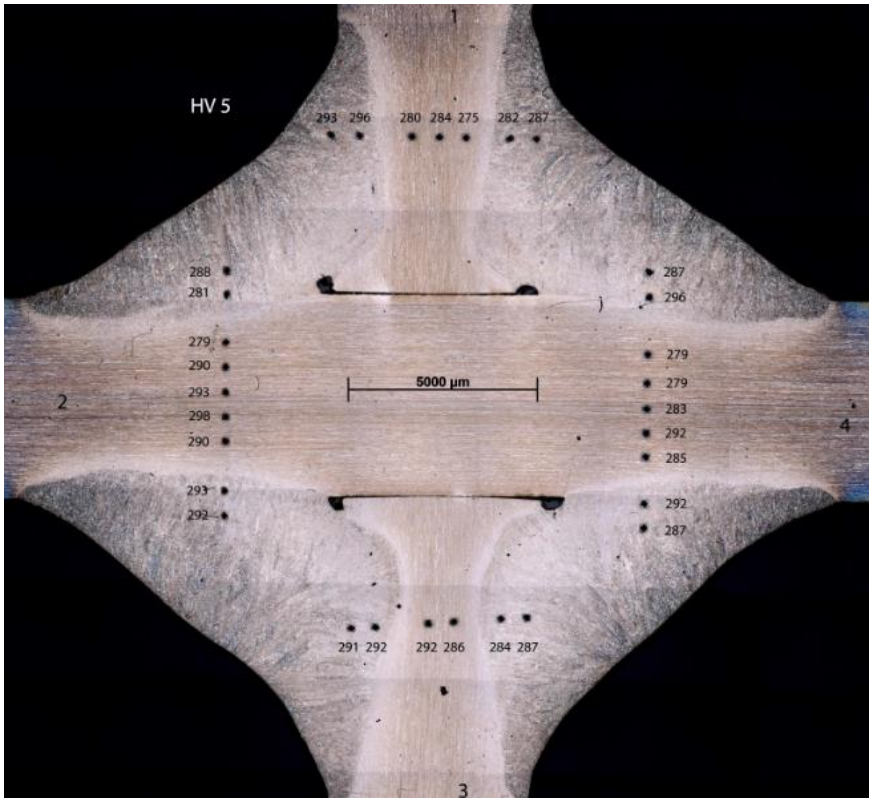

Figure 53. Macrohardness measurements and weld profile for non-load carrying joint.

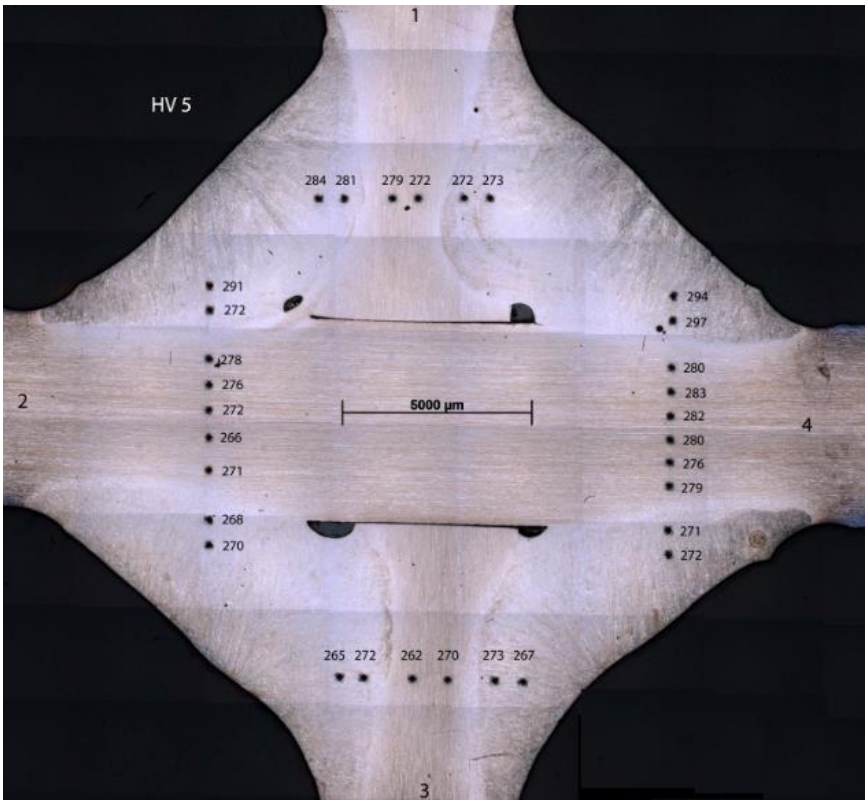

Figure 54. Macrohardness measurements and weld profile for non-load carrying HiFIT treated joints.

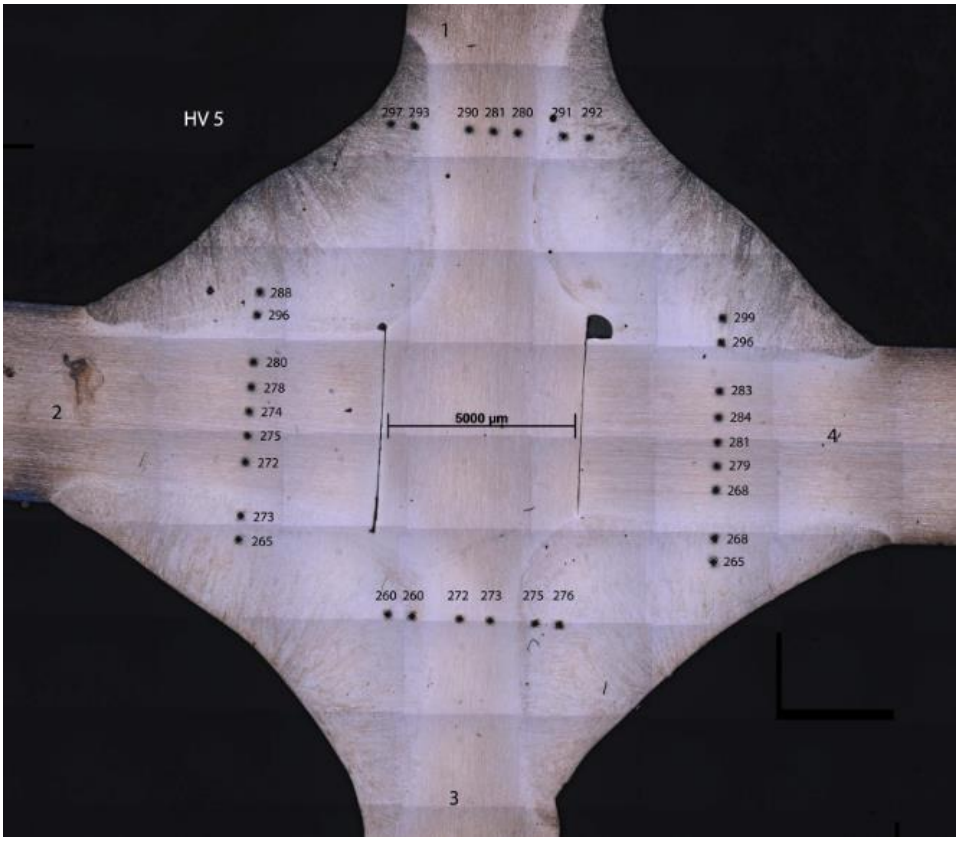

Figure 55. Macrohardness measurements and weld profile for load carrying joint.

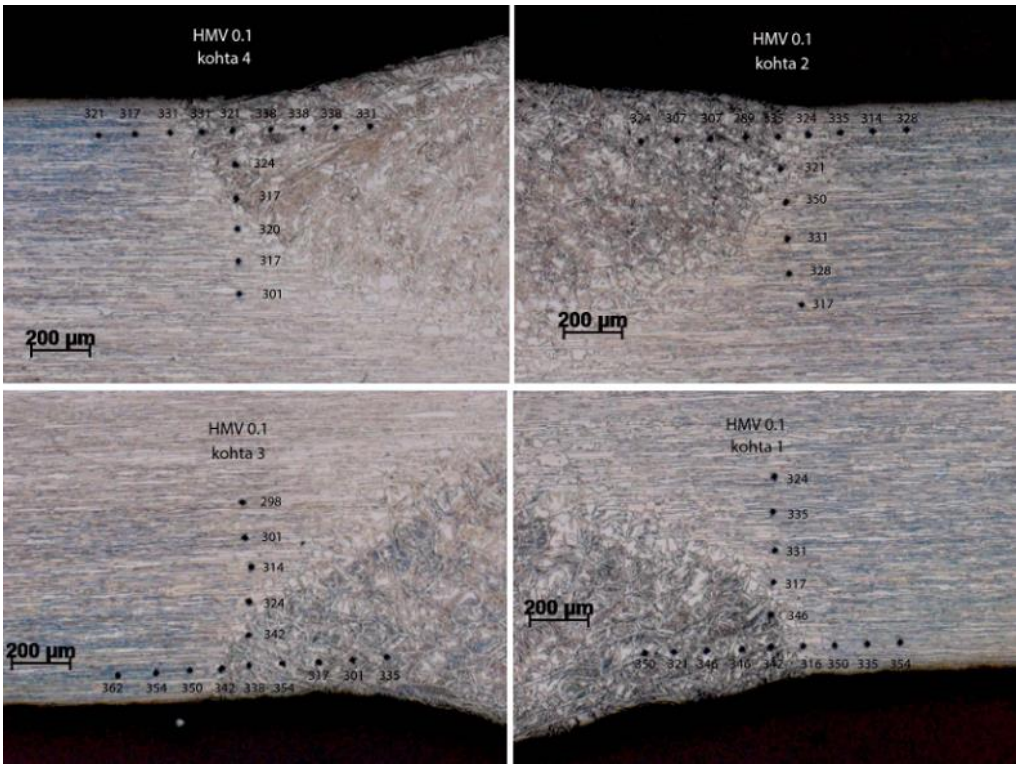

Figure 56. Microhardness measurements in the welding and HAZ area in butt welded 2507 specimen.

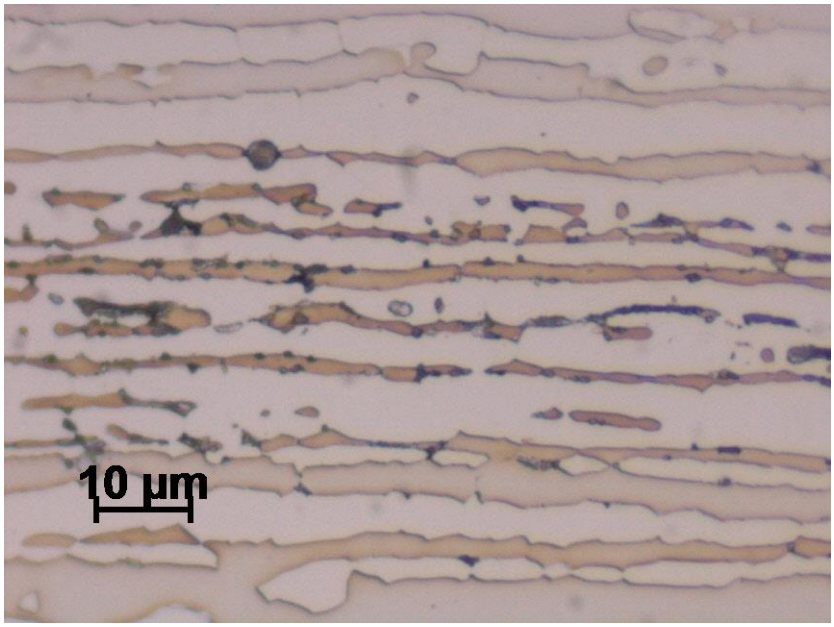

Figure 57. Sigma phase found in material about 2 mm from HAZ to the plate.

In figure 58 a close-up picture of HiFIT treatment in butt welded specimen is shown. From the figure, we can see that the HiFIT treatment makes a bump in base material next to the HiFIT treatment. More weld profile pictures are in appendix V.

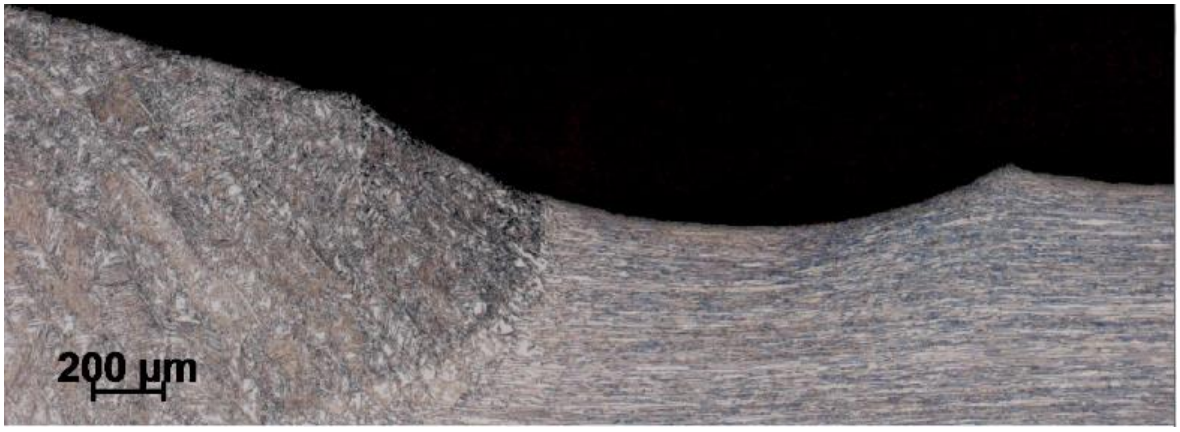

Figure 58. Close-up from butt welded specimen HiFIT treatment.

4.5.1 Scanning electron microscopy examination and welding quality

A couple of fatigue tested specimens was sent in Outotec to be examined more closely. In non-load carrying specimen SDNL.3 there was found several initiation sites and from some of the assumed initiation sites, there was found some small oxide/nitride inclusion. Also, secondary cracks at the austenite and ferrite phase boundaries existed. In non-load carrying

HiFIT treated specimen SDNL.5H crack initiation was found on many different locations. The edge was filled with small inclusions. One large initiations site was found which is shown in figure 59.

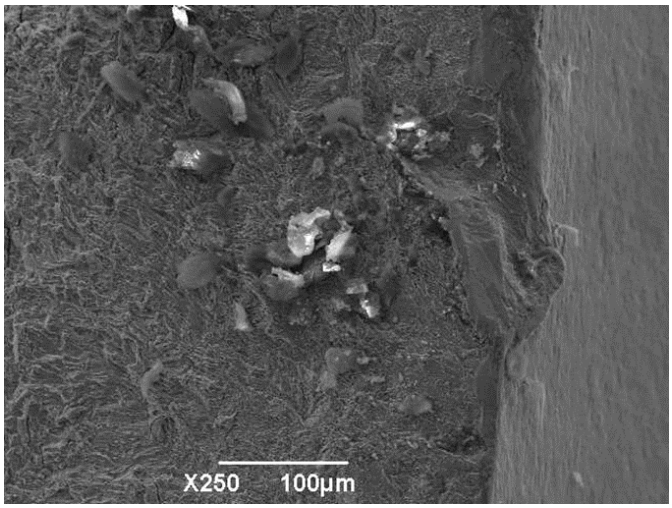

Figure 59. Large initiation site in specimen SDNL.5H.

In HiFIT treatment groove there were not found any cracks. But some irregularities on the edge of the groove and some visible regularly spaced markings. The marks are shown in figure 60. Also, some oxide/nitrate inclusion was found.

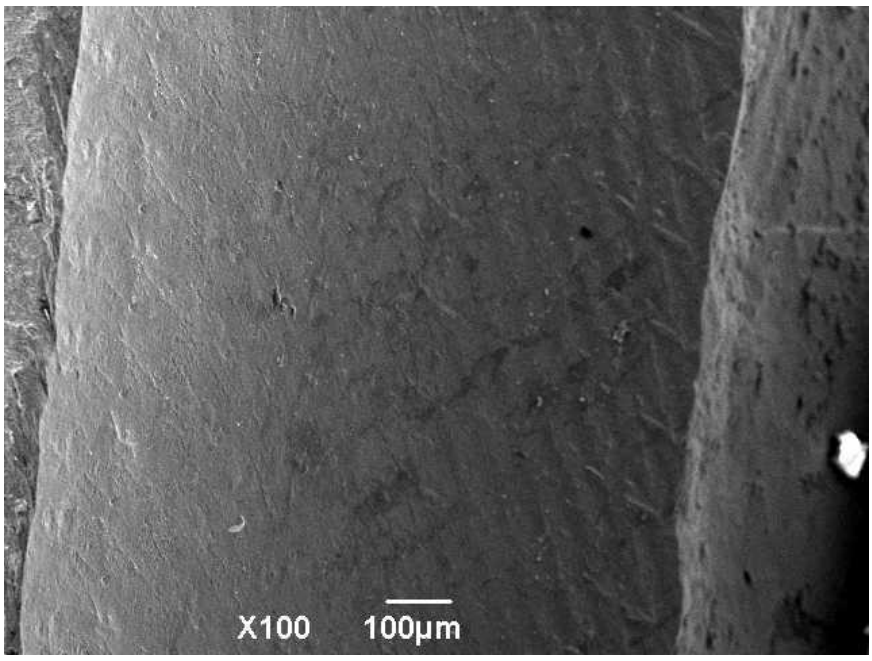

Figure 60. The HiFIT groove marks in specimen SDNL.5H.

Butt welded specimen SDBW.5H with HiFIT treatment had a lot of small inclusions, several initiation sites and secondary cracking between the phase boundaries. Load carrying specimen SDL1.4 broke from the weld root but the crack growth direction was not identified. There were large porosities found in load carrying specimen but not any secondary cracking. Porosities are presented in figure 61 and in figure 62 the fracture surface shows large caps between the weld and plate.

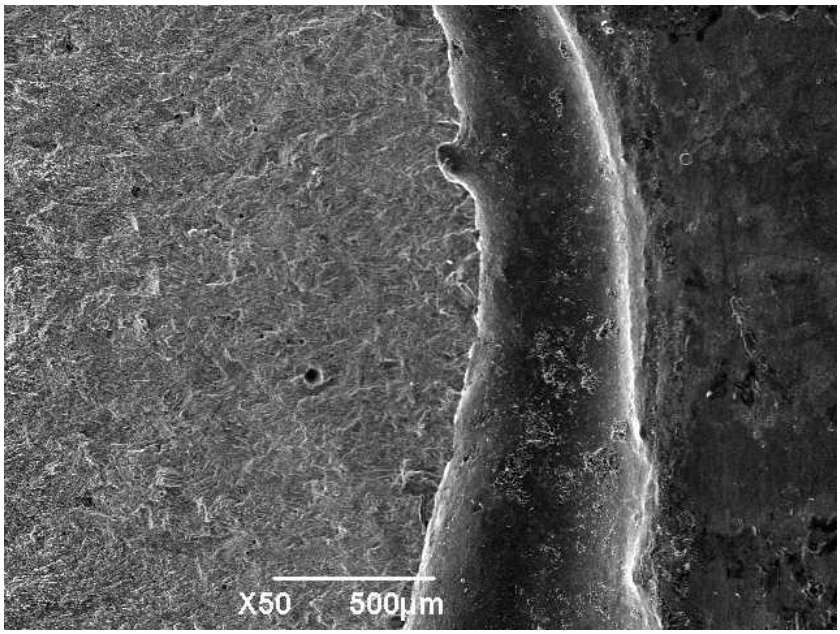

Figure 61. Large gas bubbles found in the load carrying joint specimen.

Figure 62. Fracture surface of a load carrying joint which broke from the weld root.

From the macrostructure pictures, the welding quality can be evaluated. In the cruciform joints, there were found incomplete root fusion and small pores near the weld root. Some of these presented in a fillet weld in figure 63. Generally, the welding quality is at a good level

and the weld geometers are smooth. Butt welded specimens had a little of small pores but root fusion was good and the weld profiles smooth.

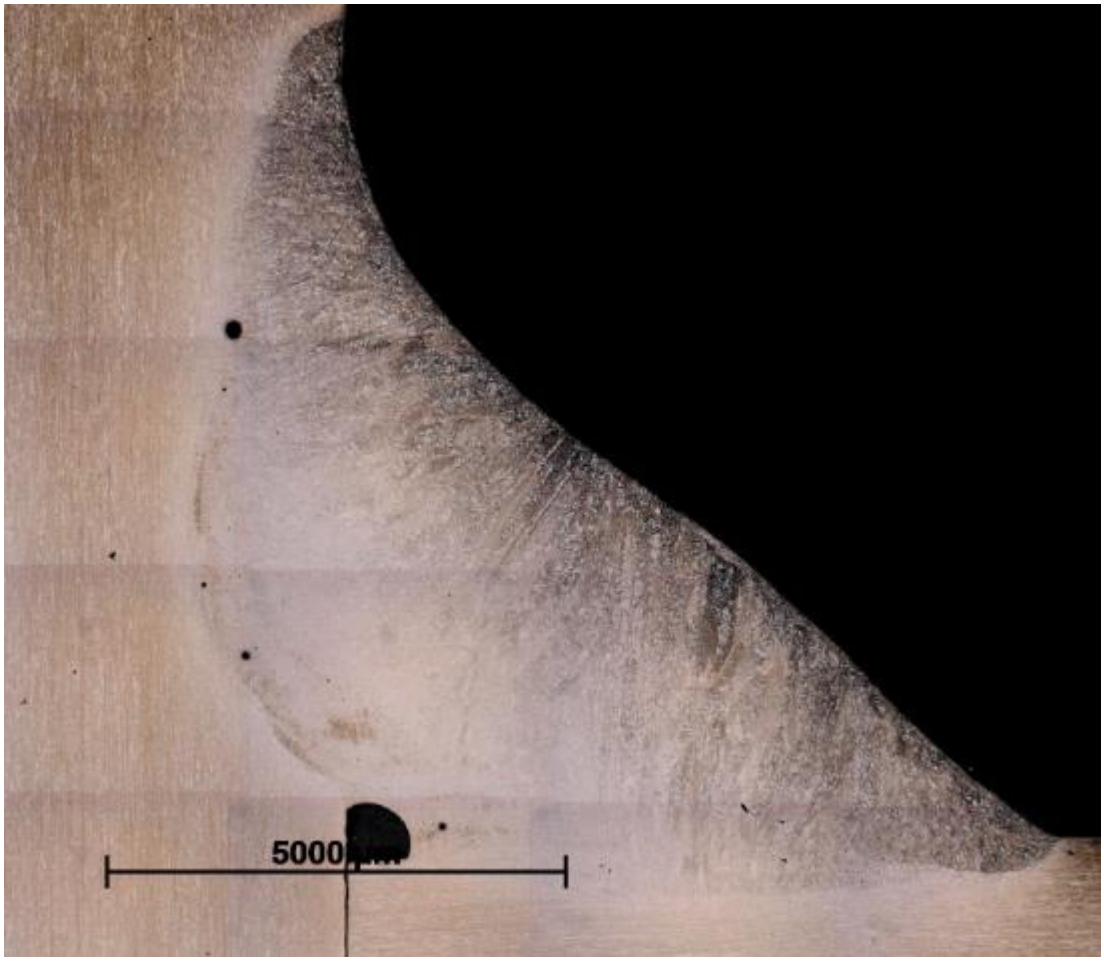

Figure 63. Pores and incomplete root fusion found in load carrying specimen.

4.6 Residual stress results

Residual stress measurement results are presented in figures 65–67 for each joint where the measurements were executed. The principle of measurement points is presented in figure 64. A chart of the numerical results can be found in appendix VI.

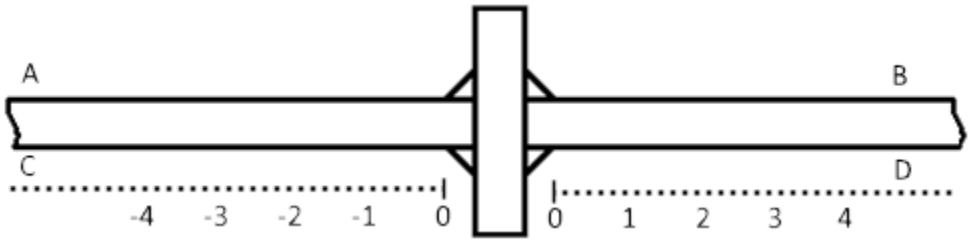

Figure 64. The principle of measurement points on residual stress.

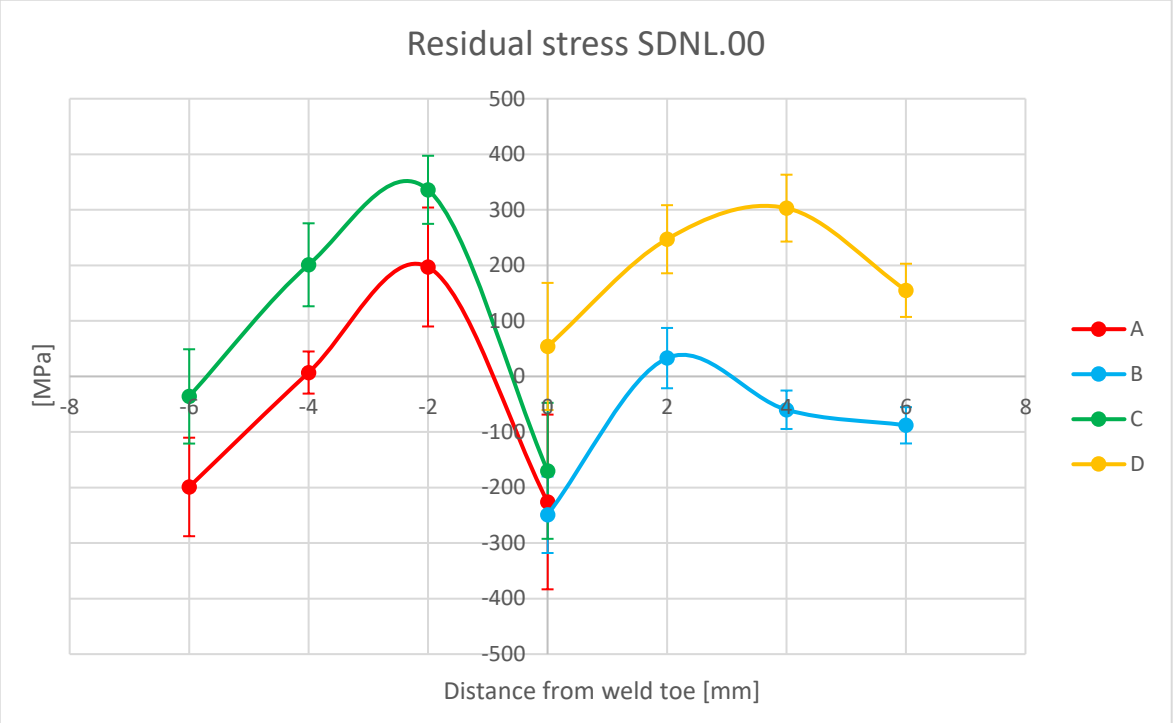

Figure 65. The residual stress measurements for non-load carrying joint.

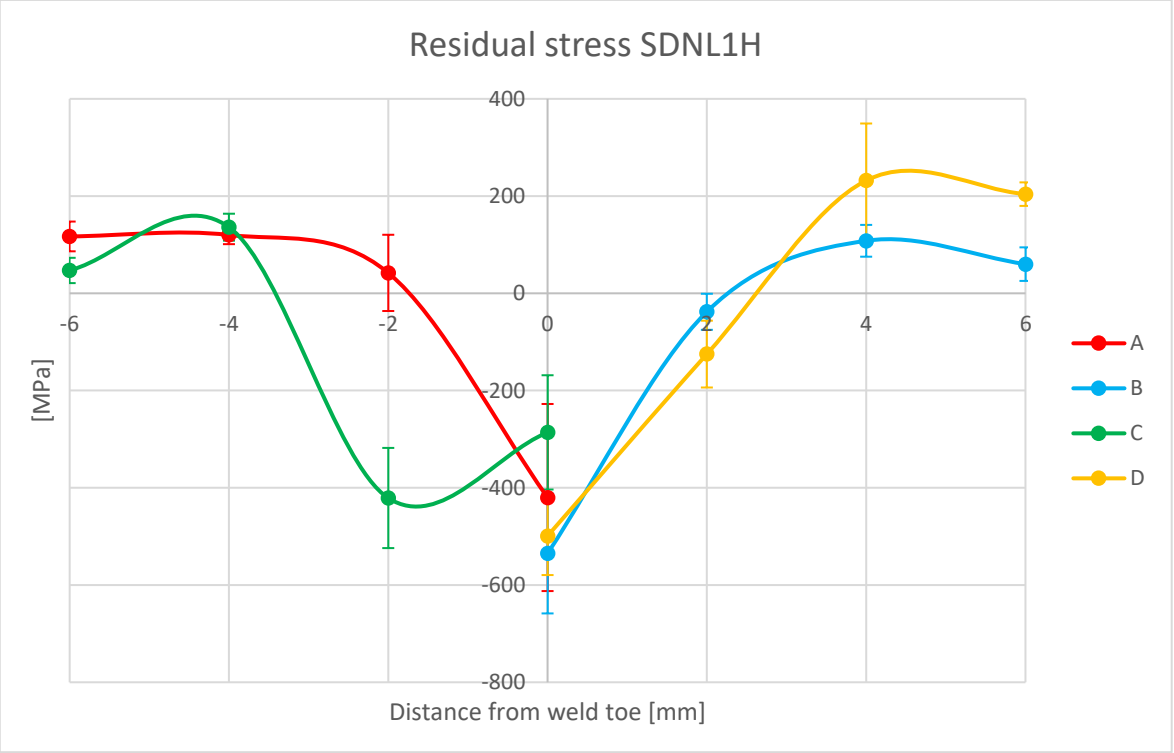

Figure 66. The residual stress measurements for non-load carrying HiFIT treated specimen SDNL.1H.

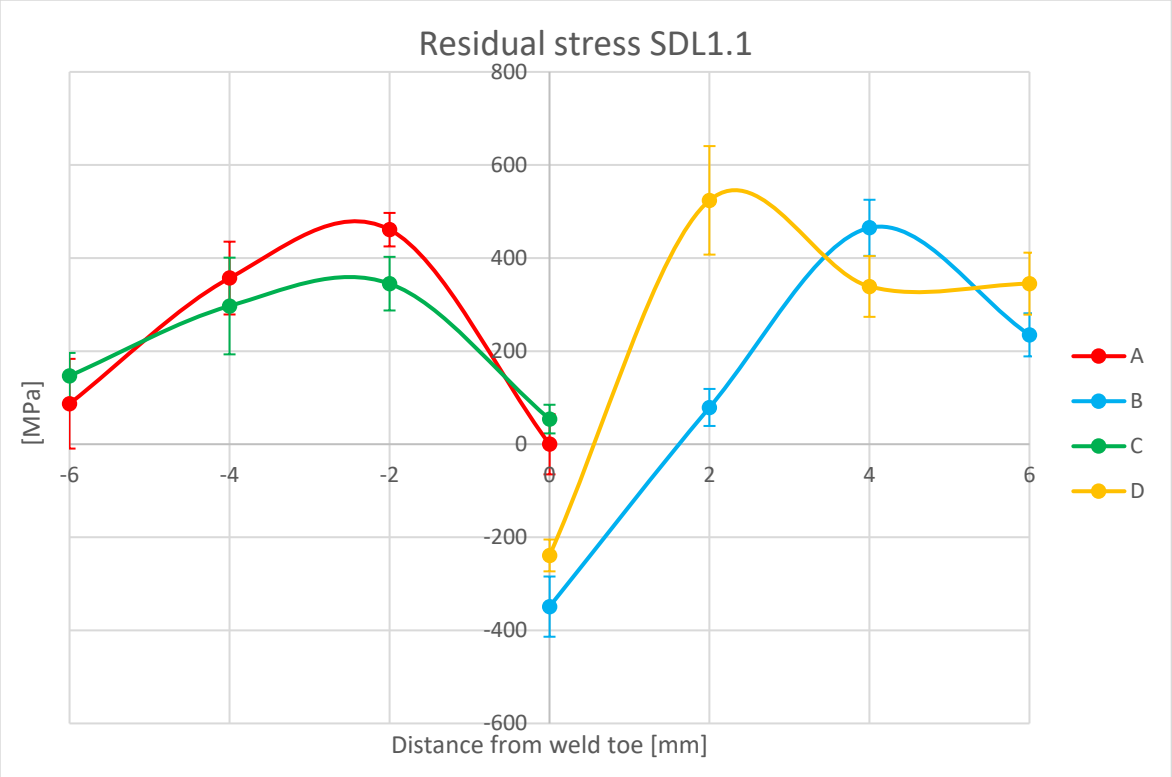

Figure 67. The residual stress measurements for load-carrying joint specimen SDL1.1

Residual stress measurements show compression in weld toe and high positive stresses in 2–4 mm from the weld toe. Non-load carrying specimen had -170 to -249 MPa compressive stress in weld toes and one side in the positive stress of 54 MPa. With HiFIT treatment the compressive stress is -290 to -500 MPa. Load carrying joint had two sides in compression of -239 and -349 MPa, one zero stress and one positive stress of 54 MPa.

5 ANALYSIS & DISCUSSION

Literature research suggested that machining the super-duplex 2507 would be more difficult than traditional stainless steels. In manufacturing the specimens this was found to be true. Machining wore down the tools fast and other methods than machining were needed to ease the process. The grinding device was used to gently cut extra material off so that there was less need for machining. For cruciform joints also wire cutting electrical discharge machining was utilized to remove extra material from the welding starting and ending points.

Shape measurement results are showed in chapter 4.1. Water cut specimens had the smallest total structural stress magnification factors $K_{m,tot}$ which is caused by angular misalignment. They had only 1.03–1.09 when plasma cut had 1.08–1.33. The cut specimen had naturally only angular misalignment. Water cut specimen and calculation data gave close to same stress range levels. Plasma cut specimens had a bit higher stress magnification factors but the measured data suggests that the stress was lower than calculated. Butt welded specimen had total structural stress magnifications factors of about 1.12–1.35 with four specimens having higher factors. Non-load carrying joints had the smallest total structural stress magnification factors in welded specimens. These joints had only attachments so the main plate is continuous and the axial misalignment is not a problem. Highest total structural stress magnification factors were around 1.45–1.65 and these are because of high, over 1.5 degrees, angular misalignment. Load carrying joints had four specimens with total structural stress magnification factors of 1.08–1.23. Two specimen SDL1.5 and SDL1.6 had much higher 1.80 and 1.86 factors. The biggest factor for these specimens large total structural stress magnification factors is a high angular misalignment of 2.16 and 3.26 degrees and also SDL1.5 had a high axial misalignment of 0.41 mm. This is shown clearly in figure 69 where the SDL1.5 and SDL1.6 have much smaller nominal stress compared to the other stresses. The differences between calculated structural stress range and measured stress range, by stain gauges, in cut edge specimens and in the butt welded specimens are presented in figure 68. In figure 69 these are presented for the cruciform joints. There are also presented the planned test stress range and nominal stress range which has been calculated from the force measured by the test equipment and cross-section area.

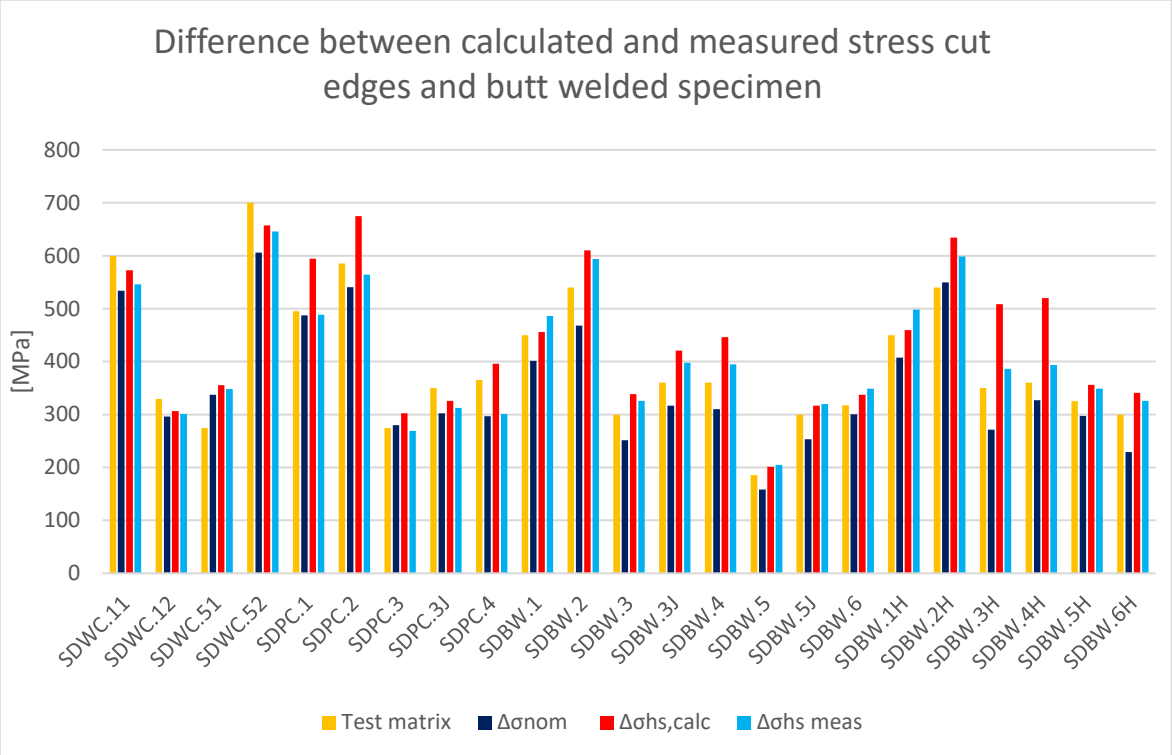

Figure 68. The comparison between calculated and measured stress in cut edges and butt welded specimen.

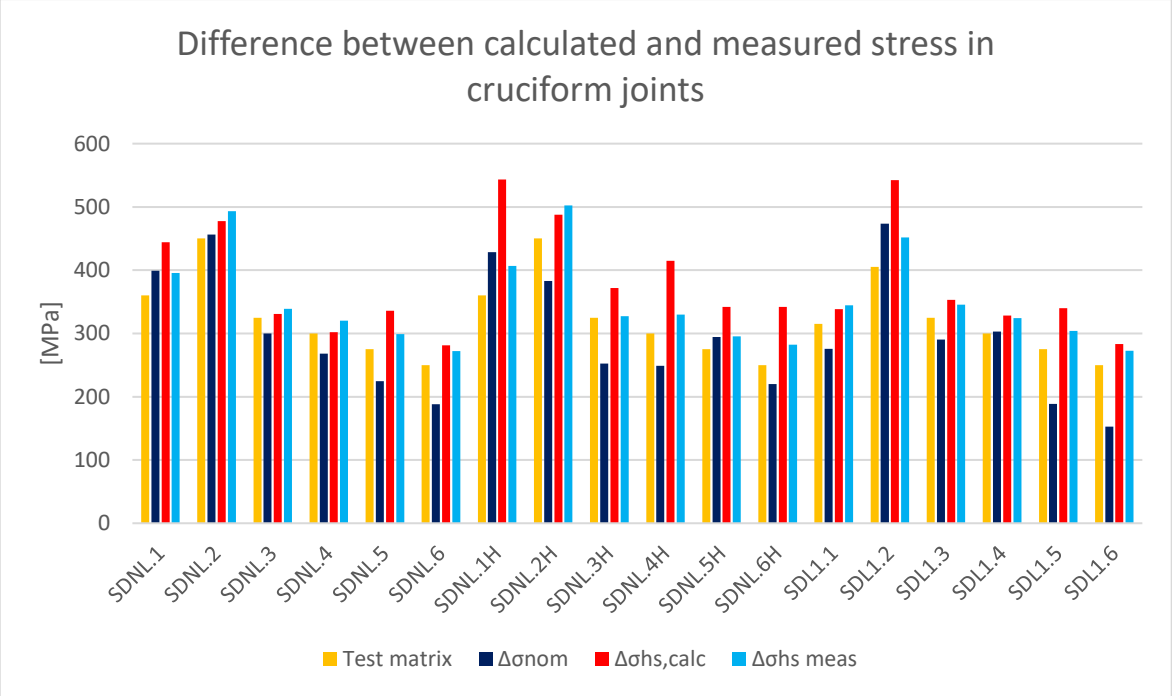

Figure 69. The comparison between test, nominal, calculated and measured stress in cruciform joints.

Some of the butt welded specimens had a little bit higher measured stress than calculated. Two butt welded HiFIT treated specimens had much lower stresses than calculated. This might be due strain gauge locating too close to the HiFIT treated area and the strain gauge is not located at the stress concentration area. A principle of this is shown in figure 70, where is a radius similar to HiFIT treatment modeled in a simplified FEM-model of a butt weld. The model shows lower stress near the HiFIT treated area. In figure 69 the cruciform joints results shows that in the as-welded specimens the strain gauge data and the calculated results with misalignments have agreed results to each other, but in HiFIT treated specimens the calculated stress is much higher in five out of six specimens. In specimen SDNL.1H the strain gauge shows smaller stress than nominal stress. It is suspected that the strain gauge showed wrong results due to wrong calibration or misplacement. The strain gauge was located on the concave side of the specimen Also, specimen SDNL.5H was tested with higher loads that it was intended.

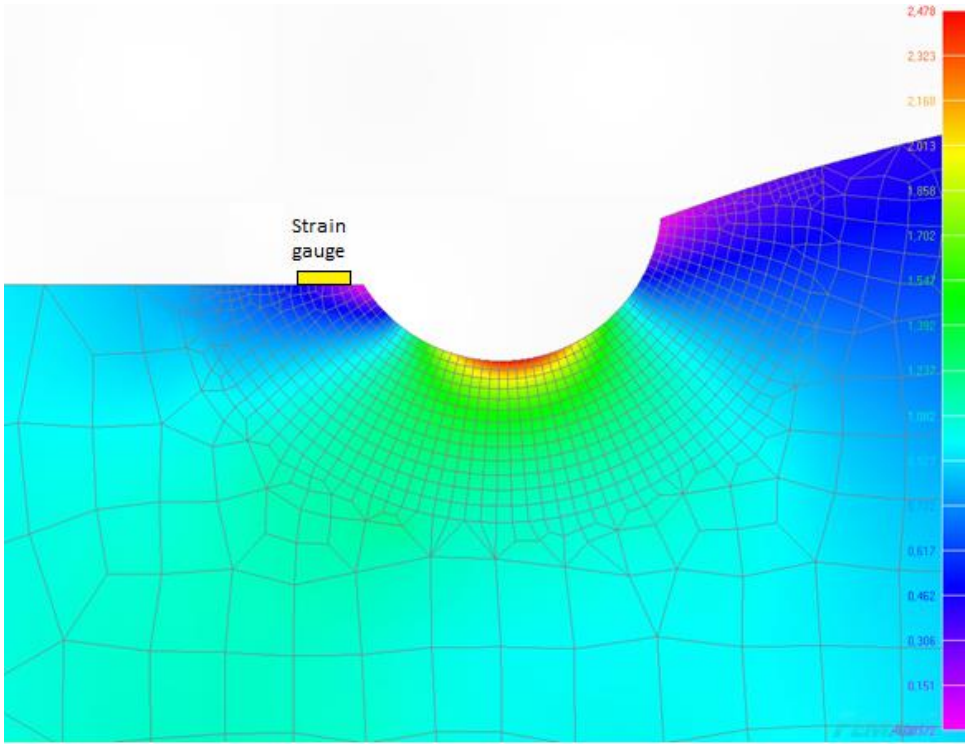

Figure 70. The principle of strain concentration missing the strain gauge.

Some of the angular misalignment is lost in stress gauge measurements as the specimen is statically pulled to the maximum strain as many times as needed to stabilize the specimen and then the strain gauge is zeroed. This may cause a little error in total structural stress

magnification factor, as angular misalignment stress is smaller in fatigue testing. Structural stress takes into account the angular and axial misalignment that is in the most likely breaking point, which is on the concave side of the specimen before testing, thus haves positive stress magnification. From the surface roughness measurements, in table 9, can be seen that the laser cutting had the smallest surface roughness arithmetic average *Ra*, followed by water cutting, while plasma cutting had the biggest average.

Static test results can be found in chapter 4.2. For base material, the ultimate nominal strength was informed earlier to be 750 MPa and the material specification says it to be 917 MPa. The static test for the base material which was, in this case, the water cut specimen showed the ultimate strength to be 871 MPa. This is much higher than the nominal strength but a little lower than material specification suggests. Butt welded specimen behaved similarly with water cut specimen, the only difference is that the elongation in the water cut specimen is a little higher. The butt weld was at least equal strength as the base material with an ultimate strength of 878 MPa. Cruciform joints had also similar behavior as base material with a little bit smaller elongation before fracture. Non-load carrying joints had an ultimate strength of 877 MPa, load carrying joint with bigger weld throat thickness 903 MPa and load carrying with smaller weld throat thickness had 867 MPa. All the specimens performed better than nominal ultimate tensile strength suggests and they broke from the base material about 50–60 mm from the weld. Even the load carrying joint with smaller weld throat thickness is at least equal strength to base material. The elongation before breaking is smaller with the welded joints. Since the SDL1.S1 specimen testing was restarted twice the stress-elongation curve is put together from three different curves which may affect the results slightly. The calculated modulus of elasticity is 204 GPa. This is just a little higher than the reported 200 GPa.

Fatigue test results and S-N curves are presented in chapter 4.3. Fatigue tests with nominal stress for cut specimen suggests that water cut specimens had slightly better FAT class than the plasma cut specimens. Both water and plasma cut specimens had better FAT class than the IIW suggested 160 MPa. Water cut specimen had 195 MPa and plasma cut 183 MPa characteristic curves and combined FAT_{char} of 198 MPa. More specific results for FAT classes on all specimen series are in appendix III. Both of series gave better results on R-value 0.1 than 0.5. With the 0.1 R-value, the stress range was higher than with 0.5 because

with 0.5 the yield limit is approached quickly when rising the stress range and with 0.1 R-value this is not a problem. Plasma cut R-value 0.1 specimens had high misalignment factors compared to water cut specimens, which explains partly the lower nominal FAT class. Calculated slope angles are slightly steeper than IIW recommended $m = 5$. All cut specimen had combined slope of $m = 3.49$. If inspecting slope angles of different R-values or separately to the water or plasma cut specimens, there are slope angle values mostly under 5 but one series, plasma cut R-value 0.5, giving a very large slope coefficient of 27.85. The large changes are explained by the small number of samples. With structural stress taken into account the FAT classes get slightly better and also they are more consistent. For all cut specimens, the structural characteristic curve is 231 MPa which is 36 MPa higher than with the nominal stress, illustrating the average structural stress concentration of 1.18. Based on the results the new suggested nominal FAT value with $m = 5$ is 200 MPa.

Butt welded specimen have IIW fatigue class of 90 MPa. The fatigue test results for all as-welded specimen with nominal stress suggest the characteristic FAT class of 123 MPa and for all HiFIT treated specimens 94 MPa, which both are better than the recommendation. Both series gave better results with 0.1 R-value than 0.5, but with as-welded the difference is small and for HiFIT treated the difference is bigger. HiFIT treated butt welded specimens performed worse than the as-welded ones, especially with R-value of 0.5. HiFIT treated butt welded characteristic curve of 81 MPa with R-value 0.5 is even below the IIW recommendation. Slope angle for as-welded is calculated to be $m = 3.44$ which is a little bigger than recommended, however, the HiFIT treated specimens suggests a slope of $m = 2.07$ which is steeper than the as-welded or IIW recommendation. Specimens SDBW.3H and SDBW.4H had large misalignments factors and both had poor fatigue performance. These specimens affect the results by giving HiFIT treated butt welded series poor performance in the high loads. However, with misalignment total structural stress factors taken into account for as-welded and HiFIT treated specimens the results are almost the same. For all HiFIT specimens with structural stress the FAT_{char} is 155 MPa and for as-welded it is 149 MPa. Now the HiFIT performed better than as-welded, but the degree of improvement was not high. The butt welded HiFIT treated slope coefficient m also gets better from nominal stress 2.07 to 3.38 which is about the same as for as-welded specimens. It is to be noted that misalignments have a large effect on the structural fatigue results. To

the butt welded joints in the as-welded condition the new suggested nominal FAT value with m = 3 is 112 MPa.

Figures of the fracture surfaces of butt welded specimens can be found in appendix IV. The as-welded specimen broke from the weld toe area and the HiFIT treated specimens broke from the HiFIT treated notch. Water cut edges specimen had multiple other places where a crack had also started to grow. This is shown in figure 71. This suggests steady performance from the cut edge.

Figure 71. Water cut specimen SDWC.51 had multiple crack locations.

Non-load carrying joints have IIW fatigue class of 80 MPa with a slope of m = 3. The combined FAT_{char} for the as-welded condition is 92 MPa and for HiFIT treated specimens it is 72 MPa. As-welded specimens performed better than IIW recommendation but the HiFIT treated specimens were worse. With both as-welded and HiFIT, the R-value 0.1 series had higher FAT_{mean} values that with R-value 0.5. But since the low number of specimens and a high slope factor of 11.25 with the R-value 0.1, the R-value 0.5 gets a better characteristic curve with HiFIT treatment because of smaller confidence boundaries. Structural stress rises the FAT_{mean} to 148 MPa and FAT_{char} to 116 MPa with as-welded and for HiFIT treated FAT_{mean} is 175 MPa and FAT_{char} is 108 MPa. Both characteristic curves are now much better than IIW recommendation. Different R-values behave the same way as with nominal stress. HiFIT treated specimens had worse characteristic curves than the as-welded condition in both cases. The new suggested nominal FAT value for the as-welded non-load carrying joints with m = 3 is 90 MPa.

Load carrying joints have IIW fatigue class of 63 MPa with a slope of m = 3. The combined results with both loading R-values had characteristic fatigue class of 71 MPa using nominal stress range. With structural stress, the characteristic fatigue class is improved to 98 MPa. Both results are better than the IIW recommendation. R-value 0.1 specimens had almost the same number of cycles before fracture despite the different stress range levels. Fixed FAT_{mean}

was better with R-value 0.1 than with 0.5, but since the unconventional results of the two specimen the FAT_{char} is better for R-value 0.5. For calculated slope coefficient, the high-stress levels and high performance makes the slope steep with m = 1.39. With only R-value 0.5 taken into account, the slope is higher 2.84 with nominal stress and structural stress makes it even bigger m = 7.85. Four of the specimens broke from the welding root. The welding throat thickness was selected to be on the limit since rounding downwards. The fatigue strength with the R-value 0.5 specimens that broke from the root is not worse than the specimens that broke from the toe. The specimens with the root critical had independent FAT_{mean} of 114 and 117 MPa while the specimens that broke from the weld toe had FAT_{mean} of 106 and 114 MPa. Even if the fatigue strength exceeds the IIW recommendation for load carrying joints when weld root is critical, the breaking from the weld root is undesirable. Weld throat thickness should be reconsidered from what was used in these specimens to make weld toe critical to all specimen but also the porosities from the weld root is a possible source of the fracture point and they should be avoided. The new suggested nominal FAT value for load carrying joints with m = 3 is 71 MPa.

For different stress ratios of the cut edges specimens and other R-value 0.1 tests the sample size was only two specimen for each R-value, which causes them to be sensitive to the scatter of results. With calculated slope, the characteristic FAT curve is the same as mean FAT since both points are directly at the curve. Hence those characteristic results are not reliable and the slope angle would possibly change if there were more tested specimens with a wider dispersion of data points. The calculated slope angles are very steep especially with HiFIT treated non-load carrying joints and load carrying joints. This might be because of high performance of the highly loaded R-value 0.1 specimens and that there were not enough specimens with high enough number of cycles. The fixed slope results describe the results better in these cases.

HiFIT treatment for butt welded joints in 5 mm plate according to these results is not recommended. The FAT_{char} is not good enough to justify extra work and costs of post weld treatment when the expected fatigue strength is about the same as as-welded. With non-load carrying joints the HiFIT treatment does not show improvement in fatigue strength overall. For both R-values, the FAT_{char} is lower than in as-welded condition. With R-value 0.1 the mean fatigue strength is improved notably but with R-value 0.5 it is about the same as as-

welded. Several studies: Nykänen & Björk (2015), Yildirim & Marquis (2012), Mikkola et al. (2015) and Maddox, Doré & Smith (2010) shows that the benefit of peening methods decrease when using: higher stress levels, maximum stress is closing to the tensile yield limit or if the R-value is over 0.5. HiFIT specimen broke from the notch area created in the peening process. In earlier figure 70 there is a model that highlights the stress concentration in the place of fracture. The fusion line is located under the treatment, this can be seen in figure 53. The fusion line location under the treatment depends on to the profile of the weld. It can be on the side of the treatment or at the bottom of the pit. It is possible that the fracture happens on the fusion line rather than the absolute bottom of the notch. It was suggested in literature research that FAT classes can increase by 4 steps in HiFIT treatment and for higher strength steels it is one more class per increase of 200 MPa in yield strength. This would mean a total of 6 FAT classes increase in 2507 HiFIT treatment. For butt welded specimen the new FAT class would be 180 MPa and for Non-load carrying joint 160 MPa. This is clearly not the case based on the results of this research with 2507. HiFIT treatment also seems to influence to the strain gauge measurements as it gives lower results.

Fatigue tests were planned by the maximum strain which was statically tested to each specimen to get the maximum force and minimum force with the R-ratio. Fatigue tests were performed by force control. In calculation between strains and stresses, there is possible of a small difference as it is calculated by the nominal modulus of elasticity reported to all Outokumpu duplex grades. With butt welded specimen the applied stress range in fatigue testing was about 9 % higher than planned. Strain gauges showed straining throughout the fatigue testing for some highly loaded specimens and for first 100 000 cycles there is plastic deformation. An example of this is showed in figure 72 where are the minimum and maximum stress and the stress range in strain gauge for plasma cut specimen SDPC.4. Even if the specimen strains the strain change in the strain gauge stays constant until the last cycles before fracture. This suggests that not cyclic hardening nor softening took place during measurement. Only one strain gauge was used per specimen due to higher costs and work amount with multiple strain gauges. They were placed in expected fracture side of the specimen. The crack initiated 10 times out of 26 from the correct side when the specimen broke from the weld toe area.

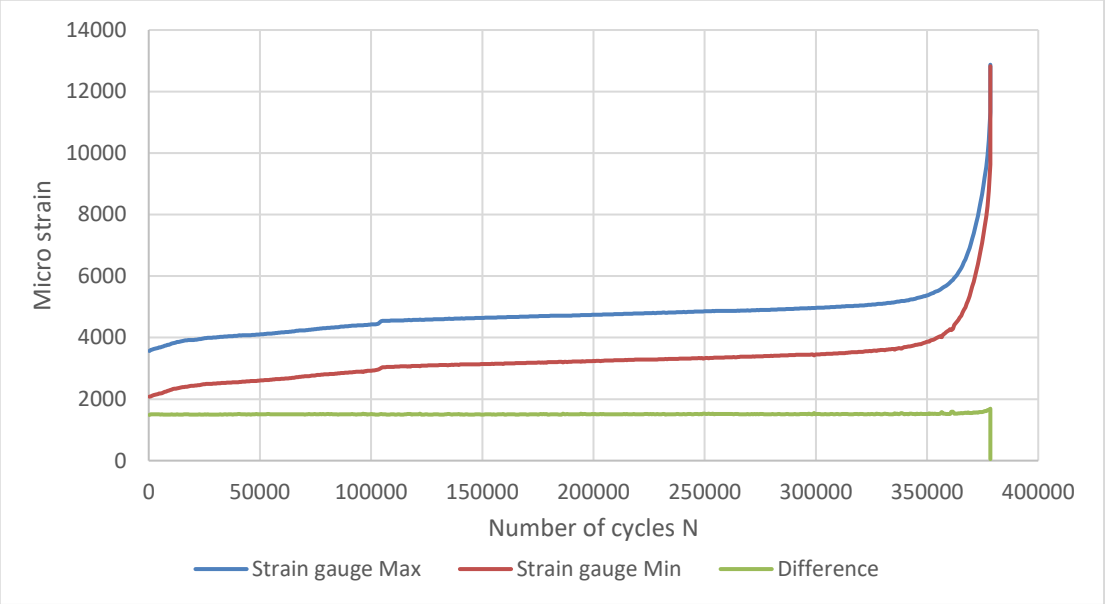

Figure 72. Strain gauge results from SDPC.4 fatigue testing.

FE-analysis with ENS-method was made to all welded specimen. The cut edges specimens were not modeled as they are not suitable for ENS-method and the stress should be equal to the loading. FE-analysis gave worse fatigue strength than the real-life fatigue tests even with using FAT_{mean} 308 MPa ENS class. The results in chapter 4.4 suggest that the FAT ENS calculated from real fatigue strength and FE-analysis, stress is about 15–60 % higher than FAT_{mean} by ENS-method for butt welded as-welded and HiFIT treated specimen. For cruciform joints the results are slightly more accurate with FAT_{mean} by ENS being averagely about 2–20 % higher than assumed FAT ENS 308 MPa. The HiFIT specimen with a larger radius in weld toe had more slightly accurate results. The ENS concentration multipliers varied between 1.58 and 1.78 for the butt welded specimens and for cruciform joints 1.64–2.40. The maximum stress in ENS-analysis in butt welded specimens is located at the side where was modeled the highest weld dome and about 2 millimeters from the side of the model. In cruciform joint types, the highest ENS multiplier is located in the smallest weld throat thickness except for specimen SDL1.4 which had weld root on the side C as the highest point of stress. FE-analysis results are a good estimation of fatigue strength, but there were some differences on experimental results. Five specimens had a better fatigue strength in FEM compared to fatigue testing. Three of them are HiFIT treated non-load carrying joints which all broke from the HiFIT groove, one is non-load carrying in an as-welded condition that broke from the toe and the last one was SDL1.4 which broke from the weld root as the FE-model suggested. The most accurate result was only 3500 cycles away from fatigue

testing while one load carrying had over 620 000 cycles better performance in fatigue testing and run out specimens had an even higher difference.

Hardness measurements show an increase of hardness in HiFIT treated specimen. Base material hardness is around 290–300 in HV0.1, which is close to the previous results. HV5 gave a bit smaller results of around 280. HiFIT treated specimens had very high hardness near the treatment surface, up to 450. The hardness is also higher for the base material and weld around the treatment. However, it decreases when going further away from the treatment. The non-treated weld toes behave in the same way as in the as-welded condition, which is not a problem since the attachment side weld toe is not critical for fatigue. The summarizing on table 20 is slightly unreliable since high local changes in hardness results especially in HiFIT treated specimens. From the additional microhardness measurements in HiFIT treated specimen, can be seen that the hardness drops slightly in the fusion line. This is presented in appendix VI figures 5 and 6. In as-welded condition, there is not a notable difference. In the fusion line, there is generated a fine line of large ferrite crystals.

In scanning electron microscope analysis, there were found several crack initiation sites on all the specimens. In both non-load carrying specimens, there was oxide/nitride inclusion found. Secondary cracks between austenite and ferrite were found in as-welded non-load carrying specimen and butt welded specimen. HiFIT treatment had some irregularities but cracks were not found. Load carrying joint had porosities in weld root which made large gaps between the plate and weld. These are a possible source of why four of the specimen broke from the weld root.

Residual stress measurements were planned to be performed to all joint types but because of butt welded specimens had been polished the measurements could not be done reliably. In chapter 4.6 is presented the residual measurements for non-load carrying and load carrying joint types. Non-load carrying joints in the as-welded condition had three out of four weld toes in compressive stress and load carrying joints in the as-welded condition had two. With HiFIT treatment there are introduced much higher compressive stresses in all weld toes compared to the as-welded condition. The as-welded specimens have a similar stress profile in the measurements. They mostly have peak stress in 2 mm from the weld toe, when HiFIT treatment had its peaks in 4 mm from the toe. Measured positive peak stress is about 150–

300 MPa for non-load carrying joints and load carrying joints 350–500 MPa. All specimens have low stresses when approaching 6 mm from the toe. In measurements, there is informed a margin of error which are drawn in the figures. The measured average error is ± 69 MPa and varies between ±19 and ±192 MPa. These results should be taken with caution as possibilities of error are high. The specimens selected to residual measurements were from fatigue testing series except for as-welded non-load carrying joint since it was measured after the fatigue test were completed thus a spare specimen SDNL.00 was used. Load carrying specimen SDL1.1 broke from the root of the weld. HiFIT treated specimen SDNL.1H broke from the same side C where was the smallest amount of compressive stress but since there is also the smallest weld throat thickness and it is located disadvantageous side of angular misalignment it was anyways the most likely fracture point.

5.1 Further research subjects improvement on current research

In this work the fatigue test especially with R-value 0.1 were set to too high load ranges. With more fatigue test results with cycle size of 500 000–2 000 000 the slope angles would be more reliable and two data points are not enough to determine a custom characteristic slope angle. Or at least the spread of current test should have been greater. With more data points on high cycles, the slope angles might be milder. Especially the as-welded condition would benefit from more specimens and more confident suggestions for the new FAT class could be made. In this study, there was focused on the many variables in the fatigue testing and the further experimental test can focus only on the most relevant ones. Since the HiFIT treatment was found to be problematic with high R-values and the costs of the material is high, other post weld treatments could be investigated. Also, the effect of the plate thickness could be interesting as these tests were made to relatively thin plate of 5 mm, but only if thicker materials are used in applications. The reason why the HiFIT treatment failed to increase the fatigue strength significantly on the 2507 super-duplex could be examined. FE-models were simplified and they didn’t take residual stresses into account in HiFIT models. Advanced modeling could be used.

Some mistakes during testing were made like with strain gauge, static test elongation limit and that the butt welded specimen could not give reliable residual stress measurements. Overall these are considered and the results should be reliable.

6 SUMMARY

Fatigue characteristic curves and static performance of super-duplex stainless steel 2507 welded joints was studied with experimental tests. Different specimen series in this research were: water and plasma cut edges, butt welded, non-load carrying, load carrying and HiFIT post weld treated butt weld and non-load carrying joint types. FE-analysis, residual stress and microstructure analysis were also utilized.

All static test specimen had much higher ultimate tensile strength than nominal of 750 MPa. The measured ultimate tensile strength with all specimens was about 870 MPa. All the specimens broke from the base material. All the welded joints were at least equal strength to the base material in static loading. The only notable difference between different series was that welded joints, compared to the base material, had a bit smaller elongation before fracture.

The characteristic fatigue performance of the 2507 super-duplex with nominal stress in water cut edges specimens was 195 MPa which is better than IIW recommendation of 160 MPa and for plasma cut edges it was 183 MPa. For combined cut edges specimens, the FAT class is 198 MPa. Based on this study the new suggested FAT class for cut edges with this manufacturing quality is 200 MPa with m = 5. Butt welded specimen characteristic FAT class was 123 MPa which is higher than 90 MPa IIW recommendation in the as-welded condition. HiFIT treated butt welded specimen performed worse than as-welded but still had a characteristic FAT class of 94 MPa. The new suggested FAT class for the as-welded butt welded joints is 112 MPa with m = 3. Non-load carrying joints in as-welded condition had 92 MPa which is better characteristic FAT class than the IIW recommendation of 80 MPa. With HiFIT treatment the fatigue strength was worse than in as-welded condition. HiFIT treated specimens had 72 MPa characteristic FAT class which is worse than IIW recommendation for the joint type in the as-welded condition. For the as-welded non-load carrying joint type the suggested FAT class is 90 MPa, with m = 3. Load carrying joints had combined characteristic fatigue value of 71 MPa which is better than IIW recommendation of 63 MPa. Load carrying joints based on these results has FAT class of 71 MPa, with m = 3. Taking structural stress into account improves the characteristic fatigue values notably.

R-value 0.1 had better fatigue results compared to R-value 0.5. HiFIT post weld treatment did not improve the fatigue strength overall in this study. Especially with R-value 0.5, the results were worse than in as-welded condition. R-value 0.1 specimens had better results with some series giving better fatigue strength than in as-welded. But overall HiFIT treatment in 2507 based on these results is not worthwhile. FEM gave decent prediction of fatigue strength but mostly smaller fatigue strength compared to experimental fatigue testing. HiFIT treatment showed high compressive stresses in weld toe.

REFERENCES

Alvarez-Armas, I. 2008. Duplex Stainless Steels: Brief History and Dome Recent Alloys. Recent Patents on Mechanical Engineering, 1: 1. Pp. 51–57.

Charles, J. 2007. Duplex stainless steels, a review after DSS ’07 held in Grado. [Online document]. [Referred 12.2.2016]. Available: http://www.aperam.com/europe/news-publications/documentation/technical-publication

Fricke, W. 2010. Guideline for the Fatigue Assessment by Notch Stress Analysis for Welded Structures. In IIW-Doc XIII-2240r2-08/XV-1289r2-08. 38 p.

Fricke, W. 2011. [Chapter 5] Fatigue strength assessment of local stresses in welded joints. In Macdonald, K. (editor) Fracture and Fatigue of Welded Joints and Structures. Cambridge. Woodhead Publishing Limited. 2011. Pp. 115–138.

GOM. 2016. ARAMIS – Optical Deformation Analysis. [Online document]. [Referred 19.4.2016]. Available: http://www.gom.com/metrology-systems/system-overview/aramis.html

Haagensen, P. J. 2011. [Chapter 11] Fatigue strength improvement methods. In Macdonald, K (editor). Fracture and Fatigue of Welded Joints and Structures. Cambridge. Woodhead Publishing Limited. 2011. Pp. 297–329.

Hobbacher, A. 2014. Recommendations for Fatigue Design of Welded Joints and Components. Paris, France. International Institute of Welding, Document XIII-2460-13/XV-1440-13. 164 p.

International Molybdenum Association (IMOA). 2014. Practical Guidelines for the Fabrication of Duplex Stainless Steels. [Online document]. [Referred 12.2.2016]. Available: http://www.imoa.info/molybdenum-uses/molybdenum-grade-stainless-steels/duplex-stainless-steel.php

Lindgren, M. & Lepistö, T. 2002. Relation between residual stress and Barkhausen noise in duplex steel. In NDT & E International, 36: 5. 2003. Pp. 279–288.

Maddox, S. J., Doré, M. J., & Smith, S. D. 2010. Investigation of Ultrasonic Peening for Upgrading a Welded Steel Structure. International Institute of Welding, Document XIII-2326-10. 23 p.

Maddox, S. J. 2011. [Chapter 7] Fatigue design rules for welded structures. In Macdonald, K. (editor) Fracture and Fatigue of Welded Joints and Structures. Cambridge. Woodhead Publishing Limited. Pp. 168–207.

Marquis, G. & Barsoum, Z. 2013. A Guideline for Fatigue Strength Improvement of High Strength Steel Welded Structures Using High Frequency Mechanical Impact Treatment. Procedia Engineering, 66. Pp. 98–107.

Mikkola, E., Marquis, G., Lehto, P., Remes, H. & Hänninen, H. 2015. Material characterization of high-frequency mechanical impact (HFMI)-treated high-strength steel. Materials and Design, 89. Pp. 205–214.

Niemi, E. & Kemppi, J. 1993. Hitsatun rakenteen suunnittelun perusteet. Helsinki: opetushallitus. 337 p.

Niemi, E. 2003. Levyrakenteiden suunnittelu. Helsinki: Teknologiateollisuus ry. 136 p.

Niemi, E., Kilkki, J., Poutiainen, I. & Lihavainen, V-M. 2004. Väsymättömän hitsausliitoksen suunnittelu, 4. Lappeenranta: LTY Digipaino. 121 p.

Nykänen, T. & Björk, T. 2015. A new proposal for assessment of the fatigue strength of steel butt-welded joints improved by peening (HFMI) under constant amplitude loading. Fatigue & Fracture of Engineering Materials & Structures, 39: 5. Oxford: Wiley Publishing Asia Pty Ltd. Pp. 566–582.

Outokumpu. 2013. Duplex Stainless Steel. [Online document]. [Referred 27.4.2016]. Available: http://www.outokumpu.com/SiteCollectionDocuments/Outokumpu-Duplex-Stainless-Steel-Data-Sheet.pdf

Pfeifer. 2009. The Revolution for Welded Constructions: HIFIT Post-Weld Treatment. [Online document]. [Referred 2.3.2016]. Available: http://www.pfeifer.de/fileadmin /user_upload/DE_doc/hifit/download/HiFIT-Produktprosp_5-2009_en.pdf

Sandvik. 2015. Sandvik SAF 2507 tube and pipe, seamless datasheet. [Online document]. [Referred 12.2.2016]. Available: http://smt.sandvik.com/en/materials-center/material-datasheets/tube-and-pipe-seamless/sandvik-saf-2507/

Sonsino, C. M., Fricke, W., de Bruyne, F., Hoppe, A., Ahmadi, A. & Zhang, G. 2012. Notch stress concepts for the fatigue assessment of welded joints – Background and applications. International Journal of Fatigue, 34: 1. Pp. 2–16.

Ummenhofer, T. et al. 2010. Refresh – Extension of the fatigue life of existing and new welded steel structures. Düsseldorf: Verlag und Vertriebsgesellschaft mbH. 58 p.

Yildirim, H. & Marquis, G. 2012. Fatigue strength improvement factors for high strength steel welded joints treated by high frequency mechanical impact. International Journal of Fatigue 44. Pp. 168–176

Welding Alloys. 2016. TETRA S D57L-G. [Online document]. [Referred 27.4.2016]. Available: http://www.welding-alloys.com/products-services/wa-welding-consumables/joining-cored-wires/welding-of-highly-alloyed-steels/tetra-s-d57l-g.html

Calculations for the equal strength weld root and toe.

Calculations for weld root and toe equal strength

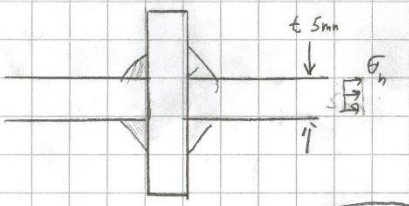

$FAT_{TOE} = 63$ (IIW 413)

$FAT_{root} = 36$ (IIW 414)

$$\Delta\sigma_{n,w} = \frac{\Delta\sigma_n \, t}{2a}$$ (Fricke 2011, p113) →

$$\begin{cases} \Delta\sigma_{n,w}^3 \cdot N_f = FAT_{root}^3 \cdot 2\cdot10^6 \\ \Delta\sigma_n^3 \cdot N_f = FAT_{toe}^3 \cdot 2\cdot10^6 \end{cases}$$

$$\begin{cases} \left(\frac{\Delta\sigma_n \, t}{2a}\right)^3 \cdot N_f = FAT_{root}^3 \cdot 2\cdot10^6 \\ \Delta\sigma_n^3 \cdot N_f = FAT_{toe}^3 \cdot 2\cdot10^6 \end{cases} \Rightarrow N_f = \left(\frac{FAT_{root}}{\frac{\Delta\sigma \, t}{2a}}\right)^3 \cdot 2\cdot10^6$$

$$\Delta\sigma_n^3 \cdot \left(\frac{FAT_{root}}{\frac{\Delta\sigma_n \, t}{2a}}\right)^3 \cdot 2\cdot10^6 = FAT_{TOE}^3 \cdot 2\cdot10^6 \quad | \cdot\sqrt{3}$$

$$\Delta\sigma = \frac{FAT_{root}}{\frac{\Delta\sigma \cdot t}{2a}} = FAT_{TOE} \rightarrow \frac{2a \, FAT_{root}}{t} = FAT_{TOE} \quad \left| \frac{2\,FAT_{root}}{t} \right.$$

$$a = \frac{FAT_{TOE}}{2\,FAT_{root}} \cdot t \qquad a = \frac{63}{2\cdot36} \cdot 5_{mm} = 4{,}375\,mm$$

Rounden downwards for root ≈ 4mm

APPENDIX II

Fatigue classifications according to IIW nominal stress method (Hobbacher, 2014, pp. 45, 47, 59 & 63).

111	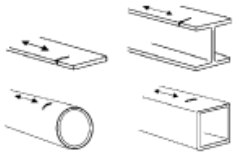	Rolled or extruded products, components with machined edges, seamless hollow sections. m = 5 Steel: A higher FAT class may be used if verified by test or specified by applicable code.	160		No fatigue resistance of any detail to be higher at any number of cycles Sharp edges, surface and rolling flaws to be removed by grinding. Any machining lines or grooves to be parallel to stresses
212		Transverse butt weld made in shop in flat position, NDT weld reinforcement < 0.1 · thickness	90	36	Weld run-on and run-off pieces to be used and subsequently removed. Plate edges ground flush in direction of stress. Welded from both sides. Misalignment <5% of plate thickness.
413	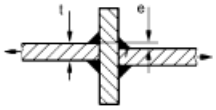	Cruciform joint or T-joint, fillet welds or partial penetration K-butt welds, potential failure from weld toe. Single sided T-joints	63 71	22 25	Advisable to ensure that intermediate plate was checked against susceptibility to lamellar tearing. Misalignment <15% of primary plate thickness in cruciform joints. Also to be assessed as 414
414	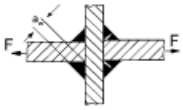	Cruciform joint or T-joint, fillet welds or partial penetration K-butt welds including toe ground joints, potential failure from weld root. For a/t<=1/3	36 40	12 14	Analysis based on stress in weld throat $\sigma_w = F/\sum (a_w \cdot l)$ l = length of weld, a_w = load carrying weld throat. Also to be assessed as 413.
500	**Non-load-carrying attachments**				
511	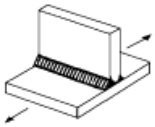	Transverse non-load-carrying attachment, not thicker than main plate K-butt weld, toe ground Two sided fillets, toe ground Fillet weld(s), as welded thicker than main plate	 100 100 80 71	 36 36 28 25	Grinding marks normal to weld toe An angular misalignment corresponding to k_m = 1.2 is already covered

Table III.1 Different FAT classes for water cut specimen.

SDWC	Nominal stress				Structural stress			
	Fixed slope		**Calculated slope**		**Fixed slope**		**Calculated slope**	
	50 %	k2 95 %	50 %	k2 95%	50 %	k2 95 %	50 %	k2 95%
ALL:	m=5		m=2,7		m=5		m=2,73	
	293,68	194,54	211,73	181,26	305,52	203,79	221,75	184,63
0,1:	m=5		m=4,51		m=5		m=6,45	
	337,33	322,17	317,73	317,73	353,67	321,62	400,26	400,26
0,5:	m=5		m=3,20		m=5		m=2,82	
	252,66	226,21	222,89	222,89	263,92	226,52	221,95	221,95

Table III.2 Different FAT classes for plasma cut specimen.

SDPC	Nominal stress				Structural stress			
	Fixed slope		**Calculated slope**		**Fixed slope**		**Calculated slope**	
	50 %	k2 95 %	50 %	k2 95%	50 %	k2 95 %	50 %	k2 95%
ALL:	m=5		m=4,40		m=5		m=4,15	
	266,80	182,97	255,77	168,49	319,54	231,58	299,86	211,09
0,1:	m=5		m=2,86		m=5		m=2,32	
	282,62	254,58	180,95	180,95	348,73	296,80	175,26	175,26
0,5:	m=5		m=27,85		m=5		m=8,33	
	256,74	144,18	282,95	275,86	301,45	197,28	315,96	255,94

Table III.3 Different FAT classes for all cut edge specimen.

ALL CUT SPECIMEN	Nominal stress				Structural stress			
	Fixed slope		**Calculated slope**		**Fixed slope**		**Calculated slope**	
	50 %	k2 95 %	50 %	k2 95%	50 %	k2 95 %	50 %	k2 95%
ALL:	m=5		m=3,49		m=5		m=3,55	
	277,69	198,06	239,18	162,94	313,23	230,97	282,08	197,56

Table III.4 Different FAT classes for butt welded specimen.

SDBW	Nominal stress				Structural stress			
	Fixed slope		**Calculated slope**		**Fixed slope**		**Calculated slope**	
	50 %	k2 95 %	50 %	k2 95%	50 %	k2 95 %	50 %	k2 95%
ALL:	m=3		m=3,44		m=3		m=3,28	
	206,42	123,04	216,03	138,86	262,46	149,11	270,57	161,93
0,1:	m=3		m=8,31		m=3		m=4,35	
	211,58	111,47	334,58	334,58	257,42	188,59	321,57	321,57
0,5:	m=3		m=4,02		m=3		m=3,26	
	204,72	111,36	217,16	141,21	264,17	132,43	269,07	142,76

Table III.5 Different FAT classes for HiFIT treated butt welded specimen.

SDBW HiFIT	Nominal stress				Structural stress			
	Fixed slope		**Calculated slope**		**Fixed slope**		**Calculated slope**	
	50 %	k2 95 %	50 %	k2 95%	50 %	k2 95 %	50 %	k2 95%
ALL:	m=3		m=2,07		m=3		m=3,38	
	160,22	94,34	114,89	56,85	220,27	155,24	239,15	176,23
0,1:	m=3		m=2,67		m=3		m=2,28	
	193,29	179,79	172,56	172,56	217,80	181,38	163,50	163,50
0,5:	m=3		m=5,24		m=3		m=3,84	
	145,87	80,61	192,47	142,23	211,52	136,70	255,17	178,20

Table III.6 Different FAT classes for non-load carrying specimen.

SDNL	Nominal stress				Structural stress			
	Fixed slope		**Calculated slope**		**Fixed slope**		**Calculated slope**	
	50 %	k2 95 %	50 %	k2 95%	50 %	k2 95 %	50 %	k2 95%
ALL:	m=3		m=1,98		m=3		m=2,82	
	121,85	92,21	77,82	64,36	148,25	115,60	140,28	107,85
0,1:	m=3		m=3,71		m=3		m=6,81	
	142,85	132,56	176,13	176,13	154,13	123,85	284,34	284,34
0,5:	m=3		m=2,68		m=3		m=5,41	
	112,54	101,57	102,68	92,98	151,58	119,06	212,94	195,07

Table III.7 Different FAT classes for HiFIT treated non-load carrying specimen.

SDNL HiFIT	Nominal stress				Structural stress			
	Fixed slope		**Calculated slope**		**Fixed slope**		**Calculated slope**	
	50 %	k2 95 %	50 %	k2 95%	50 %	k2 95 %	50 %	k2 95%
ALL:	m=3		m=0,65		m=3		m=0,572	
	126,31	72,01	5,96	1,27	175,29	107,65	4,74	0,30
0,1:	m=3		m=11,25		m=3		m=11,76	
	171,00	82,21	321,90	321,90	217,26	103,26	413,07	413,07
0,5:	m=3		m=2,84		m=3		m=0,53	
	108,56	95,34	103,50	90,32	157,45	111,75	3,19	0,61

Table III.8 Different FAT classes for load carrying specimen.

SDL1	Nominal stress				Structural stress			
	Fixed slope		**Calculated slope**		**Fixed slope**		**Calculated slope**	
	50 %	k2 95%	50 %	k2 95%	50 %	k2 95 %	50 %	k2 95%
ALL:	m=3		m=1,39		m=3		m=1,24	
	129,15	71,49	56,67	25,61	175,03	98,16	63,92	18,81
0,1:	m=3		m = -4,5E-05		m=3		m = -5,2E-05	
	169,06	46,84	65535,00	65535,00	200,45	65,51	65535,00	65535
0,5:	m=3		m=2,84		m=3		m=7,85	
	112,88	102,37	108,46	98,86	163,55	90,86	249,98	209,74

APPENDIX IV

The fracture surfaces of fatigue tested cut edges and butt welded specimen.

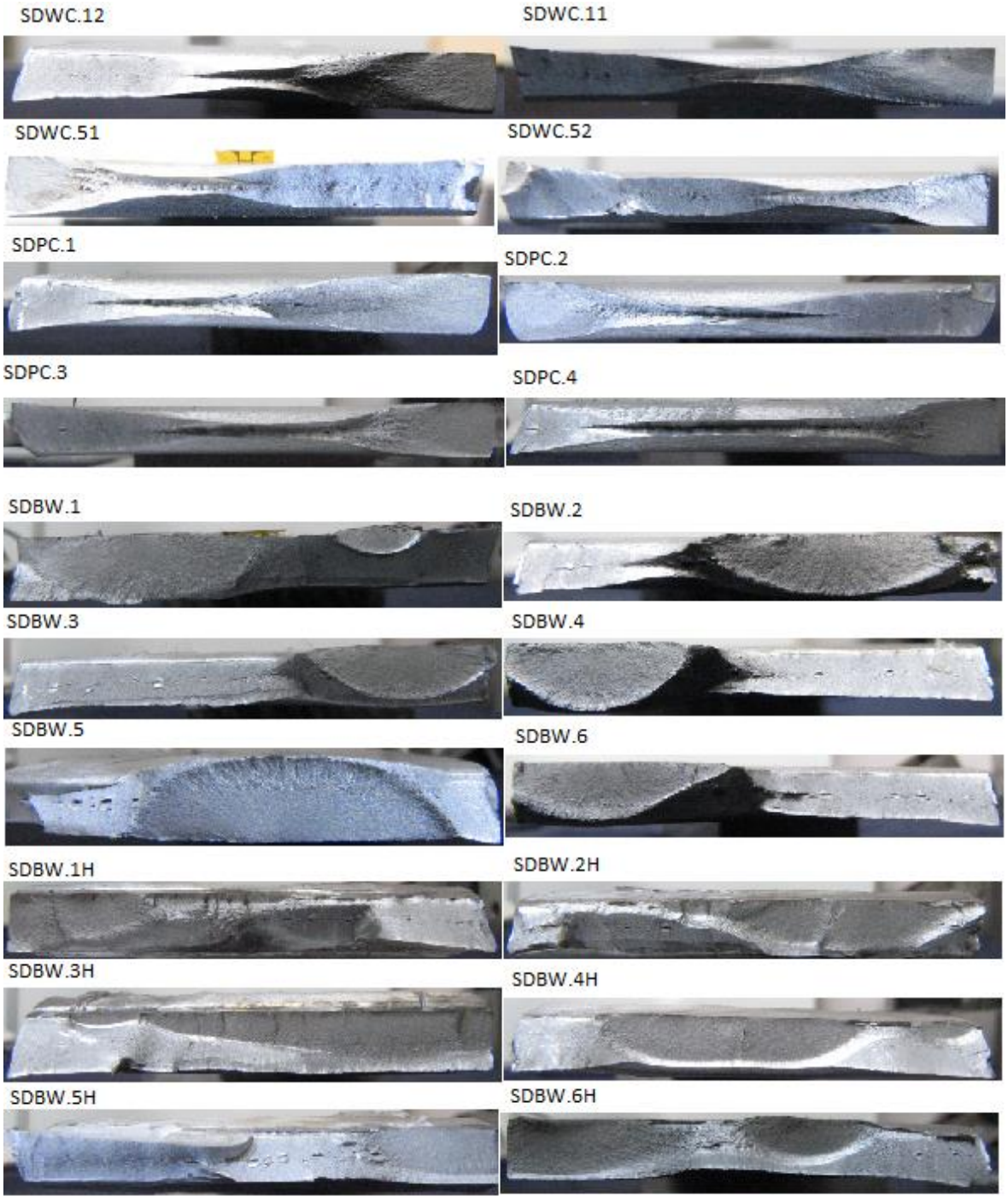

SDNL.1

SDNL.2

SDNL.3

SDNL.4

SDNL.5

SDNL.6

SDNL.1H

SDNL.2H

SDNL.3H

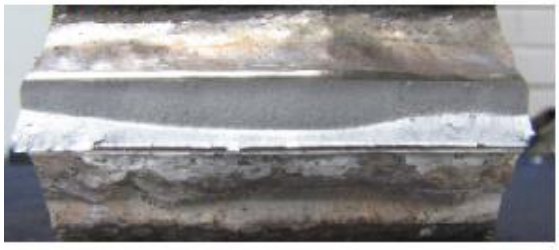

SDNL.4H

SDNL.5H

SDNL.6H

SDNL.1

SDNL.2

SDNL.3

SDNL.4

SDNL.5

SDNL.6

APPENDIX V

Photos of HiFIT treatment and breaking point of HiFIT treated specimens.

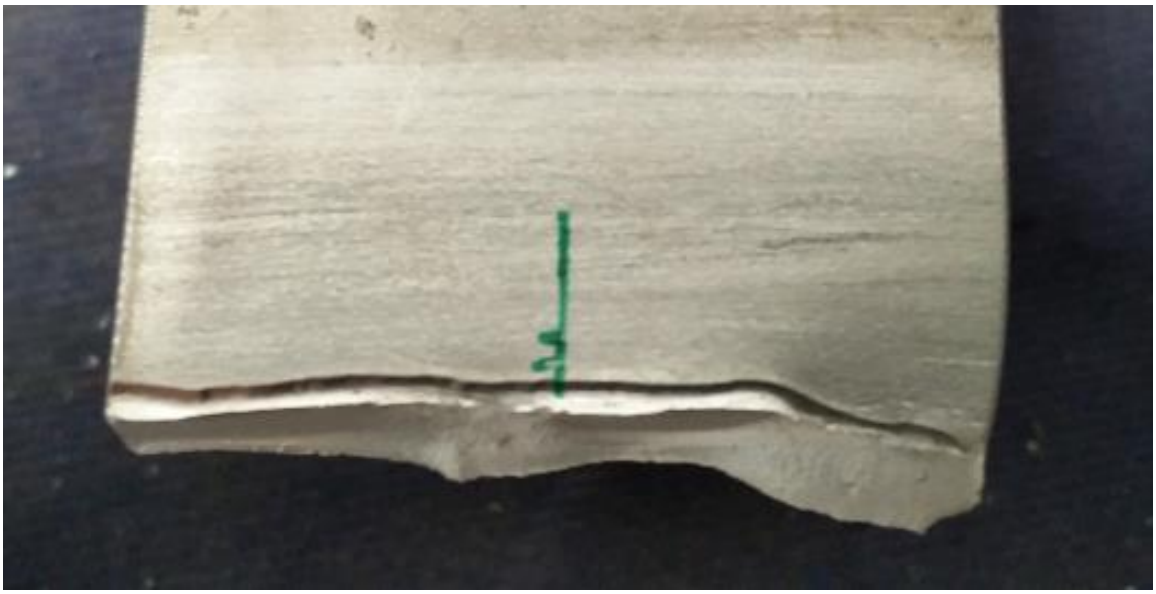

Figure V.1. Breaking of HiFIT treated butt welded specimen in treated area.

Figure V.2. HiFIT treatment in butt welded specimen

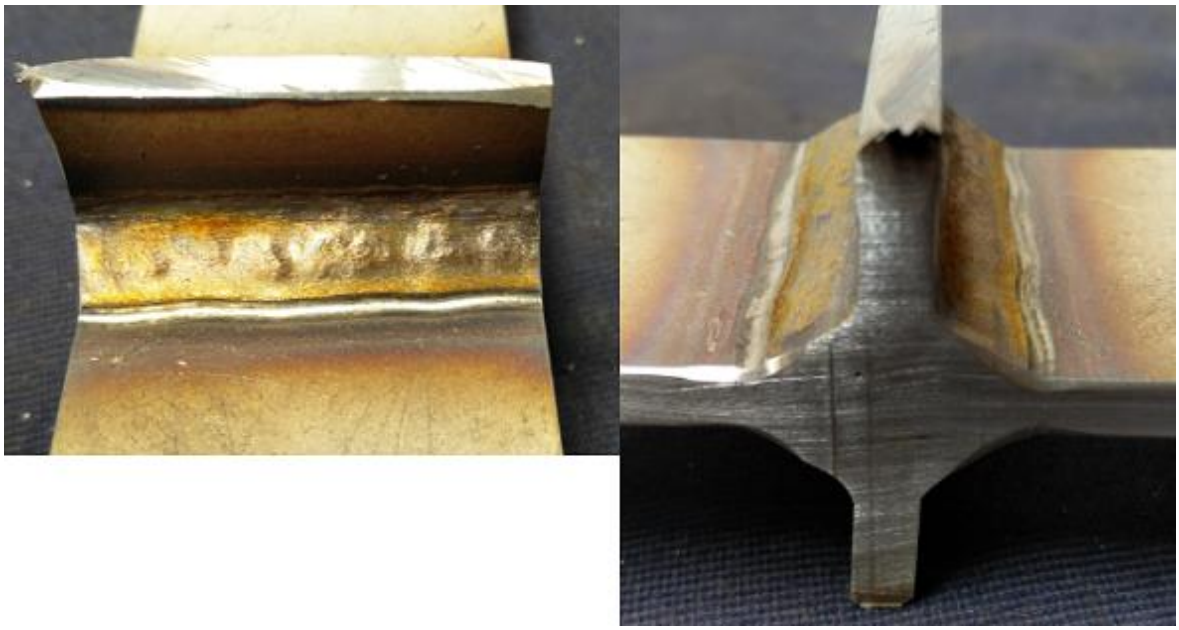

Figure V.3. HiFIT treatment in SDNL.2H specimen.

APPENDIX VI

Microhardness measurements.

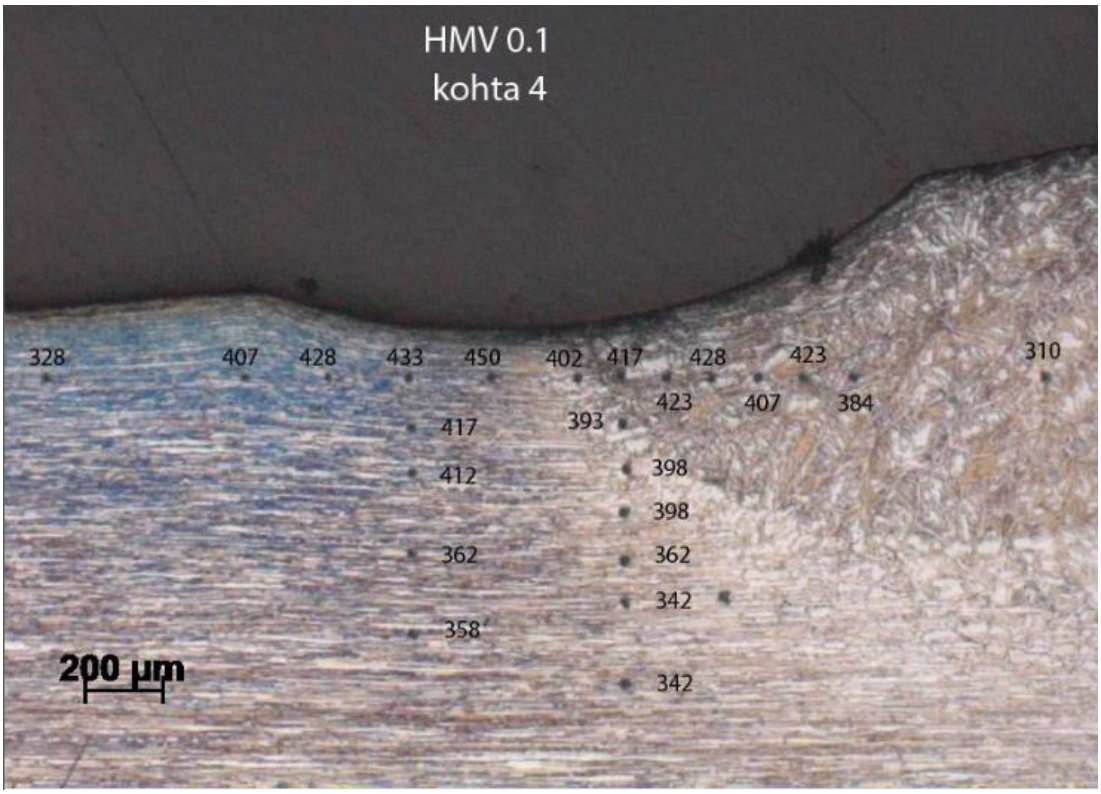

Figure VI.1. Microhardness measurements in HiFIT treated butt welded specimen.

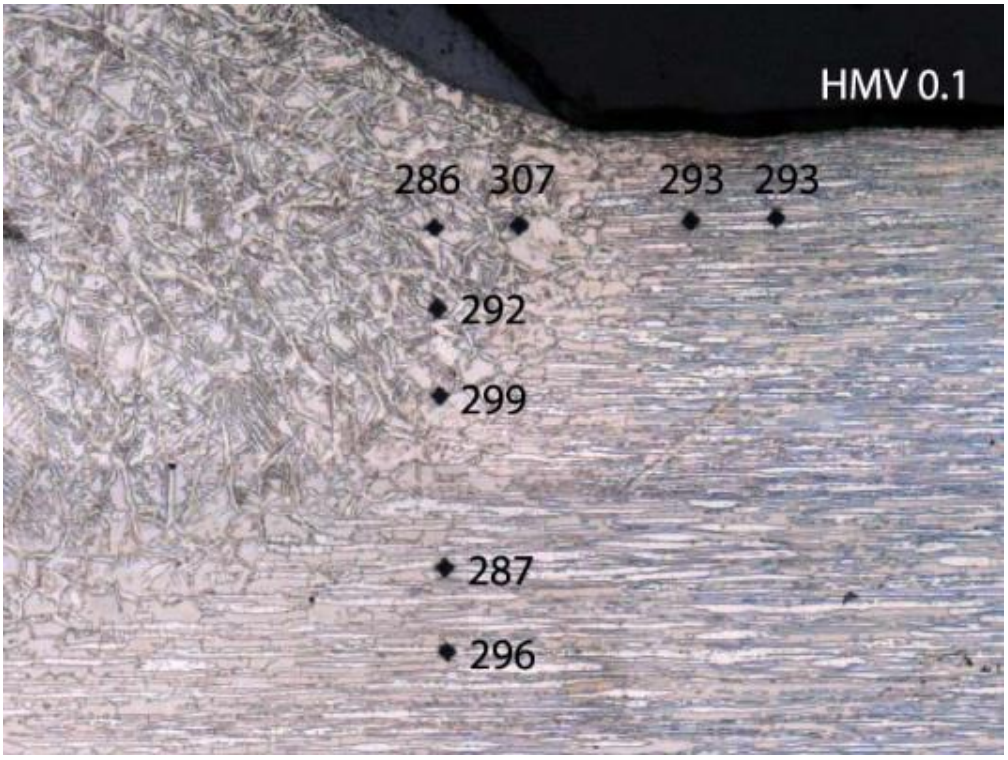

Figure VI.2. Microhardness measurements in one toe of non-load carrying specimen.

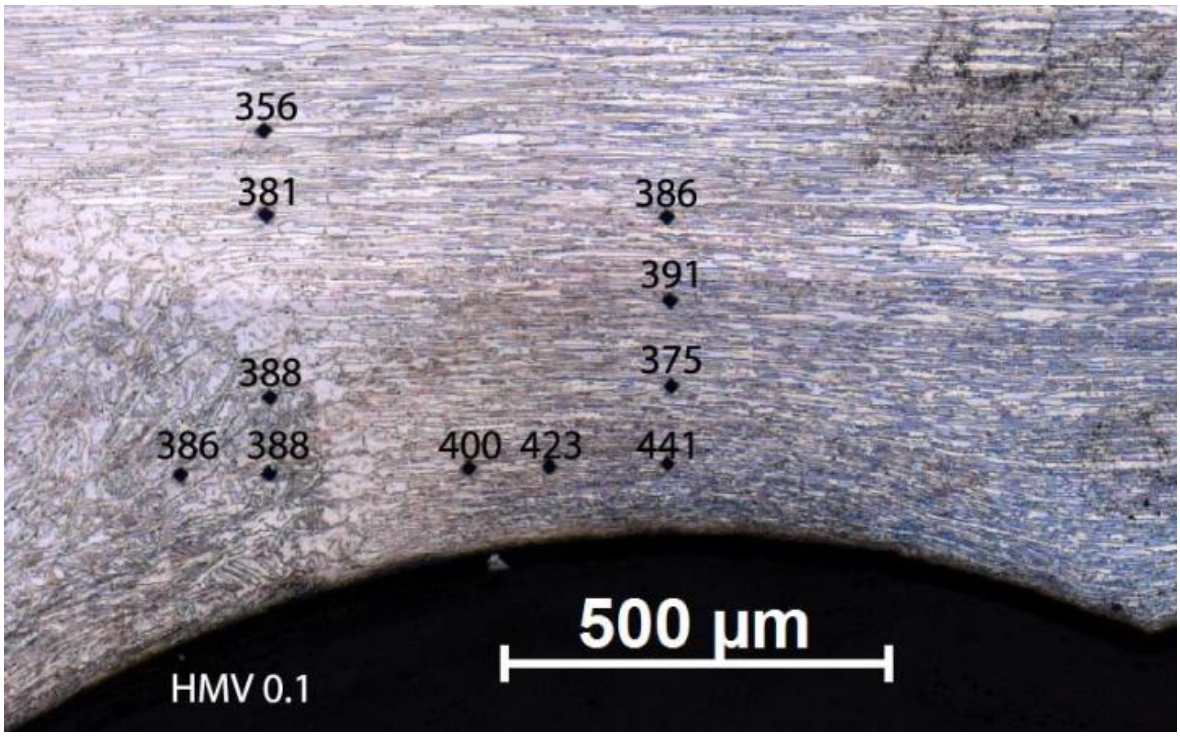

Figure VI.3. Microhardness measurements in HiFIT treated non-load carrying joint.

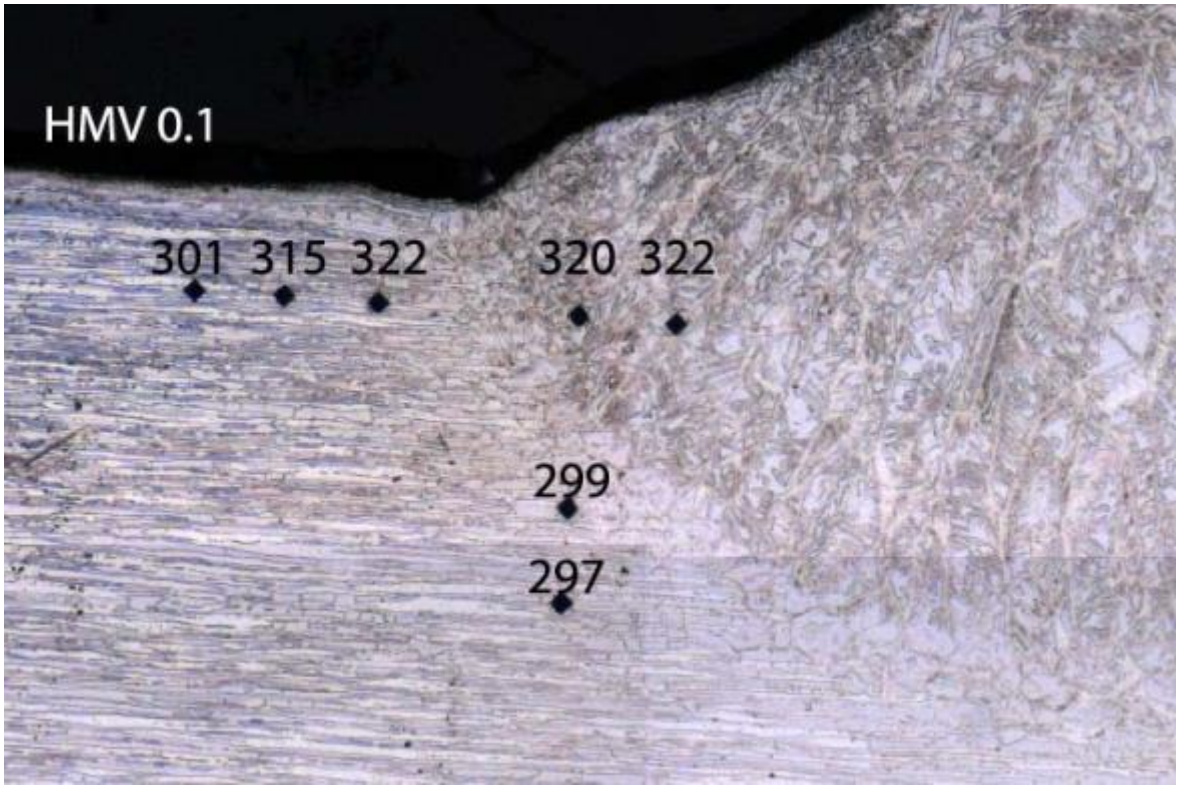

Figure VI.4. Microhardness measurements in load carrying joint.

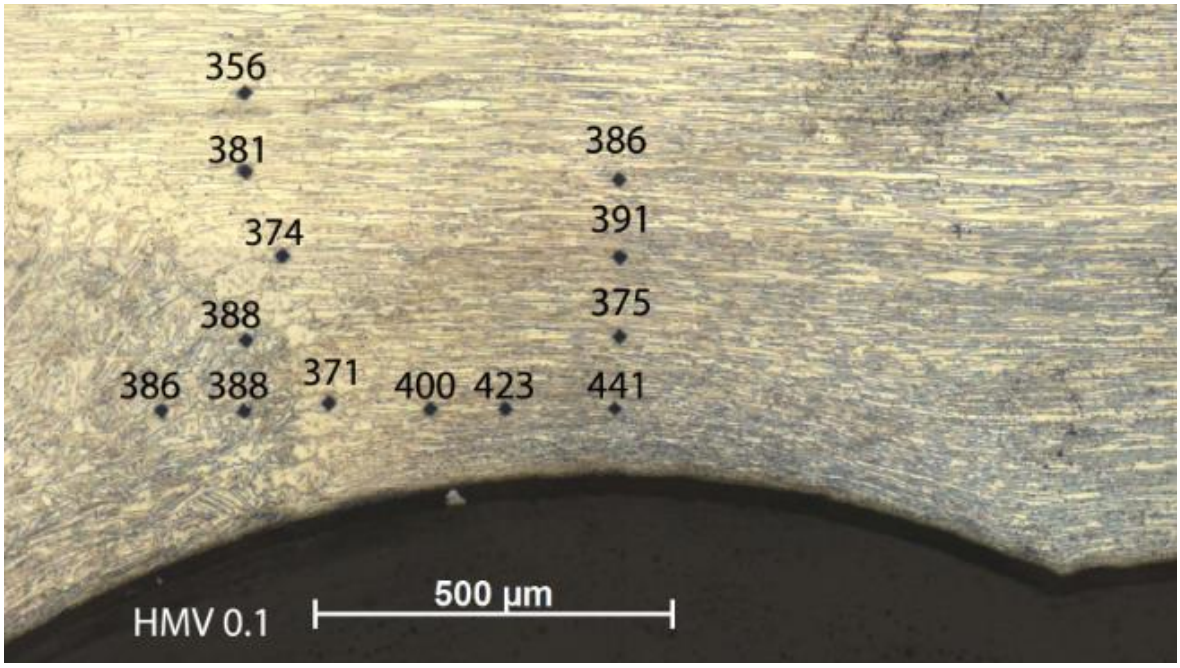

Figure VI. 5. Microhardness measurement in the non-load carrying HiFIT treated joint shows smaller hardness in fusion line.

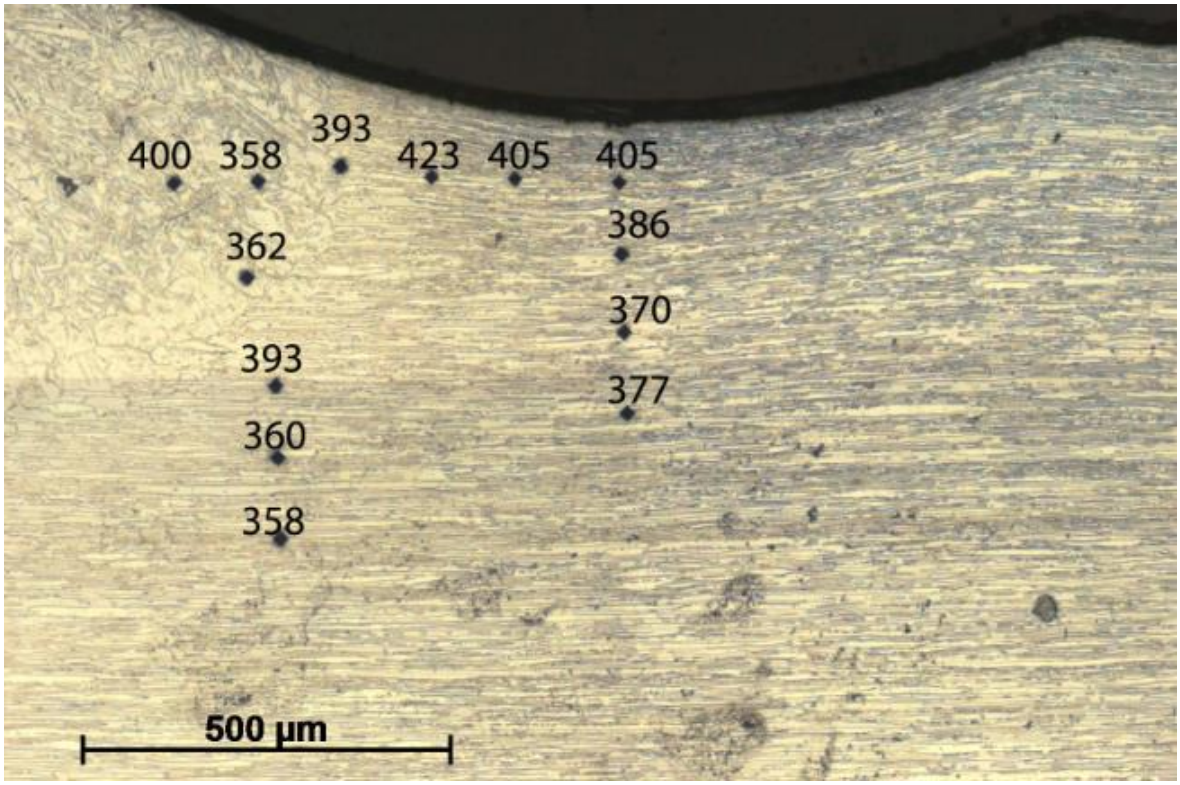

Figure VI.6. Microhardness measurement in the non-load carrying HiFIT treated joint shows smaller hardness in fusion line.

APPENDIX VII

Residual stress measurement results.

Table VI.1 Residual stress measurement numerical results.

SPECIMEN:		SDL1.1		SDNL.1H		SDNL.00	
Side	**Distance**	**MPa**	**(+/-)**	**MPa**	**(+/-)**	**MPa**	**(+/-)**
A	**0**	0	64,8	-420	192,4	-226	157,3
A	**-2**	461	36	42	78,4	197	107,1
A	**-4**	357	78,2	120	18,9	7	37,9
A	**-6**	87	96,4	117	30,6	-199	88,7
B	**0**	-349	64,7	-535	123,4	-249	68,9
B	**2**	79	39,8	-38	37,1	33	54,3
B	**4**	465	60,3	108	32,7	-60	34,6
B	**6**	235	46,3	60	34,5	-88	32,7
C	**0**	54	30,8	-286	117,5	-170	122,4
C	**-2**	345	57,6	-421	103	336	61,3
C	**-4**	297	103,9	136	27,7	201	74,7
C	**-6**	147	49,2	47	26	-36	84,9
D	**0**	-239	34,2	-499	80,5	54	114,4
D	**2**	524	116,6	-125	68,7	247	61,3
D	**4**	339	65,3	232	117,3	303	60,2
D	**6**	345	66,6	204	24,2	155	47,9